# Characterization of Temperature-dependent Gating in Archaebacterial Calcium-Activated Potassium Channel

By

Yihao Jiang

A dissertation submitted in partial fulfillment of

the requirements for the degree of

Doctor of Philosophy

(Biophysics)

at the

UNIVERSITY OF WISCONSIN-MADISON

2020

Date of final oral examination: 01/14/2020

The dissertation is approved by the following members of the Final Oral Committee:

Baron Chanda, Professor, Neuroscience

Edwin Chapman, Professor, Neuroscience

M. Thomas Record, Jr., Professor, Biochemistry

Katherine Henzler-Wildman, Associate Professor, Biochemistry

Alessandro Senes, Associate Professor, Biochemistry

# ACKNOWLEDGMENTS

I want to thank Baron and all the current and past members in the Chanda lab for their help and kindness all through my graduate life. In this long journey, I developed from an apprentice to a scientist. How I approach scientific questions, as well as how I view the world, have also changed through this practice. I want to give special thanks to my fellow graduate students, John and David. It is a pleasure to discuss science with you guys, even though our field of study different. Not to mention all the fun time we had outside the lab. To Dima, Claudia and Ana, I want to thank you all for the guidance and mentorship during my early years of graduate school. Without your help, I definitely would not be as prepared for all these obstacles in my projects as I was. I also want to thank Ana for showing me how to deal with bad days when negative results keep showing up. It is always a pleasure to discuss science with Sandipan, whose broad knowledge is very enlightening. I met Vinay and Tristan at the end of my graduate school and was impressed with your positive attitude in this short period. I have to say that I was very fortunate to meet all of you in graduate school.

I am truly happy that I enrolled in the Biophysics Graduate Program at the University of Wisconsin-Madison. I want to thank Allison and Max, the current and former program coordinators, for your help with the paperwork and responding to tons of emails from me about every detail in the program requirements. I also want to thank all my friends in the program, Gladys, Munish, and Matt. I enjoyed hanging out with you guys and if it is not for you, this journey would not have been as memorable as it was.

I also want to use this opportunity to thank my friends and family. If it were not your support, I definitely would not have been able to go through the ups and downs of graduate life. To all my friends, I am so lucky to meet you in Madison. I wish all of you good luck with your life journey, and I hope we will still be connected no matter how far apart we are. To my parents, thank you for supporting me all along, and I can only hope that I have made you proud.

In the end, I want to thank Meiqi, my fiancée, for who you are. It is tough to sustain a long-distance relationship, especially with happy endings. I cannot express how grateful I am that you sacrifice your holidays to visit me in Madison. I believe if there is someone I want to spend my rest life with, I already found her, and it is you.

# ABSTRACT

The temperature-dependent response is mediated by a structurally diverse class of eukaryotic ion channels, many of which also exhibit polymodal behavior. To probe the foundational mechanisms of temperature-sensing, we characterized the temperature-dependent activation of a calcium-activated potassium channel, MthK, derived from archaebacteria isolated from hot springs. Functional complementation studies show that these channels are 100,000-fold more efficient at rescuing a potassium uptake deficient strain, LB2003, in low potassium agar plates at 36 °C than at 18 °C. By patch clamping giant *E. coli* spheroplasts, we show that MthK expressed in *E.coli* membranes is regulated by temperature. Electrophysiological activity of the purified MthK is extremely sensitive ($Q_{10}$ ~100) to temperature change at low calcium concentrations, whereas channels lacking the calcium-sensing RCK domain are practically insensitive. Single-channel analysis of its allosteric behavior, which includes measurements under limiting conditions, shows that heat acts as an allosteric modifier by altering the coupling strength between the cytoplasmic calcium-sensing domain and pore domain. Our studies reveal a new mechanistic paradigm for allosteric regulation by physical stimuli.

It is intriguing for us to understand how this coupling interaction undergoes a temperature-dependent process to activate the channel. Collaborated with Professor Vera Moiseenkova-Bell and Dr. Yaxian Zhao in the university of Pennsylvania, we purified MthK in a calcium-free buffer and solved a 4.8 Å resolution apo structure using cryo-EM. Comparing with the calcium bound structure (PDB: 6OLY), we observed a dramatic conformation change in the linker region upon calcium activation. However, how this structural change is related to the temperature activation requests further investigation. Superposing the isolated apo RCK domain (PDB:2OGU) with our structure, we observed a conformation regulation of the RCK domain by

the pore. This result suggests the existence of coupling energy between the pore domain and the apo RCK domain.

Moreover, helped with Dr. Vinay Idikuda and Dr. Vadim Klenchin, we screened over a million MthK mutants with complementation assay. Among these mutants, we achieved hundreds of cold-sensitive mutations in MthK. Through this study, we want to get a deeper understanding of the mechanism of temperature sensing in MthK.

## TABLE OF CONTENTS

***Experimental Procedure***



**CHAPTER THREE**

***MthK expressed in E. coli is temperature-sensitive***

# CHAPTER ONE

## *Introduction*

### Overview

It is vital for the survival of an organism to be able to sense the environmental changes and react quickly and precisely to it. Complex multicellular organisms, such as human beings, have developed specialized sense organs featuring a plethora of nerve endings to perceive a variety of stimuli (Hille, 1992; Zheng and Trudeau, 2015). In these nerve endings, abundant ion channels are expressed. These ion channels could respond to a variety of environmental cues, including both physical and chemical stimuli, and act as both gatekeepers, as well as signal transducers (Hille, 1992; Zheng and Trudeau, 2015).

While most biological molecules will inherently respond to an acute physical force such as temperature or mechanical stretch, some ion channels are specialized to be multiple-fold more sensitive to such physical stimuli (Clapham and Miller, 2011; Goldschen-Ohm and Chanda, 2017; Zheng and Trudeau, 2015). For instance, compared to a $Q_{10}$ (fold change in activity for a 10-degree change in temperature) of 2-4 for most ion channels, the $Q_{10}$ is usually larger than 20 for a bonafide temperature-sensitive ion channel, such as TRPV1 (Clapham and Miller, 2011). In addition to TRPV1 (Caterina et al., 1997), the activity of TRPM8 (McKemy et al., 2002), TREK (Maingret et al., 2000), TMEM16A (Cho et al., 2012) and even voltage-gated sodium channels (Arrigoni et al., 2016; Dib-Hajj et al., 2008) have all been reported to be highly temperature-dependent.

How are some ion channels specialized to respond to a particular stimulus? Ligand-gated ion channels, for instance, have evolutionarily conserved domains, that are specialized in recognizing certain ligands (Zheng and Trudeau, 2015). For example, HCN channels (Ludwig et al., 1998) and CNG channels (Craven and Zagotta, 2006) have a conserved cyclic nucleotide-binding domain (CNBD). Upon binding to cAMP, these CNBDs will undergo a dramatic

conformation change to alter the activity of these channels (Craven and Zagotta, 2006; Lee and MacKinnon, 2017). However, for physical stimuli, such as voltage, mechanical force, and temperature, it has been pointed out that the sensors are not constrained by stereochemistry as opposed to ones that recognize chemical ligands (Kuriyan et al., 2012). Therefore, they lack a conserved recognition motif (Goldschen-Ohm and Chanda, 2017). This observation is consistent with the various structural features on these channels, thus making it difficult to probe and understand their gating mechanisms (Goldschen-Ohm and Chanda, 2017; Islas and Qin, 2014; Yuan, 2019; Zheng and Trudeau, 2015). Also, it remains unclear whether these structurally diverse channels, broadly classified as Type III ion channels, have common underlying biophysical mechanisms of activation (Goldschen-Ohm and Chanda, 2017). The complexity of this question motivated me to find a simple system that would allow us to get a glimpse at the general mechanism underlying temperature sensitivity in biomolecules in general and ion channels in particular.

**Cell membrane and membrane voltage**

To begin the story of ion channels, we have to talk about the magnificent barrier, cell membrane. This lipid bilayer protects the cell from the outside elements so that the cytoplasm maintains a controlled environment. Besides, this bilayer is hydrophobic and impermeable to water and ions, thereby upholding different ionic compositions to exist on the opposite side of the membrane.

How does membrane potential arise from this hydrophobic bilayer? In 1889, Nernst published the equation to relate the chemical potential (which arises from a difference in ionic concentrations) to membrane electric potential (Eq. 1) (Nernst, 1889), and Bernstein further applied this equation to cellular systems to understand the origin of resting membrane potential (Zheng and Trudeau, 2015).

$$E_m = \frac{RT}{F} ln\left(\frac{P_{Na}[Na]_{out}+P_K[K]_{out}+P_{Cl}[Cl]_{in}}{P_{Na}[Na]_{in}+P_K[K]_{in}+P_{Cl}[Cl]_{out}}\right) \quad \text{Eq. 1}$$

In Eq. 1, $E_m$ represents the membrane potential, $R$ is the ideal gas constant, $T$ is the temperature in kelvin, $F$ is the Faraday's constant, $P_i$ is the permeability to ion i (i represents $Na^+$, $K^+$ or $Cl^-$), and [i] is the concentration of the ion i on either inside or outside.

In cells, the internal $K^+$ concentration is much higher as compared to external $K^+$ concentration, and Bernstein hypothesized that in resting state, the cell membrane is mainly permeable to $K^+$ ions, which results in negative membrane potential (Hille, 1992). Later studies have found that this imbalance of the $K^+$ concentrations arises from the activity of the sodium-potassium pump, which uses the chemical energy stored in two ATP to pump two $K^+$ ions into the cell and three $Na^+$ ions outside (Carpenter and Alving, 1968; Clausen et al., 2017).

This equation also helps us to understand how ion channels could trigger and propagate the electrical signal. From Eq. 1, it is easy to derive that there are two ways to change the membrane potential. One is by changing the ion concentrations (actually the ratio of outside concentration versus inside concentration of a particular ion, i.e. $\frac{[Na]_{out}}{[Na]_{in}}$). The other is by changing the permeability of some ions (i.e., $P_{Na}$). For multicellular organisms, changing the ion concentrations usually takes a long time and is most likely resulting in toxicity (except for some specific ions, like intracellular $Ca^{2+}$), while changing the permeability could be well controlled by the opening or closing of certain ion channels.

**Selectivity and conductance**

Based on the discussion above, the resting membrane potential and action potential are usually determined by changing permeability to a few ions. This delicate regulation of conductance requires certain ion channels with high selectivity to a particular ion (like $K^+$). A specialized region mediates this high selectivity of one ion over another in the channel, called selectivity filter (Zheng and Trudeau, 2015). Theoretically, this high selectivity is a combination of

preferential ion binding and a high energy barrier for permeation of other ions (Jiang et al., 2002; Lee and Cui, 2010; Zheng and Trudeau, 2015). In this section, I will briefly discuss the selectivity and conductance using $K^+$ ion channels as an example.

Mutagenesis studies on fruit fly, *Drosophila*, found a mutant exhibiting uncontrolled shaking, which later on was identified as a mutation in the *Shaker* locus (Salkoff and Wyman, 1981). This gene encodes a voltage-gated potassium channel, which later on becomes one of the most well-studied ion channels in the field. Electrophysiological studies have shown that Shaker potassium channel has a 10,000-fold preference for $K^+$ over $Na^+$ (Doyle et al., 1998). Further cloning of other potassium channels has identified a conserved region with TxGYG motif (x represents an unconserved residue in this motif)(**Fig. 1A**), and mutagenesis in this region leads to dramatic changes in selectivity (Zheng and Sigworth, 1997). Later, the structure of KcsA, a bacterial potassium channel, revealed that the backbone carbonyl oxygens of T75, V76, G77, Y78 as well as the hydroxyl of T75 side-chain all point to the center of the pore and formed a narrow gate (Zhou et al., 2001), which is the selective filter, shown in **Fig. 1B**. These carbonyl oxygens will mimic an aqueous environment for dehydrated $K^+$, while $Na^+$ will not be able to fit in the selectivity filter owing to its different size. Although the structural mechanism of selectivity has been revealed, many questions remain unanswered. Different selectivities of $K^+$ versus $Na^+$ were observed with channels having similar sequences in the selectivity filter, is there any other modulators in the channel that could modify the selectivity? What causes the C-type inactivation (Cuello et al., 2010a), which is believed to be related to a conformational change in the selective filter?

Conductance in ion channel is a measurement of how fast ions could pass through the channel. However, unlike electrical resistance, the conductance of an ion channel does not increase linearly with increasing permeant ion concentration and plateaus at a saturation concentration (Hille, 1992; Michaelis; Michaelis et al., 2011). It is counterintuitive that an ion channel maintains high selectivity while having a large conductance. Later on, a ‘knock-on’ model

was proposed to explain how selectivity and large-conductance could go hand in hand in a $K^+$ ion channel, shown in **Fig. 1C** (Bernèche and Roux, 2001; Hodgkin and Keynes, 1955; Morais-Cabral et al., 2001). Based on the model, there are four binding sites for $K^+$ in the selective filter. At the same time, two potassium ion will get into the selective filter, with either $K^+$-water-$K^+$-water or water-$K^+$-water-$K^+$ position (Zheng and Trudeau, 2015). The water in between will help diminish the repulsion between the $K^+$ ions and rigidify the selectivity filter (Bernèche and Roux, 2001). MthK channel has a high conductance rate of around 220 pS (Jiang et al., 2002). Based on MthK structure and studies on its homolog, BK channels, it has been believed that this large-conductance is related to the sizeable aqueous cavity right below the selective filter and rings of negatively charged residues in the intracellular pore (Haug et al., 2004a; Haug et al., 2004b; Nimigean et al., 2003), which increases the local potassium concentration.

**Discovery of temperature-sensitive ion channels**

Temperature regulation is necessary for maintaining homeostasis. Based on experiences in daily life, we have some basic understanding of temperature sensing, such as:

1. Temperature sensing has a range. Beyond this range, it is hard to tell how hot or how cold a particular temperature is (usually ends in a painful feeling).
2. Temperature sensation could be altered. For instance, a hand from hot water (40 °C) to warm water (25 °C) feels cool, while a hand from cold water (10 °C) into warm water (25 °C) feels warm.
3. Temperature sensing has varied resolutions. Different parts of the body have different sensitivity to the temperature change.

However, a deeper understanding of temperature sensing came around the beginning of the new millennium. With anatomical studies, Darian-Smith et al. found that the tip of peripheral sensory neurons is evolved into the temperature and pressure sensors (Darian-Smith et al., 1979). However, at this point, it was not clear whether a specific tissue structure, like hair cells, was

responsible for the sensation or a particular membrane protein was enough (Islas and Qin, 2014). If it was a molecule, whether it was an ion channel or a GPCR that transmits the message by altering ion channels was also not known.

The breakthrough came through studies on the transient receptor potential (TRP) channel family (Patapoutian et al., 2003). TRP ion channels derive their name from a phototransduction mutant of *Drosophila* (Cosens and Manning, 1969; Islas and Qin, 2014; Zheng and Trudeau, 2015). Upon light activation, the fruit flies with this mutation show a transient instead of sustained response (Cosens and Manning, 1969). Later studies have shown that this channel in *Drosophila* belongs to subclass TRPC (Islas and Qin, 2014). The bridge between TRP channels and temperature sensing is the study searching for a capsaicin-sensitive ion channel (Caterina et al., 1997; Harteneck et al., 2000). Worldwide, pepper, or to say spicy food, is one of the main flavors for cooking, which brings a burning feeling. So, instead of finding an ion channel that responds to heat, scientists put effort into finding an ion channel that could be activated by capsaicin. In this pursuit, Caterina et al. found vanilloid receptor 1 (VR1) (Caterina et al., 1997), which was further identified to be a member of the TRP family, and named as TRPV1 (Harteneck et al., 2000).

Based on sequence similarity, more channels in the TRP channel family were discovered. Among them, TRPV1-4, TRPM8, TRPA1, and more are all found to be temperature sensitive, and after that, categorized as thermoTRP channels (Islas and Qin, 2014; Patapoutian et al., 2003). Heterologous expression of these channels in eukaryotic cell lines (i.e., human embryonic kidney (HEK) cells (Caterina et al., 1997), insect Sf9 cells (Liao et al., 2013), and *Xenopus* oocytes (Brauchi et al., 2004)) has shown robust temperature response. Further bilayer studies of the purified thermoTRP channel (Cao et al., 2013a) demonstrates an intrinsic temperature-sensitive in these channels, without interactions with cellular modulators. Furthermore, studies in TRPV3 knock out mice showed that their sensitivity to noxious heat is compromised (Moqrich et al., 2005). Taken together, these results prove that thermoTRP channels act as the temperature sensors in the cell.

Besides temperature activation, some of the thermoTRPs are also sensitive to pressure. In vitro studies have shown that TRPV2 is sensitive to osmotic stress and stretch (Caterina et al., 1999; Muraki et al., 2003). As an ion channel sensitive to moderate temperature, TRPV4 also has a potential role in mechanosensation (Alessandri-Haber et al., 2003) and hearing (Liedtke et al., 2000; Voets et al., 2005). Moreover, it was shown in heterogeneous expression systems that TRPM8 could be activated by increased osmolality (Quallo et al., 2015). And this osmosensation in TRPM8 is responsible for the eye-blinking regulation in mice (Quallo et al., 2015). However, how mechanical forces regulate these channels remains unknown.

Although multiple temperature-sensitive ion channels have been found, the thermal perception in complex multicellular organisms is still not well understood because of many reasons. First, there are likely more temperature-sensitive ion channels than we have discovered (Gong et al., 2019), which covers the full range of the temperature response. Second, multiple temperature-sensitive ion channels are coexpressed in the same sensory neuron, and differences in the expression pattern of these temperature-sensitive ion channels will give us a fine map of the temperature sensitivity (Cheng et al., 2010; Cheng et al., 2007; Saito et al., 2012). Another hypothesis is that the temperature response of each channel can be altered by cellular conditions (Islas and Qin, 2014). As eukaryotic temperature-sensitive ion channels have a polymodal gating process, cells can use secondary messengers and other factors, like pH, to fine-tune the temperature response of each channel. Any or all of these mechanisms may contribute to the temperature sensitivity in eukaryotic organisms.

For the known temperature-sensitive ion channels, to describe how temperature-sensitive these channels are, $Q_{10}$ is a standard parameter used, which corresponds to change in activity for a 10 ºC increase in temperature (Clapham and Miller, 2011; Islas and Qin, 2014; Zheng and Trudeau, 2015). It can be calculated using Eq. 2:

$$Q_{10} = \left(\frac{A_{T1}}{A_{T2}}\right)^{\frac{10}{(T1-T2)}} \qquad \text{Eq. 2}$$

Most temperature-sensitive ion channels in the thermoTRP family have a significant high $Q_{10}$, which were listed in **Table one**.

**Animal models used in thermal sensation studies**

The thermoTRP family has been found to be temperature sensitive (Patapoutian et al., 2003). However, whether these channels are the only temperature sensors in sensory neurons remains unanswered. To study this question, animal models that have a fast and efficient temperature response is needed.

Many species demonstrate dramatic temperature sensing abilities. For example, a snake could sense one milidegree difference of the temperature difference between the environment and prey (Bullock and Diecke, 1956). However, a straightforward mutagenesis system was not available in snakes. To systematically understand the molecular mechanism of temperature sensors, we need an animal system that has a robust response to temperature and tolerates mutagenesis studies. These requirements lead us to the use of established model animals (Islas and Qin, 2014).

*Caenorhabditis elegans* has been found to have a significant temperature preference around 27℃, and avoidance behavior will be observed for both higher and lower temperatures (Garrity et al., 2010; Glauser, 2013; Glauser et al., 2011; Gong et al., 2019). Large scale mutagenesis could be applied by mutagen ethyl methanesulfonate (EMS) in *C. elegans*. With this, Gong et al. have found that glutamate receptors also function as temperature sensors in *C. elegans* (Gong et al., 2019). However, these glutamate receptors have lost their glutamate sensitivity. Furthermore, the homolog of these glutamate receptors in human and mouse are also temperature sensitive based on fluorescence assays (Gong et al., 2019). Thus, these glutamate receptors represent an evolutionarily conserved temperature-sensitive family.

Besides *C. elegans*, fruit fly, *Drosophila melanogaster*, could also serve as a good model system for genetic studies on temperature-sensitive ion channels (Garrity et al., 2010; Hoffmann

et al., 2003; Patapoutian et al., 2003). Even in the larval stage, drosophila could sense and respond to temperature change effectively (Liu et al., 2003b). It has been found that specialized organs in fruit flies' head antenna were activated at uncomfortable temperatures. Later molecular studies have found that TRPA1 is responsible for its heat avoidance behavior, and during transcription, the mRNA of this channel exhibits alternate splicing, which results in diverse channel formations (Neely et al., 2011; Zhong et al., 2012).

Other than these eukaryotic models, *E. coli* is also widely used in the discovery of temperature-sensitive ion channels (Maeda et al., 1976). It has been observed that this Gram-negative bacteria could flee from undesirable temperatures by using their flagellar motors (Islas and Qin, 2014). Later studies show that the thermosensation has similar behavior with chemotaxis in *E. coli* (Block et al., 1982; Maeda et al., 1976; Paster and Ryu, 2008). Based on this observation, the chemoattractant receptors may also function as the temperature sensors in bacteria. Under this hypothesis, researchers have found that chemoreceptors Tar, Tsr, Trg, and Tap could all respond to temperature change (Islas and Qin, 2014). Among them, Tar and Tsr have also been shown to be heat-sensitive (Falke and Hazelbauer, 2001; Sourjik and Wingreen, 2012). Besides these channels, Arrigoni et al. found that the voltage-gated sodium channels (BacNav) are also temperature-sensitive (Arrigoni et al., 2016). However, little is known about how temperature sensitivity is perceived in microbes besides these studies.

**Principles of the temperature-dependent gating mechanism**

Now let us consider what is known about the gating mechanisms of temperature sensing. Temperature could change many physical properties of the cell components, from the formation of the lipid bilayer to the activity of electrolytes (intracellularly and extracellularly). It is well known that bilayers undergo a phase transition at specific temperatures, depending on the lipid composition (Träuble and Eibl, 1974). At low temperatures, lipids are in a highly ordered structure like a gel with low fluidity and high rigidity. At higher temperatures (usually around the optimum

growth temperature for the corresponding organisms), the lipids remain to be ordered but more flexible. However, for extreme temperatures (> 40℃), the lipids are disordered and form a nonlamellar structure. As many temperature-sensitive ion channels, such as TRPV1, TRPV2, and TRPV3, all have a threshold higher than 40 ºC (Clapham and Miller, 2011; Patapoutian et al., 2003), membrane disruption may play a role in their temperature sensitivity. Furthermore, the activity of ions is also temperature-dependent (Hille, 1992; Islas and Qin, 2014), which may alter the activity of thermoTRPs since some of them are activated upon ion binding. (Diaz-Franulic et al., 2016; Islas and Qin, 2014; Jara-Oseguera et al., 2016; Patapoutian et al., 2003).

**Enthalpy and entropy theory**

The open probability ($P_O$) of an ion channel is related to the energy difference between its closed and open state, illustrated in Eq. 3:

$$P_O = \frac{1}{1+e^{\frac{\Delta G}{RT}}} \quad \text{Eq. 3}$$

$$\Delta G = \Delta H - T\Delta S \quad \text{Eq. 4}$$

Eq. 4 defines free energy relation with enthalpy (ΔH) and entropy (ΔS) change. By implying Eq. 4 to Eq. 3, we could achieve Eq. 5:

$$P_O = \frac{1}{1+e^{\frac{\Delta H}{RT}-\frac{\Delta S}{R}}} \quad \text{Eq. 5}$$

From Eq. 5, we could see that the thermal sensitivity of a channel is dependent on the enthalpy change during channel opening process. Moreover, whether it is heat-sensitive or cold-sensitive is determined by the polarity of the enthalpy change (ΔH) (Islas and Qin, 2014).

Based on this theory, to achieve a highly temperature-sensitive ion channel, like TRPV1, the enthalpy change required during the close-open transition is around 100 kcal/mol (Islas and Qin, 2014; Yao et al., 2010). This energy change is equivalent to a voltage-gated ion channel that has 85 unit charges across an electrical potential of 50 mV during the opening process, which is way larger than any known voltage-gated ion channels (Yao et al., 2010).

It has been a matter of debate in the field, whether there is a temperature sensor involved in the temperature activation process (Arrigoni and Minor, 2018; Clapham and Miller, 2011). Theoretically, temperature is a physical entity that could affect all the parts of the channel, which may not require a localized domain for temperature sensing.

Mutagenesis studies from different groups have found that multiple regions in thermoTRP channels may contribute to temperature sensitivity (Brauchi et al., 2006; Cordero-Morales et al., 2011a; Feng, 2014; Grandl et al., 2008; Islas and Qin, 2014; Jabba et al., 2014; Patapoutian et al., 2003; Voets et al., 2007; Yang et al., 2010; Zhong et al., 2012). To illustrate the location of these critical structural elements, the structure of a TRPV1 monomer is shown in **Fig. 2**. Replacement of the ankyrin repeats and proximal N-terminus in temperature-insensitive TRPVs (human TRPV2 and mouse TRPV4) with the functional counterpart of heat-sensitive TRPV1 will make these chimeras sensitive to elevated temperatures (Islas and Qin, 2014). Moreover, Grandl et al. found the external pore linker is vital for the temperature sensitivity of TRPV3 with random mutagenesis screening (Grandl et al., 2008). Later, a chimera of Shaker ion channel with its pore domain replaced with the TRPV1 pore was reported to be heat-sensitive (Zhang et al., 2018). This study further illustrates the importance of pore domain in temperature sensing. Studies on TRPM8 and TRPV1 show that swapping of the C-terminus between TRPV1 and TRPM8 will reverse their temperature sensitivity (Brauchi et al., 2006), which suggests that the C-terminus is essential for temperature regulation. From these studies, one can conclude that there is not a single conserved domain, which accounts for temperature-sensitivity in thermoTRP channels. However, one disadvantage of these studies is that the identified area could interfere with the temperature-dependent activation by manipulating the coupling between the temperature sensor and the pore or just the pore gating itself without modifying the temperature sensor. As of now, there is no consensus on the location of a temperature sensor in thermoTRPs based on structural or functional evidence (Arrigoni and Minor, 2018; Clapham and Miller, 2011; Islas and Qin, 2014; Yuan, 2019).

**Heat capacity change theory**

A few years ago, Clapham and Miller suggested that a heat capacity change ($\Delta C_P$), which correlates with changes in solvation of side chains in the channel opening process can explain temperature sensitivity (Clapham and Miller, 2011).

In Eq. 6 and Eq. 7, the relationship of enthalpy change (ΔH) and entropy change (ΔS) with the heat capacity change are shown respectively:

$$\Delta H = \Delta C_P(T - T_0) \quad \text{Eq. 6}$$

$$\Delta S = \Delta S_0 + \Delta C_P \ln(T/T_0) \quad \text{Eq. 7}$$

Substituting the values of ΔH and ΔS into Eq. 4, we could get:

$$\Delta G(T) = \Delta H_0 + \Delta Cp(T - T_0) - T\Delta S_0 - T\Delta Cp \cdot \ln(T/T_0) \quad \text{Eq. 8}$$

This equation solves the source of the large enthalpy and entropy changes in the temperature activation process and set the heat capacity change as a primary determinant of the temperature dependence in the ion channels (Chowdhury et al., 2014; Clapham and Miller, 2011). Based on this equation, it appears that there is no need for a discrete domain to sense the temperature change. Instead, a bunch of micro-domains could work together to facilitate the temperature sensitivity in the ion channel.

From **Fig. 3**, which is adapted from Chowdhury et al.'s paper (Chowdhury et al., 2014), we can see that the free energy change versus temperature is a U-shaped curve, which is concave for the positive $\Delta C_P$, and convex for negative $\Delta C_P$. From this U-shaped curve, we could easily interpret that temperature-sensitive ion channels will be heat-sensitive in one temperature range while cold-sensitive in another temperature range. However, this dual-response to heat and cold has not been observed for thermoTRP channels (Islas and Qin, 2014). This discrepancy could be either due to our inability to measure activity at extreme temperatures or other processes that may obscure temperature-dependent gating, such as inactivation. Recently, Moparthi et al.

used single channel recordings to show that human TRPA1 has a U-shaped activity curve when plotted with respect to temperature ($Q_{10}$ ~ 6) (Moparthi et al., 2016).

Furthermore, based on this hypothesis, Chowdhury et al. used the Shaker potassium channel as a model (Chowdhury et al., 2014). By mutating critical residues undergoing changes in solvation during the gating process, they identified many mutants that change this temperature-insensitive ion channel to a highly temperature-dependent ion channel, which has comparable $Q_{10}$ to thermoTRPs. However, a thorough study of the $\Delta C_P$ on these Shaker mutants is challenging with electrophysiology, as it requires an accurate calculation of ΔG close to critical temperature ($T_C$), where the derivative of ΔG versus T equal to zero. This is because, far away from the critical temperature, the curve will be quasilinear, which is not ideal for an accurate calculation of the $\Delta C_P$.

However, this theory is also controversial. For thermoTRPs, outside the activation range, they are nominally temperature-dependent like other ion channels, which gives $\Delta H_0$ around 20 kcal/mol, then the heat capacity change would have a value around 4 kcal/mol·K. On average, one hydrophobic residue contributes a heat capacity of about 30-40 cal/mol·K (Islas and Qin, 2014). Thus exposure of 100 hydrophobic residues or 25 residues per subunit is required during the open process. However, this profound conformational change is not observed from the structures of TRPV1, between the open state [agonist bound structure (PDB: 3J5R)] and the closed state [the apo structure (PDB: 5IRZ)].

**Hysteresis of thermoTRPs**

Hysteresis in temperature activation of thermoTRPs has been commonly observed (Islas and Qin, 2014; Liu et al., 2011) especially involving the Peltier temperature controller to alter the buffer temperature.

As shown in **Table one**, the $Q_{10}$ calculated from different laboratories sometimes even vary multiple folds. This, in large part, is due to hysteresis during activation, which happens during

the slow speed of temperature change. To solve this problem, Qin et al. developed a fast temperature control based on high power infrared laser diodes, which can give a temperature jump as fast as 100,000 ºC/s (Yao et al., 2009). This technique also shortens the time duration for the experiment which makes it possible to complete the experiment without damaging the patch. Furthermore, it can be used in experiments with extremely high temperatures (> 50 °C).

Using a similar fast temperature jump set up, Sanchez-Moreno et al. studied hysteresis of TRPV1 on excised patches and found that hysteresis may result from the irreversible inactivation of the channel (Sánchez-Moreno et al., 2018). However, it is still unknown why a channel would evolve that responds to temperature activation only once and then becomes unfunctional. Interestingly, this irreversible behavior is also observed in TRPV3 channels but in the opposite direction (Liu et al., 2011). Instead of irreversible inactivation upon heat in TRPV1, TRPV3 has irreversible activation with physical and chemical stimuli. When first activated by either heat or chemical agonists (i.e., 2-APB), TRPV3 only shows small activity. However, with repeated stimuli, the activity of the channel increases progressively. This potentiation process could be accelerated by using the fast $Ca^{2+}$ chelator, 1,2-Bis(2-aminophenoxy) ethane-N, N, N', N'-tetraacetic acid (BAPTA), in the cytoplasmic buffer, which suggests that $Ca^{2+}$ may play a role in this potentiation (Islas and Qin, 2014). With this irreversible inactivation or activation processes, thermoTRPs seem to be imperfect channel models for thermodynamic analysis.

**Prokaryotic temperature sensors**

For decades, most of the studies in the temperature activation mechanism field are done in eukaryotic temperature-sensitive ion channels. Using eukaryotic ion channels has a particular advantage as their physiological roles are better established with knockout and knockdown experiments in mice (Caterina et al., 2000; Islas and Qin, 2014; Moqrich et al., 2005). Besides, multiple ligands, both biological-based and chemically synthesized, have been discovered and developed for these channels, especially for thermoTRPs (Islas and Qin, 2014; Patapoutian et al.,

2003). These agonists and specific blockers form an excellent toolkit for electrophysiological studies.

However, these eukaryotic channels have polymodal gating processes and many of them undergo irreversible conformational changes upon temperature activation. Both of these make it almost impossible to proceed with a thermodynamic analysis of these channels and extract the temperature-activation mechanism. By using prokaryotic voltage-gated sodium (BacNav) channels, Minor and his colleagues have combined electrophysiology and structural biology to study the mechanism of temperature activation in these channels (Arrigoni et al., 2016). A coiled-coil domain in the proximal C-terminal was shown to undergo conformational changes upon temperature activation. Later studies in proton channel $H_V1$ also found that a similar coiled-coil domain can account for temperature response observed in these channels (Takeshita et al., 2014). These studies shed light on the possibility of using prokaryotic ion channels to study the mechanism of temperature activation.

**Allosteric mechanisms**

Allosteric activation is also referred to as ‘action at a distance’. The word ‘allostery’ initially was used to describe the binding of two different ligands to the same enzyme at different binding pockets. The presence of either ligand could interfere with the binding affinity of the other through reversible conformational changes. In this manner, Monod, Wyman, and Changeux devised the MWC model to describe the cooperative binding of oxygen to hemoglobin (Monod et al., 1965). This model has been widely used in modeling the cooperativity of ligand-gated ion channels. But here, we will discuss the allosteric activation model for BK developed by Horrigan and Aldrich (Horrigan and Aldrich, 2002), which is based on the MWC model (**Fig. 4A**).

**Horrigan-Aldrich (HA) Model**

To study the intracellular calcium and membrane potential effects on the gating of large-

conductance $Ca^{2+}$-activated $K^+$ (BK, Slo1) channel, Horrigan and Aldrich inspected the steady-state and kinetic properties of BK's ionic and gating currents over a wide range of membrane potentials and calcium concentrations (Horrigan and Aldrich, 2002). Through this study, they found that without calcium, gating charges' movements shift to more depolarized voltages, while at very negative membrane potentials (-80 mV), calcium could still activate the channel. These results suggest that calcium sensors and voltage sensors in the BK channel act independently to activate the channel. With this dual-allosteric mechanism, Horrigan and Aldrich built a model (Horrigan and Aldrich, 2002) shown in **Fig. 4B**.

In the HA model, there are three modules, namely, pore, voltage sensor, and calcium sensor. The intrinsic close-open equilibrium of the pore is defined by L, transition of voltage sensor between active and rest states is defined by J(V), and equilibrium of occupied versus apo calcium sensor is defined by binding affinity K. Activation of voltage sensor and calcium sensor additively promotes the closed to open transition in pore, which are defined by D and C. While a slight interaction between the voltage sensor and calcium sensor is defined by E, independent of the closed or open of the channel. This model fits the experimental data in most circumstances and has been widely used to study the gating mechanism of BK.

**$\chi$-value analysis of the coupling energy**

As discussed above, allosteric interaction is widely distributed in ion channels, but it is not trivial to study the coupling energy between a specific structural domain with the pore. To solve this problem, Chowdhury and Chanda demonstrated that the $\chi$-value analysis can be used to directly extract the interaction energy of a particular site with the pore based on open probabilities at limiting conditions (Chowdhury and Chanda, 2010, 2012).

In their study, Chowdhury and Chanda used the voltage-gated system as an example. Since at very negative membrane potentials, all the voltage sensors prefer resting state, while at

saturation depolarized potentials, all the voltage sensors are in the activated state (Chowdhury and Chanda, 2012). With a Hill transformation, the equilibrium $x = \ln(P_O/P_C)$ varies linearly in response to driving force at extreme conditions. And the slope of these linear lines represents the intrinsic voltage dependence of the pore, as the stimulus is the voltage. From this analysis, they showed that the difference between the $\ln(P_O/P_C)$ values at the two extremes correspond to the coupling energy of the stimuli sensor (voltage sensor) to the pore (Chowdhury and Chanda, 2010, 2012). This method greatly simplifies the analysis of complicated allosteric systems as long as we are able to measure activities at extreme potentials accurately.

**Figures**

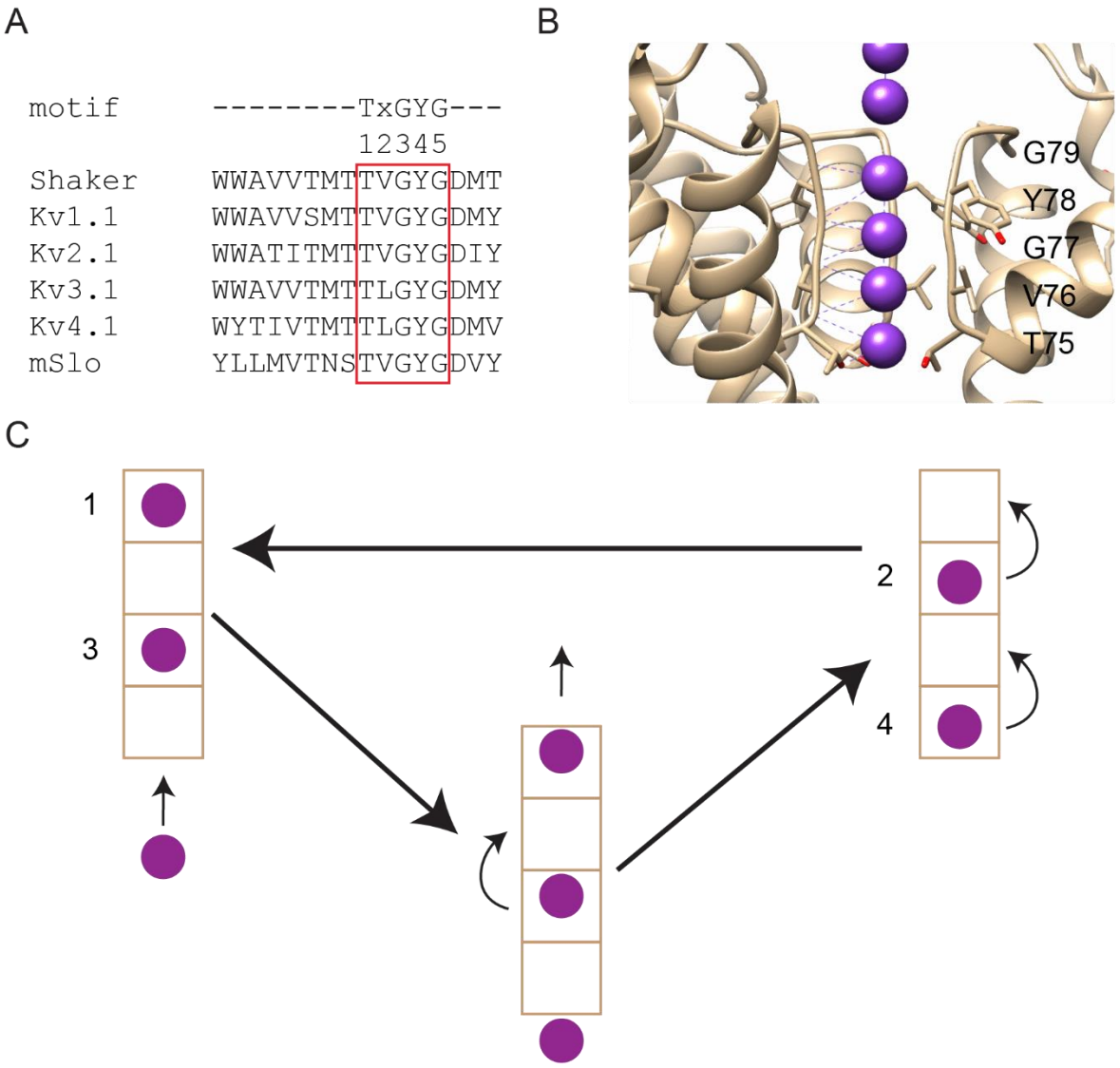


**Figure 1 | Selective filter of potassium ion channels**

**A.** Sequence alignment of the pore region of selected potassium channel [adapted from **Fig. 1** (Heginbotham et al., 1994)]. The sequence motif was highlighted in the red box. **B.** The enlarged structure of the selective filter in KcsA (PDB:1K4C). $K^+$ is marked as a purple ball and the side chain of contiguous sequence TVGYG is shown. The front subunit is removed for clarity. Four potassium binding sites were shown, and all occupied with potassium ions. However, the structure is solved based on the average density of all the unit cells, and it is believed that only two

potassium can co-exist in the selective filter. **C.** A simplified cartoon of the 'Knock-on' model for the potassium channel. The four binding sites shown in **B** are represented as rectangle boxes here. Two potassium ions occupy either 1,3 sites or 2,4 sites in the selective filter. Same color code is used as **B**. The incoming ion to site 4 will push the $K^+$ in site 1 out, which results in the outward current. Figure adapted from **Figure 2.5** of *Handbook of Ion Channels* (Zheng and Trudeau, 2015).

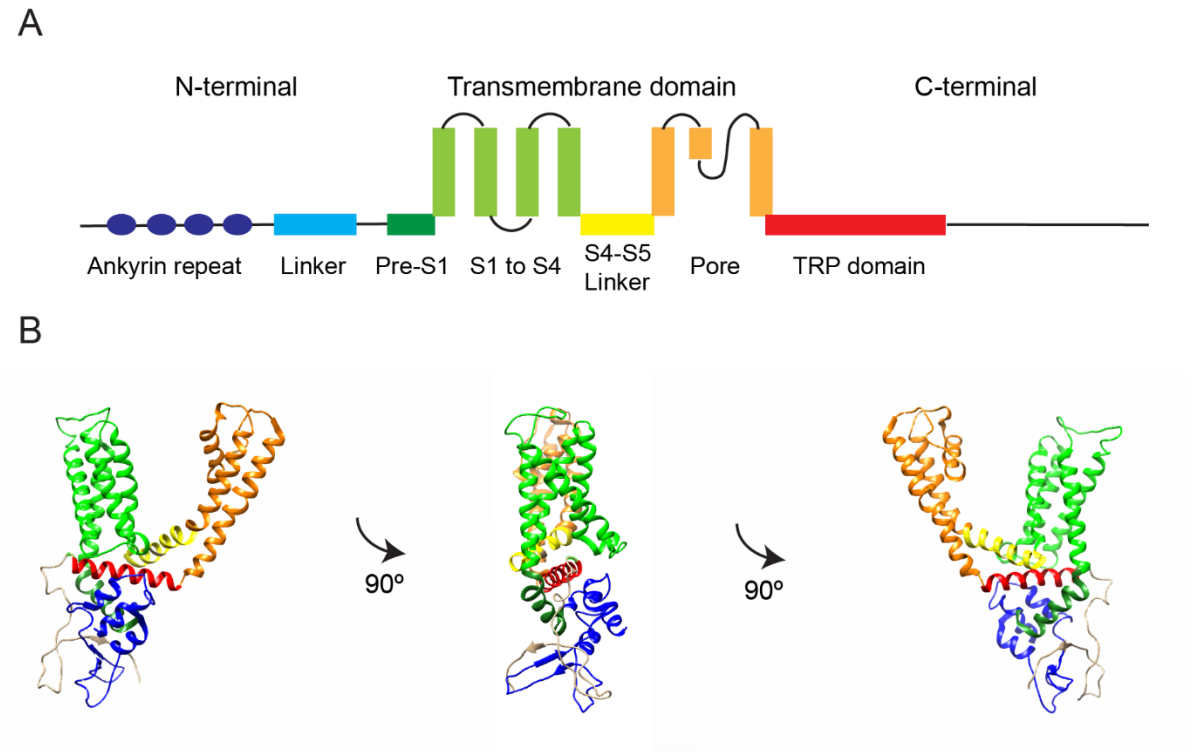


**Figure 2 | Structural representation of TRPV1 monomer**

**A.** Liner diagram of a TRPV1 monomer. All the important structural domains are indicated and color-coded. The color code is based on light wavelength from N-terminal to C-terminal. This figure is replotted based on **Figure 3A** (Liao et al., 2013). **B.** The structure of the TRPV1 monomer, isolated from TRPV1 channel in a lipid environment (PDB:5IRZ). The color code is the same as in **A** to represent these important structural elements better.

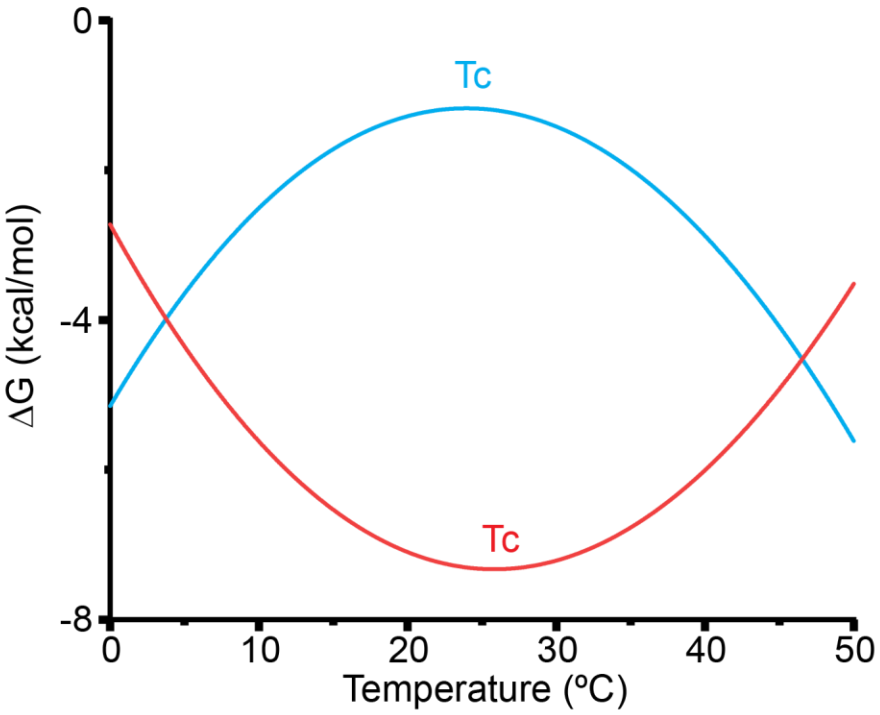


**Figure 3 | Gibb's free energy change (ΔG) versus temperature relation based on heat capacity change theory.**

The relationship of ΔG versus temperature was simulated based on the equation: $\Delta G(T) = \Delta H_0 + \Delta Cp(T - T_0) - T\Delta S_0 - T\Delta Cp \cdot \ln(T/T_0)$. As shown in the graph, ΔG is a curve and $\frac{d\,\Delta G}{dT}$ change its polarity at Tc. For the blue curve, $\Delta H_0$ = 35 kcal/mol, $\Delta S_0$ = 120 cal/mol·K$^{-1}$, $\Delta C_P$ = 4 kcal/mol, $T_0$ = 306 K. As for the red line, $\Delta H_0$ = 28 kcal/mol, $\Delta S_0$ = 120 cal/mol·K$^{-1}$, $\Delta C_P$ = -4 kcal/mol, $T_0$ = 290 K. This figure is replotted based on **Figure 1B** (Chowdhury et al., 2014).

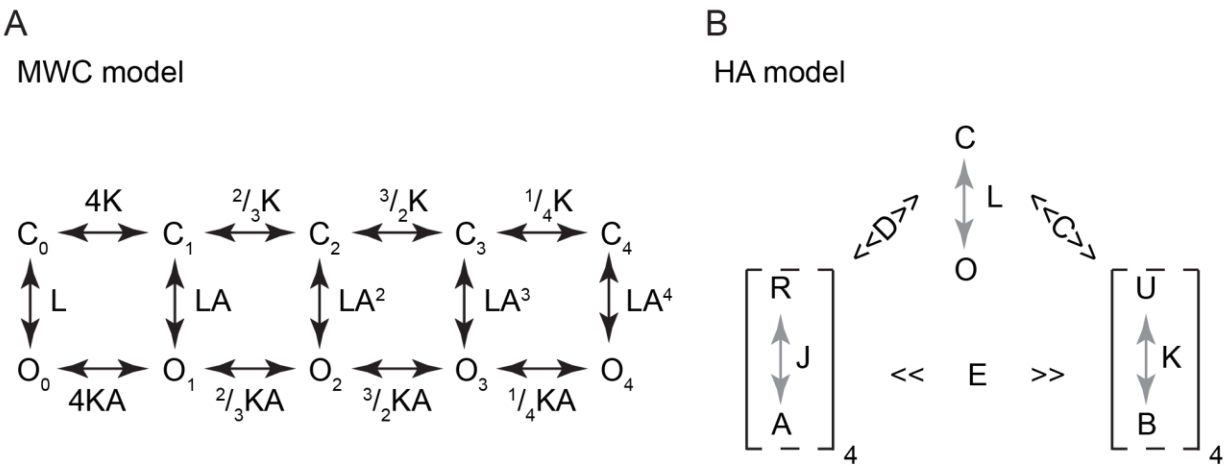


**Figure 4 | Examples of classic allosteric models**

This figure is adapted from **Figure 7.5** of Handbook of Ion Channels (Zheng and Trudeau, 2015) with minor modifications. **A.** Monod-Wyman-Changeux (MWC) allosteric model. This model is based on a tetrameric ion channel with five open (O) and five closed (C) states with four identical ligand binding sites. The intrinsic equilibrium of open-close is defined by L. K is the binding affinity of the ligand, while A is the allosteric factor. With A > 1, it means the ligand binding has a positive effect on pore opening. **B.** Horrigan-Aldrich (HA) model for $Ca^{2+}$-activated large-conductance $K^+$ (BK) channel. In this model, the pore is either in closed (C) or open (O) state, four voltage sensor is in rest (R) or activate (state) with a voltage-dependent equilibrium J, and four $Ca^{2+}$ sensors in either unbound (U) or bound (B) state with affinity constant K. The interaction between these three modules is defined by C, D, E.

**Table one. $Q_{10}$ of representative thermoTRP channels**

| Channel | $Q_{10}$ |
|---|---|
| TRPV1 | 20.6 (Welch et al., 2000), 25.6 (Vlachová et al., 2003), 27 (Liu et al., 2003a) |
| TRPV2 | >100 (Leffler et al., 2007) |
| TRPV3 | 6.6 (Peier et al., 2002), 23.3 (Xu et al., 2002) |
| TRPV4 | 10 (Güler et al., 2002), 19 (Watanabe et al., 2002) |
| TRPM8 | 24 (Brauchi et al., 2004), 40 (Zakharian et al., 2010) |
| TRPA1 | 8.8 (Gracheva et al., 2010),13.7 (rattlesnake) (Gracheva et al., 2010), 129 (Drasophila) (Kang et al., 2011) |
| TRPC5 | 10 (Zimmermann et al., 2011) |

This table is adapted from **Chapter Two** of the book *Thermal Sensors* (Islas and Qin, 2014).

# CHAPTER TWO

## *Experimental Procedures*

### Materials

The wild-type MthK gene in pQE82L plasmid was a generous gift from Dr. Brad Rothberg (Temple University). All the primers were synthesized by Integrated DNA Technologies (Coralville, Iowa). The PFU-Ultra DNA polymerase was from Agilent Technologies (Santa Clara, California), and Taq DNA polymerase was from New England Biolabs (Ipswich, Massachusetts). All the DNA loading dye, DNA ladder, restriction enzymes, and dNTP were purchased from New England Biolabs (Ipswich, Massachusetts). Genemorph II random mutagenesis kit was purchased from Agilent Technologies (Santa Clara, California). BigDye and BigDye buffer were purchased from the Biotechnology Center at University of Wisconsin-Madison. For *E. coli* cell lines, $K^+$ uptake deficient strain *LB2003* was a generous gift from Dr. Inga Hanelt (Goethe-University, Frankfurt), XL1-Blue were obtained from Agilent Technologies (Santa Clara, California), BL21 (DE3) and OverExpress C43 cells were purchased from Lucigen. Ready-Lyse Lysozyme solutions and OmniCleave Endonuclease for spheroplast making were purchased from Illumina (San Diego, California). Antibiotics were obtained from Gold Biotechnology. Reagents for home-made SDS-PAGE, protein ladders and precast SDS-PAGE were purchased from Bio-Rad (Hercules, California). All the detergents and lipids were purchased from either Anatrace (Maumee, Ohio) or Avanti Polar Lipids (Alabaster, Alabama). Thrombin protease (Bovine) was obtained from GE Healthcare Life Sciences. All other chemicals were purchased from Research Products International, Fisher Scientific, or Sigma-Aldrich.

### Chemical *E. coli* Competent Cell Preparation

This protocol is modified from a previous version organized by a former lab member, Dr. Vadim A. Klenchin. The competent cells of LB2003 and XL 1-Blue were created with this protocol.

250 ml of super optimal broth (SOB) media was inoculated with one aliquot of the competent cell and grew at 18 ºC to $OD_{600}$ around 0.5-0.6. (All sodium chloride is replaced by potassium chloride for LB2003 strain). Then the cells were spun down at 3,000 rpm, 4 ºC for 15 mins in 50 ml Falcon tubes, and the supernatant was carefully removed. After cell collection, all the procedures were done in a cold room with refrigerated buffers. 3.5 ml of "CCMB80 buffer" (10 mM K-Acetate, 80 mM $CaCl_2$, 20 mM $MnCl_2$, 10 mM MgCl2, 10% (v/v) glycerol, pH 6.4, sterilized by filtration) were added into each tube and resuspend the cell pellets by tapping. Add 20 ml of CCMB80 buffer into each tube and spin down the cells again at 3,000 rpm, 4 ºC for 15 mins. Repeat the previous resuspension, and aliquot 50 µl per sterile 1.5 ml Eppendorf tubes.

Based on previous tests, the key points are probably water quality and glassware cleanliness. MilliQ water from the Milli-Q Synthesis A10 (Millipore) is used in our lab. However, occasionally if the MilliQ water is contaminated, the alternative is using UHPLC-grade water. As for glassware, detergent-free is required. To achieve this, we first clean the glassware thoroughly with MilliQ water and then fill it with MilliQ water and autoclave it at 120 ºC for 30 minutes with alumina foil cover. Afterward, pour the water out before it fully cools down, and rinse the glassware additionally with MilliQ water. Drain it on a clean surface.

**Transformation**

Thaw an aliquot of frozen competent cells on ice and add 1 ul of a sterile solution of neutralized 1M TCEP with 0.1 mg of target plasmid. Mix by gentle tapping and incubate on ice for 30 mins. Then heat shock for 35 sec in a water bath at 42 °C, and quickly place the tube on ice for 2 mins. Add 0.5 ml of sterile SOB media and transfer to a 15 ml culture tube. The transformed cells were recovered in the incubator at 37 °C for 1 hour, spread on LB agar plates with the corresponding antibiotic.

**Cloning, expression, and purification of MthK in *E. coli***

The MthK $K^+$ channel gene from *M. thermoautotrophicum* was cloned into expression vector pQE82L as described previously (Parfenova et al., 2006). N-terminal (2-17 amino acid position) was deleted in MthK IR construct. MthK ΔC was generated by introducing a stop codon after H117 position in the MthK IR background. The constructs were expressed in *E. coli* XL1-Blue cell cultures and induced overnight at 24°C with 1 mM isopropyl-β-D-thiogalactopyranoside (IPTG). Protein was purified according to the protocol described by Jiang *et al* (Jiang et al., 2002) with minor modifications. Cell pellets were broken by sonication and solubilized with 40 mM n-decyl-β-D-maltopyranoside (DM) (Anatrace) in lysis buffer (20 mM Tris, pH 8.0, 100 mM KCl and 20 mM imidazole). Insoluble fraction was pelleted by high speed centrifugation at 20,500 rpm (50,228g) for 40 min in SS-34 Rotor (Sorvall). The supernatant was loaded on either Talon $Co^{2+}$ affinity (Clontech) or Ni-NTA Agarose (Qiagen) columns. Nonspecific binding proteins were washed with lysis buffer containing 5 mM DM. To elute MthK, the imidazole concentration was increased to 250 mM. His tag was removed by Thrombin (GE) digestion (10 NIH units per 5 mgs of protein) for 2 hours at room temperature. The digested protein was concentrated and injected into Superdex-200 (10/300 GL) size exclusion column (GE) with 25 mM Hepes, pH 7.6, 100 mM KCl and 5 mM DM.

MthK pore only domain was purified as described previously (Li et al., 2007; Posson et al., 2013). Briefly, following gel filtration, the purified MthK IR was collected and incubated with 1:50 (w/w) Trypsin type I (Sigma, T8003) for 2 hours. The reaction was stopped by adding two-fold excess Trypsin inhibitor type II-O (Sigma, T9253) and the cleaved protein was purified on a Superdex-200 (10/300 GL) size exclusion column (GE) using buffer containing 25 mM Hepes, 100 mM KCl, 1 mM (n-Dodecyl β-D-maltoside) DDM, 5 mM DM pH 7.6 in 4°C.

**Complementation assay**

For complementation assay, LB2003 competent cells (Parfenova et al., 2006) were transformed and plated in Luria broth (LB) plates containing 100 mM KCl. pQE32 (Qiagen)

plasmid was used as a negative control. After O/N incubation at 37 °C, the colonies from each of the plates were pooled and after serial dilution, they were plated in low potassium (4 mM KCl) plates containing IPTG. Without IPTG plates were used as control. To normalize for differences in growth rate, all the plates were grown until MthK FL colonies were observed at the lowest dilution and then imaged (ChemiDoc MP imaging system, BIO-RAD).

**High throughput screen of MthK mutants**

The temperature-sensitive clones generated from error-prone PCR were stored at -80 °C. These clones were streaked onto high potassium agar plates without IPTG and left overnight to grow at 37 °C. The following day a single colony was picked and allowed to grow in High $K^+$ liquid medium (10 g Tryptone, 5 g Yeast extract, 10 g KCl in 1L MilliQ water) overnight. After overnight growth of bacterial culture in high $K^+$ medium without IPTG, the optical density was measured on Nanodrop. The optical density (OD) values at 600 nm of various clones were adjusted to 0.5, and four serial dilutions were made. 4ul of the resulting bacterial cell suspension was seeded on to agar plates containing high $K^+$ (described above) and low $K^+$ (10 g Tryptone, 5 g Yeast extract, 10 g NaCl, 400 ul of 2.5M KCl, add MilliQ water to 1L) agar plates. The bacteria were grown in the presence of 1 mM IPTG whenever the channel expression was desired. To monitor complementation at various temperatures, the resulting bacterial plates were grown at two different temperatures 20 °C and 37 °C.

**Giant *E. coli* spheroplasts**

This protocol is optimized from previous protocols (Martinac et al., 2013; Sun et al., 2014). *E. coli* OverExpress C43 (DE3) competent cells (Lucigen) transformed with MthK IR were grown to an optical density of 0.7 for making giant spheroplasts. 6 ml of this liquid culture was combined with 55 ml LB containing antibiotic and 50 μg/ml cephalexin at 42 °C. After 2 hours of incubation, 1 mM IPTG was added to this culture and incubated for another hour at 37 °C. Following induction,

the cells were harvested by low speed centrifugation, the pellet was gently resuspended in 3 ml of 1 M sucrose. The resuspended cells were incubated with 240 μl Tris, pH 8.0, 67500 units of Ready-Lyse Lysozyme solutions (Illumina), 1600 units OmniCleave Endonuclease (Illumina) and 20 μl of 500 mM EDTA. After incubation at room temperature for approximately 10 minutes, the digestion was stopped by adding 1 ml of stop buffer (0.8 M sucrose, 80 mM Tris, pH 8.0, 12 mM $MgCl_2$). The cells were aliquoted into PCR tubes, flash frozen in liquid nitrogen and stored in -80 °C freezer.

**Reconstitution of the purified protein in liposome**

This protocol is based on methods used to reconstitute KcsA in soybean polar lipids (Chakrapani et al., 2007). 25 mg/ml lipids (Avanti) in chloroform were dried under argon and kept overnight in a vacuum. The dried lipids were resuspended using bath sonication in 250 mM KCl, 30 mM Hepes, pH 7.6 and 0.1 mM $CaCl_2$ to a final concentration of 15 mg/ml. 5 mM DM was added to the suspension so that the protein: lipid molar ratio was 1:500 to 1:1000 for single-channel recording studies. Detergents were removed by O/N dialysis using either 25 KD cutoff Slide-A-Lyzer Dialysis cassette for MthK IR or 7 KD cutoff Slide-A-Lyzer Dialysis cassette for MthK pore. The dialysis buffer was refreshed the next day and, after 4 hours, the proteoliposomes were aliquoted and stored at -80 °C.

**Electrophysiology**

For patch clamping spheroplasts, the bath solution was 150 mM KCl, 20 mM $MgCl_2$, 15 mM Tris, pH 8.0, and sucrose was used to make up for differences in osmolarity. MthK currents were blocked using 0.3 mM $BaCl_2$. The recording pipette was filled with 150 mM KCl, 20 mM $MgCl_2$, 15 mM Tris, pH 8.0, 0.1 mM $CaCl_2$ and 450 mM sucrose. All the microelectrodes (Drummond) for electrophysiological measurements had a resistance of around 3.5 MΩ, and a tip

size ~ 5.0-5.5 bubble number (Mittman et al., 1987). Digidata 1440A interface (Axon instrument) was used to collect the data with a 250 kHz sampling rate and low-pass filtered at 5 kHz. Currents were elicited from a holding potential of -10 mV by a 300 ms pulse ranging from -100 mV to +100 mV stepping at 20 mV intervals.

Single-channel recordings were obtained by inside-out patch-clamping of reconstituted proteoliposomes. 30 μl of proteoliposomes were placed on a clean glass slide and dried in a desiccator under vacuum at 4 °C. The sample was then rehydrated with 50 μl buffer (250 mM KCl, 30 mM Hepes, pH 7.6, and 0.1 mM $CaCl_2$) for more than 2 hours, which yielded giant multilamellar vesicles (GMV). The pipette solution contained 200 mM KCl, 1 mM NaCl, 30 mM Hepes, pH 7.6, 0.1 mM $CaCl_2$ and 30 mM sucrose and bath contained 150 mM KCl, 50 mM NaCl, 30 mM Hepes, pH 7.6. The calcium concentration was varied from 0.1 to 10 mM in the bath, and the osmolarity was adjusted with sucrose. For MthK pore, symmetrical buffers containing 200 mM KCl, 30 mM Hepes, 1 mM $CaCl_2$, 27 mM sucrose, pH 7.6 were used. For temperature control, SC-20 dual in-line heater/cooler (Warner Instrument) was used with a single channel bipolar temperature controller CL-100 (Warner Instrument). Recording temperatures were monitored with a bead thermistor (TA-29; Warner Instrument) within 5 mm of the microelectrode tip.

**Data Analysis**

For macroscopic recordings, currents were normalized to the maximum currents at 42 °C in presence of $Ca^{2+}$. Since MthK channels exhibit voltage-dependent rectification at positive potentials (Li et al., 2007), steady-state currents at -100 mV were used for the analysis of macroscopic conductance changes. Single channel data was digitally low pass filtered at 1.4 kHz and analyzed using Clampfit 9.0 (Axon Instrument). The integrated Single-channel Search module was used to detect any open and close event that is longer than 0.05 ms, and the $nP_O$ was determined. $nP_O$ is defined as

$$nP_O = \sum_1^n iP_i,$$

where $n$ is the number of channels present in a patch, $i$ indicates the number of the open channel and $P_i$ is the probability of the corresponding level. For high $Ca^{2+}$ and high-temperature conditions, it is straightforward to determine the total number of channels in a particular patch because MthK is fully activated by $Ca^{2+}$. However, for low $Ca^{2+}$ concentrations or at low temperatures, the open probability is too low to determine the total number of channels in a patch. Therefore, for every condition, we decided the total number of channels in a patch by going to high temperatures and high $Ca^{2+}$. We cannot use this method for MthK Pore only construct because they are insensitive to $Ca^{2+}$. In this case, we did not calculate the absolute Po but only relative changes in Po.

The temperature coefficient ($Q_{10}$) was calculated using the following equation (Islas and Qin, 2014):

$$Q_{10} = \left(\frac{A_2}{A_1}\right)^{\frac{10}{T_2 - T_1}},$$

where $A_2$ and $A_1$ are either subtracted currents (macroscopic current recordings from giant *E. coli* spheroplast) or $P_O$ estimated from single-channel recordings at temperature $T_2$ and $T_1$ (in Kelvin).

For coupling energy analysis, the open probability ($P_O$) was fitted to the Hill plot using the following equation using Origin 2018b:

$$y = start + (end - start) * \frac{x^n}{K^n + x^n},$$

where the start is the value at low $Ca^{2+}$, the end is the plateau value at high $Ca^{2+}$, K is equal to $K_d$ of the $Ca^{2+}$ binding, and n is the Hill coefficient. With these constants, we can fit $\ln [Po/(1\text{-}Po)]$ with the temperature.

**Negative stain screening**

Dr. Yaxian Zhao organizes this protocol. Applying 3 µl of purified MthK IR in digitonin (0.2–0.9 mg/ml) onto glow-discharged electron microscopy (EM) grids covered by a thin layer of the continuous carbon film. Afterward, the grids were stained with 2% (w/v) uranyl acetate. Negatively

stained EM grids were imaged on a Tecnai microscope (FEI Company) operated at 120 kV. Images were recorded at a nominal magnification of 67k and a defocus set to 2.5 µm.

**Electron Microscope sample preparation and imaging**

Our collaborator, Dr. Yaxian Zhao, helped to wrap up this protocol. 3.5 µl of the purified MthK IR (~2 mg/ml) in the presence of 5 mM EGTA and 5 mM HEDTA was pipetted onto a glow-discharged 200 mesh Quantifoil 1.2/1.3 grids (Quantifoil Micro Tools). After 12s blotting at 100% humidity at room temperature and plunge frozen in liquid nitrogen-cooled liquid ethane using Vitrobot (FEI), grids were imaged using Titan Krios Cryo-electron microscope at an acceleration voltage of 300 keV. Images were recorded in an automated fashion on a Gatan K2 Summit (Gatan) direct detector. 40-frame movies were collected in super-resolution mode, resulting in a pixel size of 0.55 Å at the sample level and a dose rate of ~8 $e^-$/pixel/s in the detector. Total exposure time for each movie was 10 s, with one frame collected every 0.2 s. Images were collected 1.5–2.5 µm under focus with imaging software Leginon.

**Cryo-EM images processing**

This protocol is achieved from Dr. Vera Moiseenkova-Bell's lab following a protocol from their TRPV2 structure paper (Pumroy et al., 2019). All movies were motion-corrected with the MotionCor2 algorithm implemented in RELION 3.1. Contrast transfer function (CTF) estimation was performed in CTFFIND4.1 on non-dose-weighted micrographs, while subsequent data processing was done on dose-weighted micrographs.

Approximately 26,000 particles were picked using LoG-autopicking to generate 2D class templates, which were subsequently used to automatically pick ~2,700,000 particles. The autopicked particles were subjected to 3 rounds of 2D classification to remove false positives and suboptimal particles. The best 2D classes (~304,000) particles were then subjected to 3 rounds of 3D classification with C1 symmetry, using the published MthK structure (PDB 1LNQ) as an

initial model. After the final round of 3D classification, only one class (~38,000 particles) shows features of the linker region. Thus, this class was selected for 3D refinement with C4 symmetry. The resulting 3D refined map shows a poorly resolved transmembrane domains comparing to RCK domains, presumably due to the heterogenicity of the particles. Therefore, additional rounds of 3D classification without angular sampling was conducted by masking the transmembrane domains and the linker region of the channel. The best 3D class, containing 15,000 particles, was used in the final 3D refinement and post-processing to yield a map at an overall resolution of 4.8 Å based on the 0.143 cutoff criterion.

**Nanodisc reconstitution**

This protocol is following Kenton's protocol for voltage-gated potassium channel with minor modifications (Matthies et al., 2018). MSP1E3D1 was purchased from Sigma, and before reconstitution, it is dialyzed against 25 mM Hepes pH 7.6, and 150 mM KCl in 7KD cut-off dialysis bag. *E. coli* lipids solubilized in chloroform (Avanti) were dried under the stream of Argon and placed under a desiccator overnight in vacuum to remove residual chloroform completely. Dry lipids were resuspended in water thoroughly at a concentration of 20 mg/ml, and formed vesicles were sonicated until the solution became translucent. DM was added to a concentration of 26 mg/ml and divided into smaller aliquots, which were kept frozen at −80°C until further use. To begin nanodisc assembly, purified MthK IR in 1mM DDM and 5mM DM was mixed with the solubilized lipids and MSP in the molar ratio indicated at room temperature for 30 min. The protein concentrations were calculated by measuring the absorbance at 280 nm using molar extinction coefficients of 28,950 $M^{-1}cm^{-1}$ and 28,590 $M^{-1}cm^{-1}$ (calculated from ATT Bioquest) for the MthK IR and MSP1E3D1, respectively. The solution was then transferred to a tube containing Biobeads (30 fold of detergent weight) that were previously washed with methanol and equilibrated in 25 mM Hepes pH 7.6 and 150 mM KCl buffer to initiate nanodisc assembly and mixed at room temperature for 2 to 3 hours. Biobeads were separated by high-speed centrifuge, and the

supernatant was injected into Superose 6 5/150 GL column using a buffer with 25 mM Hepes, pH 7.6, 100 mM KCl, 5 mM HEDTA, 5mM EGTA. The fluorescence detector (Shimadzu Corporation) is set as excitation at 295 nm and emission at 335 nm.

# CHAPTER THREE

## *MthK expressed in E. coli is temperature-sensitive*

### Introduction

The ability to sense temperature is essential for the survival of all forms of life. In mammals and higher eukaryotes, the thermal stimulus is detected by specialized ion channels found in peripheral nerves (Islas and Qin, 2014). Much less is known about temperature-sensing in prokaryotes, many of which thrive at temperatures above 100 °C (in deep-sea under high pressure) or as low as around 0 °C (Deming, 2002; Stetter, 2006).

**Fig. 1A** shows a photo of the Grand Prismatic Spring in Yellowstone National Park I took in the summer of 2018. The rainbow-like colors radiating from its center make this place one of the most popular tourist destinations in North America. As illustrated in **Fig. 1B**, this eyecatching image originates from the temperature sensitivity of varied microbes. The rings of different colors are actually rings of different bacteria and archaea that have adapted to different conditions, mainly temperature and acidity (pH) (Nugent et al., 2015). In the center, the highest temperature can reach more than 90 °C, where few organisms can survive. The dark blue appearance in this area is primarily a result of the light scattering, as is the case for sky and ocean. The yellow band is mainly due to two photosynthetic pigments, chlorophyll (green) and carotenoid (orange) in cyanobacteria *Synechococcu*s, which lives at a temperature of around 74 °C (Nugent et al., 2015). Chlorophyll can transfer the energy from light to chemical energy, while carotenoid protects the microbe from the radiation damage caused by short-wavelength light. Outside the yellow band, temperature decreases to a comfortable zone to support more organisms. The mixture of these organisms gives the orange to red color of the outer concentric rings. Besides their scenic views, these thermophiles in the hot spring also provide the opportunity for studying thermal stability and temperature sensing.

MthK is an archaebacterial calcium-activated potassium channel from *Methanobacterium thermoautotrophicum*, a thermophile that was discovered in the hot springs of Yellowstone National park (Jiang et al., 2002). Previously, Rothberg and his colleagues recorded the activity of MthK in the bilayer with heated buffer and observed robust activity at a low $Ca^{2+}$ condition (Parfenova et al., 2006). However, how temperature-sensitive MthK is and the molecular mechanism of temperature activation were not illustrated in their study. Here, we assayed the temperature-dependent activity of MthK based on the recovery of a $K^+$ uptake deficient strain, LB2003, on low $K^+$ plates (i.e., Luria Broth). Furthermore, by patch clamping giant *E. coli* spheroplast, we showed that the activity of MthK expressed in *E. coli* membrane is regulated by temperature.

## Results

### Complementation assay shows the temperature-dependent activity of MthK

To probe the temperature sensitivity of MthK in bacteria, we utilized a complementation assay based on *E. coli* LB2003 strain, a potassium-uptake deficient bacteria which does not survive in a typical low potassium medium such as Luria broth (LB) (Hänelt et al., 2010; Parfenova et al., 2006; Smith et al., 2013). Rothberg and his colleagues have previously shown that functional MthK can rescue LB2003 strain (Parfenova et al., 2006) and that the open probability of MthK is directly correlated with its survival (Hänelt et al., 2010; Parfenova et al., 2006), analogous to studies on KcsA potassium channel (Cuello et al., 2010b). This assay can potentially allow us to test the temperature sensitivity of MthK rapidly. We hypothesize that if the temperature can activate MthK, then it should increase complementation at elevated incubation temperatures compared to low temperatures.

To test the effect of temperature on activation of MthK, we set up complementation assays at various temperatures for the full-length (FL) MthK channel. As shown in **Fig. 2A**, compared to the uninduced controls, the cells expressing the MthK FL channels are able to rescue 100,000-

fold more efficiently at 36 °C compared to 18 °C. To determine whether this increased survival is mainly due to growth complementation, we compared the plates grown in the presence and absence of IPTG since the MthK constructs are all under the control of lac Y inducible promoter. Serial dilution was used in this assay to get a more quantitative readout, summarized in **Fig. 2D**. The comparison between induced and uninduced controls is necessary at each temperature because the bacterial growth rate is much slower at lower temperatures. We corrected for bias in the growth rate by letting the MthK FL expressed bacteria grow to the same level at varying temperatures.

In addition to the full-length channel, we tested the inactivation-removed (IR) version of the MthK channel and the pore only domain construct which lacks the C-terminal of the RCK domain, shown in **Fig. 2C**. The presence of inactivation obfuscates channel opening and thereby complicates the interpretation of the equilibrium gating properties (Hoshi et al., 1994). In order to focus on the temperature-dependence of activation, we generated an N-terminal deletion construct, which was previously shown to eliminate fast inactivation (Kuo et al., 2008). Note that MthK channels reconstituted in planer bilayer do not exhibit any measurable inactivation, but macroscopic recordings in bacterial spheroplasts show an apparent inactivation phenotype (Kuo et al., 2008). This contradicts observation of single-channel recordings from patch clamping, and bilayer setup may result from the variation of membrane thickness (Personal discussion with Dr. Crina Nimigean). The organic solvent used in the bilayer setup will increase the thickness of the lipid bilayer, compared to the patch of proteoliposomes. Finally, to test the role of the cytoplasmic RCK domain, we also created a C-terminal deletion construct that lacks the entire RCK domain by deleting the sequence after Histidine 117, as shown in **Fig. 2E**.

Serial dilution and plating of the various MthK constructs show that the survival of the LB2003 strain (empty vector) is much higher at low temperatures compared to high temperatures (**Fig. 2B**). This, in part, may reflect the more extended incubation periods for low-temperature conditions. Cells expressing MthK IR exhibit similar complementation patterns, whereas the MthK

ΔC construct shows reduced complementation compared to the other two constructs. The differences in growth complementation are quantified and plotted in **Fig. 2D**. These findings indicate that both MthK FL and MthK IR are much more efficient in rescuing cell growth at higher temperatures and that the cytosolic C-terminal domain is required for robust complementation. We focused our efforts on the inactivation removed construct in the following studies because the presence of inactivation obfuscates the interpretation of the equilibrium gating properties. This complementation assay also brings an opportunity for fast and high-throughput screening of the temperature-sensitive mutants in MthK, which will be further discussed in **Chapter Six**.

**Inside-out patch clamping of giant *E. coli* spheroplasts shows temperature-dependent activation of MthK IR**

As MthK shows temperature sensitivity in the complementation assay with LB2003 cells, we want to further examine the function of MthK channels in *E. coli* membrane and measure macroscopic current responses. Most ion channels were located in the inner membrane of Gram-negative bacteria, *E. coli*. To study MthK, we removed the outer membrane and generated giant *E. coli* spheroplast using a method described previously (Kikuchi et al., 2015; Kuo et al., 2008; Martinac et al., 2013), which is explained in detail in the method section. The main modification in our protocol is that we used the C43 cell lines. C43 is a new version of the C41 *E. coli* strain, and it shows better toxic resistance to protein overexpression (Dumon-Seignovert et al., 2004). As previously demonstrated in KcsA channels, although the growth of bacteria requires $K^+$, overexpression of a potassium channel in regular strains could still be toxic to cells (Tilegenova et al., 2016). In our experience, C43 strain tolerates the expression of potassium ion channel and cephalexin treatment better than other strains, i.e., XL 1-blue.

As the *E. coli* spheroplasts lack the outer membrane and cell skeleton, it is not trivial to patch these cells using standard patch-clamp techniques. In order to obtain reproducible seals, we have to use fairly tiny pipette tips with 0.5-micron diameters. To measure the size of the tips,

we used a ‘bubble number’ method (Mittman et al., 1987). With the tip submerged in methanol, we can increase the pressure in the glass pipette and measure the bubble-start-forming pressure. This pressure, also called ‘bubble pressure’, is directly related to the diameter of the pipette. In this way, we could measure the diameter of the tips without damaging them.

With the help from Professor Sergei Sukharev, we learned how to patch these giant *E. coli* spheroplasts. Inside-out patch-clamping recordings of *E. coli* spheroplast membranes from bacteria expressing MthK IR show that the macroscopic currents increase with increasing temperature (**Fig. 3**). These recordings were obtained in the presence of 1.5 mM $Ca^{2+}$, which is around the $EC_{50}$ at this pH (Pau et al., 2010) (**Fig. 3A**). As shown in the figure, the activation at high temperature (42 °C) mimics an MthK current activated by calcium with the inward rectification. This rectification is believed to be transiently blocking by the calcium from the inside of the channel (Li et al., 2007). Even with the removal of the first 17 amino acids, there is still a slight inactivation of the channel, as seen by the time-dependent decay in current amplitude. We also tested the patches with a saturating concentration of calcium and observed activation currents as expected, shown in **Fig. 3B**. This calcium response illustrates that the currents we observed are from MthK IR channels. With saturating calcium concentrations, slight increases in the currents were still observed at elevated temperatures. However, these increases could result from a higher leaking current, or from single-channel conductance changes with temperature without changing the open probability.

From this set of experiments, we can see that MthK seems to be more temperature-sensitive at a $Ca^{2+}$ concentration around the $EC_{50}$. Combined with the complementation assay, this result suggests that the RCK domain plays a vital role in temperature activation. However, as these recordings are contaminated with the leaking currents, channel blockers must be used to observe the actual change of MthK currents with temperature.

**Tetraethylammonium (TEA) and barium blocking of MthK are temperature-dependent**

To obtain a better estimate of temperature effects on MthK currents, we need to measure the leak currents at different temperatures to estimate their impact on the currents of interest. As temperature could affect the ion activity, which will give a $Q_{10}$ ~2 for the conductance (Hille, 1992; Islas and Qin, 2014), we think that the leak currents will show a similar increase. To test this, we used general potassium channel blockers to estimate the leak currents, such as tetraethylammonium (TEA) chloride (Lenaeus et al., 2005; Posson et al., 2013) and barium (Guo et al., 2014; Jiang and MacKinnon, 2000).

Barium, as a permeable blocker, will mimic $K^+$ and stick into the selective filter (**Fig. 4A**). Based on the study of Guo et al., barium mainly occupies site 2 in the selective filter, but in the presence of potassium, barium could reach even deeper into sites 3 and 4, which has a better blocking effect (Guo et al., 2014). Besides being a pore blocker, barium could also activate MthK through the RCK domain. $EC_{50}$ for barium is 54.8 mM at pH 7.7 (Smith et al., 2012); therefore, at the experimental concentration (0.3 mM), we mainly observe the blocking effect of barium. Another blocker is TEA. Based on the structure of MthK with the tetrabutylantimony (TBSb) (PDB:4HZ3), a quaternary ammonium blocker similar to TEA, TEA should bind right below the selective filter of the MthK channel (**Fig. 4C**). At positive voltages, potasium currents could knock off TEA from its binding site, which explains the voltage-dependent blocking of TEA at depolarizing potentials (Posson et al., 2013).

After blocking the MthK currents using 0.3 mM barium inside (**Fig. 4B**), we show that the baseline leak is not regulated by temperature. The temperature-dependent increase in MthK macroscopic currents becomes evident upon the subtraction of the baseline leak (**Fig. 4E**). These observations indicate that the MthK currents increase significantly above 25 °C, with the nominal $Q_{10}$ of activation around 6. Our macroscopic current measurements likely underestimate the real change in the current amplitudes because the barium could not fully block MthK at higher temperatures. A better approach to address these concerns will be to measure the temperature dependence of MthK open probability directly by single-channel recordings.

As shown in **Fig. 4B** and **D**, we could see that with millimolar calcium, the blocking of the channel with either TEA or Barium is temperature-dependent. However, this temperature-dependent blocking may result from different mechanisms.

**Calcium response curves of MthK at various temperatures from macroscopic recordings**

The complementation assay shows that without the RCK domain, MthK couldn't recover the potassium uptake at elevated temperature (**Fig. 2**). Furthermore, at different $Ca^{2+}$ concentrations, the temperature dependence of MthK varied, and it seems to be more dramatic around $EC_{50}$ (**Fig. 3**). With these results, it appears that the RCK domain is playing an essential role in the temperature sensing of MthK. To further address this, we studied the temperature effects on the calcium response curve by using the inside-out patch clamping on giant *E. coli* spheroplasts.

However, these experiments are incredibly challenging. An inline temperature control system is used to change the bath temperature, which requires continuous perfusion. Patch clamping of the *E. coli* cell is already tricky. To study the temperature effect, we need to hold the fragile patch in constant perfusion for an hour to get a full response curve, which makes this set of experiments almost impracticable. Moreover, although we picked a single clone of transformed bacteria and induced with the same amount of IPTG under the same conditions, each *E. coli* cell still has a varying expression level. To achieve a quantitative result, we need to get the full $Ca^{2+}$ binding curve at various temperatures under the same patch. On average, for every 20 to 30 patches formed, we may only achieve one set of usable data, which takes weeks of effort.

We applied a constant flow setup with eight lines, giving us the potential to have eight $Ca^{2+}$ concentrations for each temperature. Fortunately, we succeeded in getting the set of data, as shown in **Fig. 5A**. Calcium dramatically activates the MthK channel at each temperature, and an inward rectification is observed with saturation levels of calcium. With 0.1 mM $Ca^{2+}$, the elevated temperature barely activates the MthK, and we do not observe any inward rectification at heat in

this condition. Further recordings show that there is not much change in currents in the presence of 0.1 mM calcium, with and without TEA. Furthermore, many studies on thermoTRP channels have found that the temperature activation of these eukaryotic channels is irreversible. Unlike these eukaryotic temperature-sensitive ion channels, by returning to a lower temperature, the activity of MthK is reversible, shown in **Fig. 5B**.

As a next step, we normalized the currents to the maximum currents at each temperature and got **Fig. 5C**, showing the binding affinity of the calcium doesn't change much at different temperatures, which is consistent with the finding that the neutralized mutations of glutamates at the calcium-binding site does not alter the complementation much compared to the wild type MthK (Parfenova et al., 2006). Although the combined mutation of D184N and E210Q do not entirely abolish the $Ca^{2+}$ activation of MthK, the mutations still decrease the binding affinity dramatically (Pau et al., 2011). Putting these together, it seems temperature does not activate MthK by enhancing the calcium-binding affinity.

## Discussion

Most of the temperature-sensitive ion channels known are of eukaryotic origin. These channels have a polymodal gating mechanism and are regulated by endogenous as well as exogenous ligands (Islas and Qin, 2014), which makes the study of temperature-activation mechanism complicated. Previously, by using a prokaryotic voltage-gated sodium channel, Minor et al. could address the temperature-dependent activation mechanism through structural biology (Arrigoni et al., 2016). This study demonstrates that prokaryotic temperature-sensitive ion channels, which are structurally tractable, could be good systems to study temperature activation mechanisms. Based on this, we want to find another prokaryotic temperature-sensitive ion channel that has a dramatic temperature response comparable to eukaryotic temperature-sensitive ion channels and is amenable to thermodynamic analysis as well as structural studies.

Through complementation assay, as well as inside-out patch clamping of the giant *E. coli* spheroplast, we revealed that temperature activates the MthK channel in *E. coli*.

With the complementation assay, we tested different MthK constructs. We found that elevated temperatures could activate MthK in *E. coli* cells. Previous studies have shown that the MthK requires millimolar concentrations of calcium to be activated (Zadek and Nimigean, 2006), which is above the 'physiological calcium concentration'. In *E. coli* cells, the intracellular calcium concentration is far below the $EC_{50}$ of calcium response curve for MthK, but the expression of MthK could still recover the potassium deficiency at elevated temperatures (Parfenova et al., 2006). This observation seems to imply that temperatures may activate MthK in vivo. As MthK is originally from a thermophile (Jiang et al., 2002), whose optimum growth temperature is around 65 °C (Zeikus and Wolfe, 1973), MthK could be even more active at this temperature and may function as a temperature sensor in these archaea.

However, in *E. coli* patch clamping recordings, we did not observe any significant activation in the presence of 0.1 mM calcium, shown in **Fig. 5A**. This lack of activation could result from the heat-activated Po ends in a range that is hard to observe with macroscopic recordings with deficient calcium. Contamination of the leak currents makes this observation even harder. Although we have TEA and barium as blockers to estimate the leaking currents, they are neither specific nor can they entirely block the MthK currents. Furthermore, we observed a temperature-dependent blocking behavior of these blockers, which may have different mechanism origins. For barium, we think this phenomenon results from a dilation in the selectivity filter. As has been seen previously, the folding of most proteins change at varying temperatures (Islas and Qin, 2014). As selectivity filter is considerable 'flexible' compared to secondary structures such as α-helixes, they may be even less rigid at higher temperatures. Actually, compared to other potassium channels that have the same GYG motif in selective filters, such as Shaker and BK channel, MthK has a lower selectivity to $K^+$ versus $Na^+$ (Zheng and Trudeau, 2015). For TEA, besides the structural changes, the binding process itself can be temperature-dependent.

We observed robust heat activation of MthK with 1.5 mM calcium in the cytoplasmic part of the channel. Furthermore, the calcium response curves at various temperatures indicate that the temperature effect is more significant around the $EC_{50}$, shown in **Fig. 5A** and **B**. But the binding affinity of the calcium does not seem to change much with temperature. Based on the normalized curves in **Fig. 5C**, we can see that the Hill coefficient increases with temperature. Previously it has been observed that the calcium activation of MthK has a steep hill slope, which suggests strong cooperativity between the binding sites in the RCK domains. Although the Hill coefficient and cooperativity are not the same, this increase in steepness of the Hill plot suggests a tighter interaction between the RCK domains. But how a tighter interaction in the RCK domain results in the temperature dependence is still unknown.

In this chapter, we have illustrated that the activity of MthK is temperature-dependent. And as complementation assay is useful in screening the temperature sensitivity of different MthK constructs, it could be further used as a high throughput screen assay for the cold-sensitive MthK mutants, which will be further described in **Chapter Six**.

**Figures**

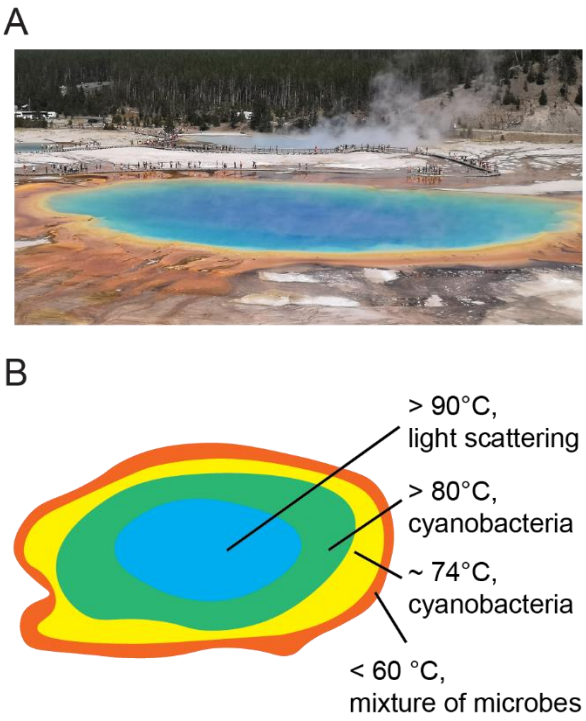


**Figure 1 | Grand prismatic spring in Yellowstone National park.**

**A.** This is a photo of Grand prismatic spring that I took in the summer of 2018. MthK originates from *Methanobacterium thermoautotrophicum*, which lives in the hot spring of Yellowstone National park. Ever since I worked on this project, I have always wanted to visit there. The multiple concentric colored rings are quite clear from this viewpoint. **B.** A graph indication of the color formation for the concentric color rings.

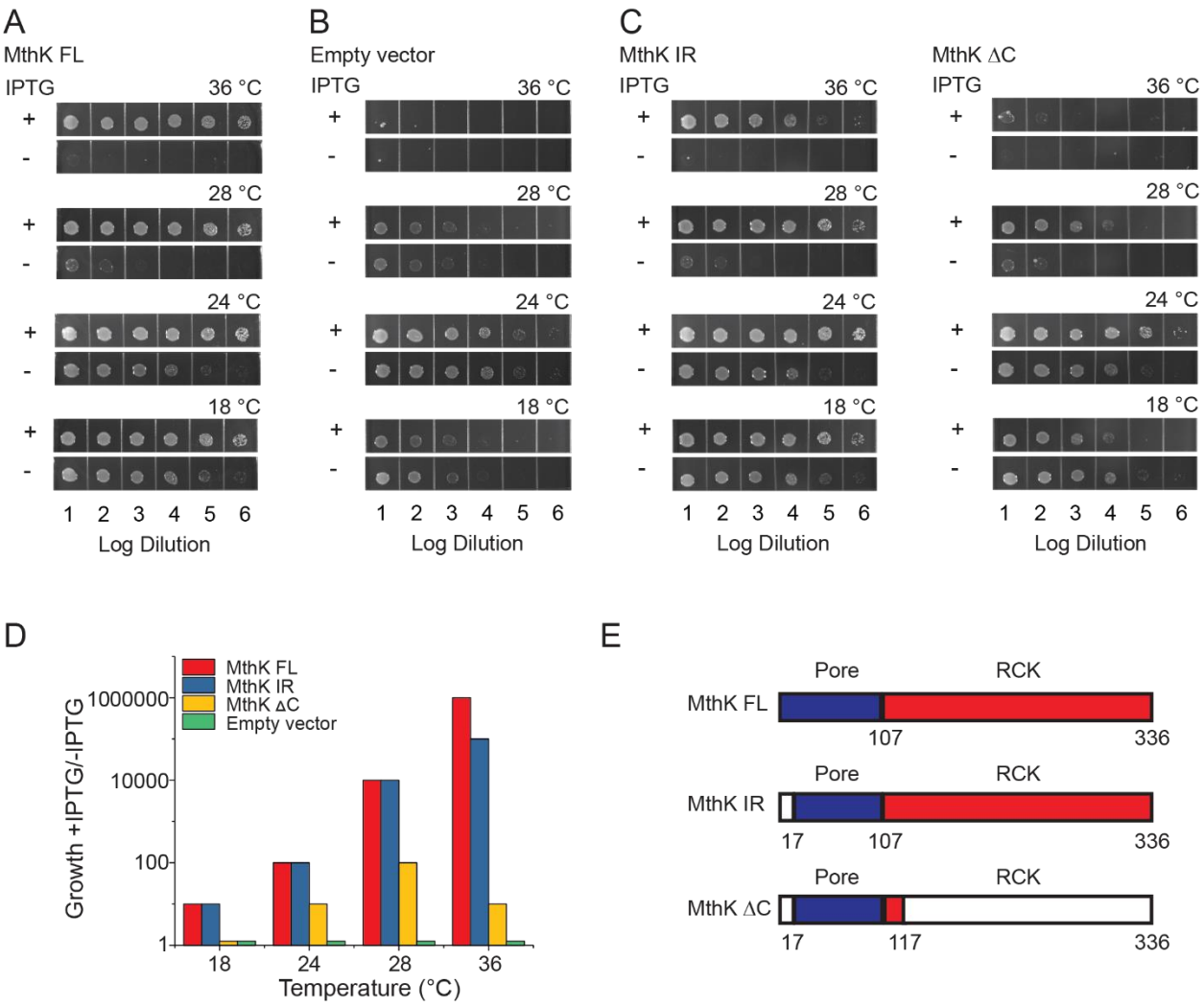


**Figure 2 | Complementation of growth with various MthK constructs in *E. coli* LB2003 cells at different temperatures.**

**A.** and **B.** are panels of serially diluted LB2003 strain, which expresses the full-length MthK constructs and empty vector control respectively, in low potassium plates at various temperatures. The log dilution factor is indicated below each panel. **C.** The same panel of serially diluted complementation assay as **A** and **B** for inactivation removed MthK (MthK IR) and C-terminal deleted MthK (MthK ΔC). **D.** Summary of growth complementation at different temperatures. The ratio of growth difference in the presence and absence of IPTG is plotted with respect to temperature to normalize differences in growth rate and survival at various temperatures. **E.** A schematic of the three different MthK constructs used in this assay. The first 107 amino acids,

which include the short cytoplasmic N-terminus up to Lysine 17 and the two transmembrane helices are highlighted in deep blue. The C-terminus cytoplasmic region containing the RCK domain is shown in red.

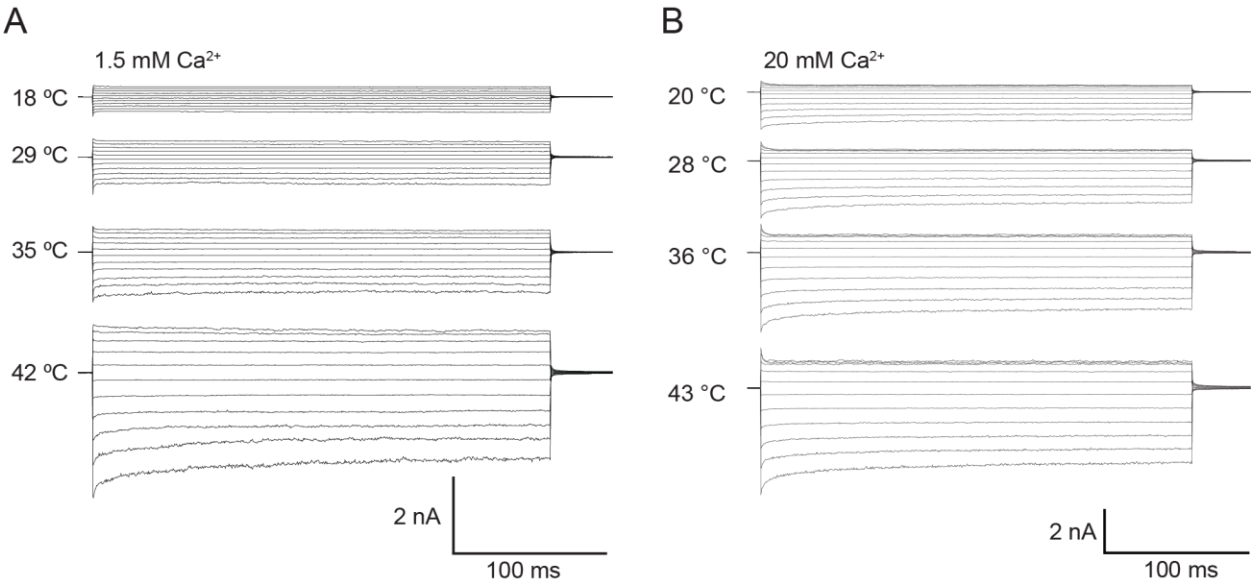


**Figure 3 | MthK IR channel expressed in bacterial membranes is active with high temperature.**

**A.** Representative macroscopic recordings of MthK IR channel with inside-out patch-clamp in giant *E. coli* spheroplast with 1.5 mM calcium at varying temperatures. All currents were obtained from the same patch in 150 mM symmetrical potassium. [Voltage steps are from -100 mV to 100 mV with 20 mV increment]. Temperatures are verified with a thermometer in a 5 mm-range of the patch. **B.** Representative macroscopic recordings of MthK IR with 20 mM calcium in the buffer at various temperatures.

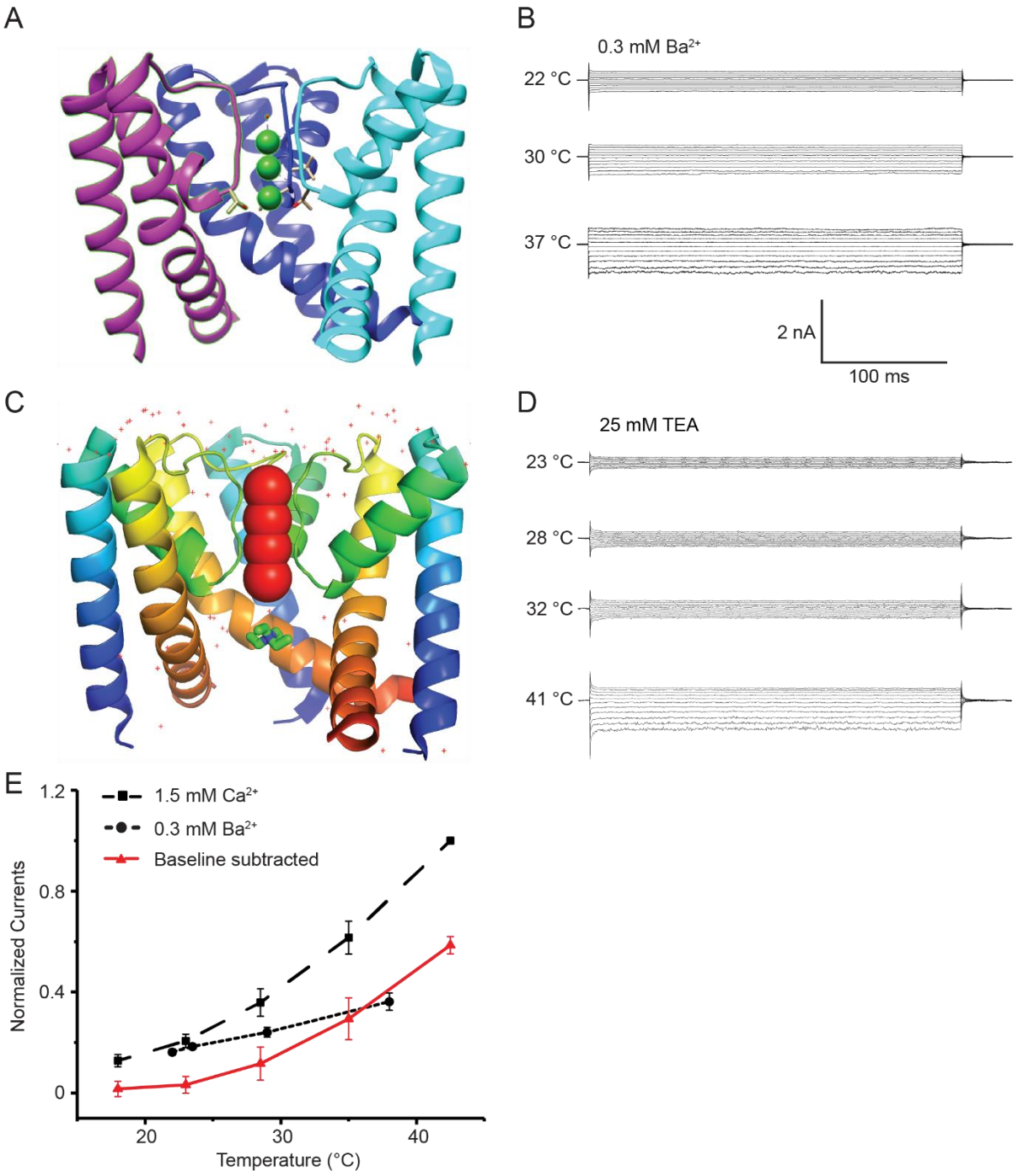


**Figure 4 | Barium and tetraethylammonium (TEA) blocking of MthK in inside-out patches of giant *E. coli* spheroplasts.**

**A.** Structure assemble of the MthK pore in the presence of barium (PDB:4QE7). The PDB file was shown as a trimer instead of a tetramer for clearance (modified in Chimera). The selectivity filter

is narrower in the presence of barium compared with occupied by potassium. **B.** Representative macroscopic recordings of MthK IR channel with inside-out patch-clamp in giant *E. coli* spheroplast with 0.3 mM $Ba^{2+}$ at varying temperatures. All currents were obtained from the same patch in 150 mM symmetrical $K^{+}$. **C.** Tetraethylammonium (TEA) docking into the structure of MthK pore with tetrabutylantimony (TBsb) (PDB:4HZ3). As can be seen, the blocker binds directly below the selective filter. **D.** Representative macroscopic recordings of MthK IR in the presence of 25 mM TEA and 1 mM calcium. **E.** The normalized current-temperature relationship for MthK IR. The current at each temperature was normalized versus maximum current at 42 °C with 1.5 mM calcium. Dashed black line with a square is the 1.5 mM calcium data, dotted black line with square corresponds to 0.3 mM barium, and the solid red line with triangle symbol is the normalized currents after baseline subtraction using the barium blocking data. Error bars are SEM from n = 4 independent measurements for 1.5 mM calcium and n = 3 independent measurements for 0.3 mM barium.

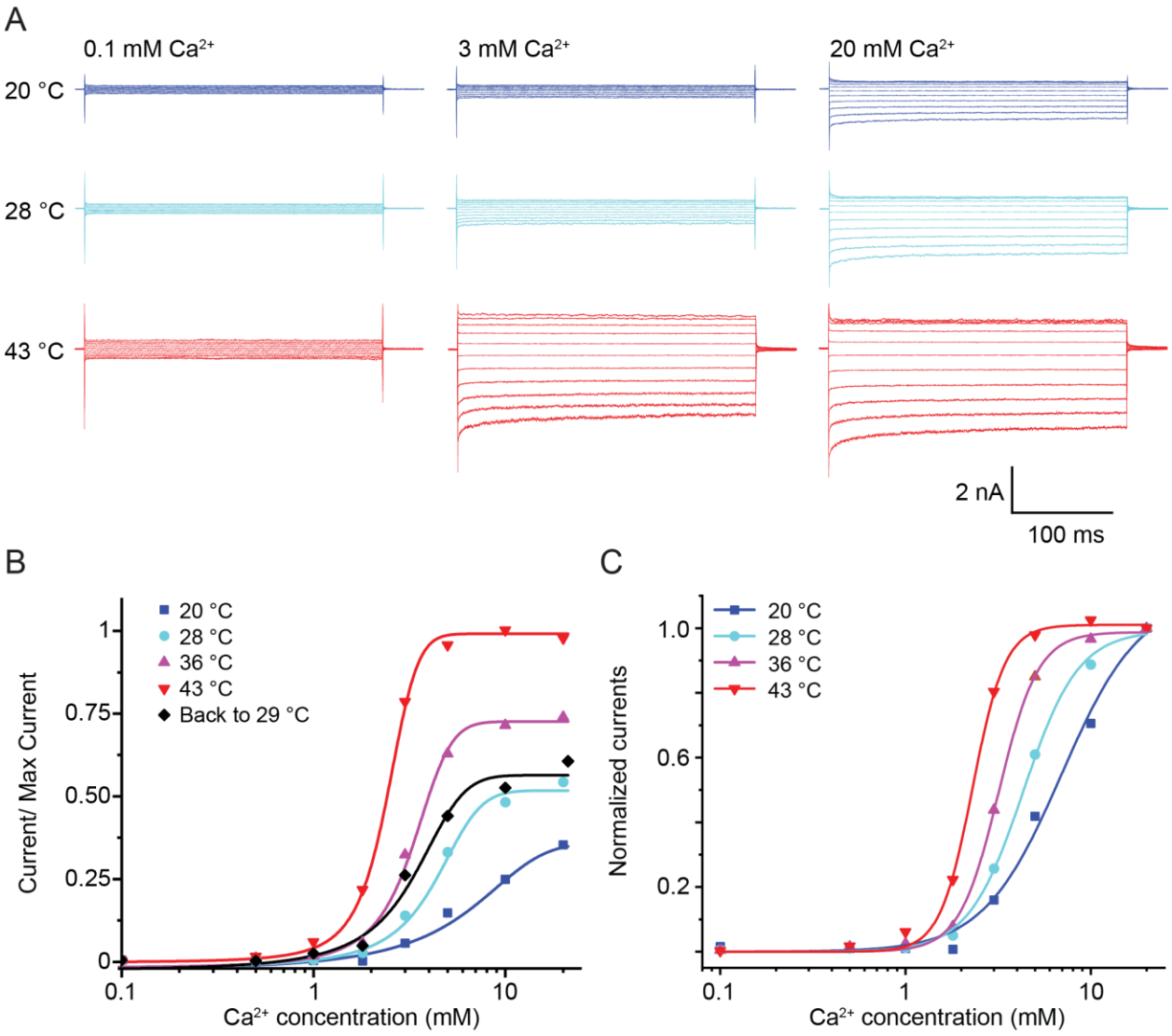


**Figure 5 | Calcium dose-response curves of MthK in inside-out patches of giant *E. coli* spheroplasts.**

**A.** Representative MthK IR channel recordings in giant *E. coli* spheroplast at a constant temperature with various calcium concentrations and then changing temperatures with the inline temperature controller to get the response curve at different temperatures. All currents were obtained from the same patch. **B.** Calcium response curves at different temperatures, summarized from recordings shown in **A**. The currents were baselined to 0.1 mM calcium, as no significant temperature-dependent activation was observed with this amount of calcium. **C.** The

normalized plot of the calcium response curve of MthK. The data is normalized from **B** to demonstrate the calcium affinity change at different temperatures.

# CHAPTER FOUR

## *Unique allosteric mechanism underlies robust temperature-sensing in MthK*

### Introduction

All of the highly temperature-sensitive channels are of eukaryotic origin, and from a biophysical perspective, these are complex systems that often exhibit irreversible gating and are biochemically recalcitrant to detailed thermodynamic analysis (Liu et al., 2011; Sánchez-Moreno et al., 2018). Many prokaryotic ion channels have become model systems to probe foundational mechanisms that underlie gating behavior and transport characteristics of their eukaryotic counterparts. For a variety of reasons, these ion channels are more tractable to structural and biochemical analysis. For instance, much of the understanding of ion selectivity comes from studies on bacterial KcsA (Doyle et al., 1998) and NaK (Shi et al., 2006) channels. KcsA ion channels have also become exemplars to understand the structural mechanisms that underlie C-type inactivation (Cordero-Morales et al., 2011b; Cuello et al., 2010a). Prokaryotes, particularly archaebacteria, can thrive in every habitat, including in extreme environments such as hot springs and deep ocean vents. Although prokaryotic ion channels that sense physical stimuli such as light, voltage, and stretch have been well-characterized, very few studies have examined the temperature-sensitive gating of archaebacterial ion channels.

As shown in **Chapter Three**, the activity of MthK is regulated by temperature in *E. coli* membranes. However, many questions remain unanswered from this study. Is the temperature sensitivity intrinsic to the MthK channel, or does it require additional cellular cofactors? What is the mechanism of temperature-dependent activation of MthK? To answer these questions, we need to purify MthK expressed in *E. coli* to rule out the effect of additional cellular proteins. In addition, we will also investigate the temperature activation mechanism of MthK using an allosteric coupling model.

## Results

### Intrinsic temperature-dependence of purified and reconstituted MthK

We sought to determine whether the observed temperature-sensitivity of MthK gating is intrinsic to the protein or is mediated by additional cellular cofactors. MthK IR was purified using metal affinity and size exclusion chromatography (SEC) from *E.coli* expression system as described previously (Jiang et al., 2002). The SEC elution profile and SDS-PAGE analysis of purified protein are shown in **Suppl. Fig. 1A** and **1B**. The purified MthK protein was reconstituted into soybean polar lipids to form proteoliposomes. Giant multilamellar vesicles were generated and currents were recorded using inside-out patch electrophysiology (Chakrapani et al., 2007).

Single-channel recordings from a single patch at different temperatures in the presence of 0.1 mM calcium are shown in **Fig. 1A**. The $EC_{50}$ of calcium dose-response is at 3.8 mM at room temperature and therefore at 0.1 mM calcium, these channels are primarily unliganded (Pau et al., 2010; Zadek and Nimigean, 2006). Large conductance of the open MthK channel allows us to resolve opening events easily. Up until 32 °C, single-channel openings are rare but upon elevating the temperature to 39 °C we observe a large increase in single-channel activity. Plotting the current amplitude distributions at various temperatures shows clearly that the channel remains closed till 32 °C but upon further increase in temperature to 39 °C, the channel opening events increase dramatically (**Fig. 1B**). The open dwell time distributions clearly indicate the presence of multiple kinetically distinct open states. The mean open dwell time changes from 4.9 ms at 21 °C to 3.3 ms at 39 °C (**Fig. 1C**). Due to the presence of at least two channels in the patch, we were not able to obtain a direct estimate of the mean closed times. However, the open probability, $Po$, calculated from 5 minutes of continuous single-channel recordings, shows that at 39 °C, *Po* is more than two orders of magnitude higher than those measured at lower temperatures (**Fig. 2D**). Therefore, the high temperature must profoundly shorten the residence times of the channel in the closed states.

The observed temperature dependence of single channel activity of purified MthK reconstituted in soybean lipids corresponds to a $Q_{10}$ of ~100, which is comparable to the canonical eukaryotic temperature-sensitive ion channels, TRPV1 and TRPM8. Our findings also establish that temperature-sensitive activation is an intrinsic property of the channel and does not require cellular cofactors.

These observations of purified MthK in proteoliposome establish that temperature-sensitive activation is an intrinsic property of the channel and does not require its interaction with endogenous proteins. The high-temperature sensitivity of MthK suggests a possible physiological role in the thermophilic archaebacteria, which grows optimally around 65 °C (Zeikus and Wolfe, 1973). We speculate that these channels likely shut down potassium uptake and thus inhibit cell growth when the temperature falls below 35 °C. Calcium activation may act as an alternate signaling pathway for potassium uptake at sub-optimal temperatures, but, at high temperatures, calcium has a modest effect on channel activity.

**The MthK pore domain is not responsible for temperature sensation**

Gating of MthK has been described via an allosteric scheme where the pore isomerizes between a closed and open state with an intrinsic bias towards the closed state and calcium binding shifts this bias towards the open state (Jiang et al., 2002; Li et al., 2007). Our single-channel measurements were performed at very low calcium concentrations and so we wondered whether temperature skews the innate conformational bias of the pore domain. Such a hypothesis would parallel a recent study which showed that the pore domain of the heat-sensitive TRPV1 channel when fused to the voltage-sensing domain of the prototypical Shaker potassium channel, results in a chimeric channel with strong heat sensitivity, suggesting that pore domain of TRPV1 might retain the essential structural elements for temperature sensitivity (Zhang et al., 2018).

To directly test the temperature sensitivity of the pore domain, we adapted a previously reported protocol to purify a ‘pore-only’ MthK channel (MthK PO) (Li et al., 2007; Posson et al.,

2013). Purified MthK IR channels, were treated with trypsin to cleave off the RCK domains and the “pore-only” domain was subsequently isolated via gel-filtration chromatography (**Suppl. Fig. 2A and 2B**). MthK PO was reconstituted into soybean polar lipids and its single-channel activity was measured at 20 and 36 °C (**Fig. 2A)**. Although MthK PO has higher opening events at 36 °C, the calculated $nPo$ at 20 °C is 4.8 fold higher. Furthermore, the mean open dwell time of MthK ΔC channels decreases from 11.2 ms at 20 °C to 2.1 ms at 36 °C (**Fig. 2B and 2C**). It is noteworthy that this ~5.5 fold change in the mean open dwell times (and thus closing rate) can almost entirely account for the change in the equilibrium constant for channel opening (derived from the open probability measurements). These effects are in stark contrast to those observed in MthK IR where the open probability increases by at least two orders of magnitude upon heating. Taken together, these results prove the pore domain of MthK is not intrinsically sensitive to temperature and that structural elements from RCK domains are required for its exquisite temperature-sensitivity.

**Coupling of RCK domains with the pore**

The classical view of calcium activation of MthK channels is that under low calcium conditions, the pore domain has an intrinsic bias towards closed conformation. This is consistent with the low single-channel activity of MthK PO (Li et al., 2007). Binding of calcium to the octameric ring of RCK domains drives channel opening through long-range interactions. To probe the allosteric nature of temperature-induced conformational changes, we measured single-channel activities at different calcium concentrations at two temperatures, 21 °C and 39 °C (**Fig. 3A and B**).

The calcium dose-response curves of MthK obtained from $Po$ estimates exhibit high Hill-coefficients (Zadek and Nimigean, 2006), which makes it very challenging to obtain accurate measurements of $EC_{50}$. Nevertheless, the saturating regimes of calcium concentrations constrain these values within a specific range. Our measured dose-response curves of MthK reveal that

the $EC_{50}$ of calcium at 21 and 39 °C are only modestly different ($EC_{50}$ ~ 0.9 mM). Our experiments show that most temperature dependence of activity is observed at the lowest concentrations of calcium where the RCK domains are primarily in apo-state (**Fig. 3C**). The lowest calcium concentration tested was 0.1 mM because patches became unstable below this concentration even in the presence of millimolar concentrations of magnesium as has been reported previously (Coronado, 1985; Graber et al., 2017). In the most parsimonious allosteric model, the apo RCK domain does not interact with the pore. Upon calcium binding, it undergoes a conformational change and stabilizes the open pore resulting in increased $Po$. However, given our observations, we must conclude that the RCK domain influences pore gating even in the absence of ligand.

In our revised model, the pore and the calcium sensor each exist in two different conformations, analogous to the classical model. The transition of the pore, from the closed to open state, has an intrinsic equilibrium constant and the binding of calcium to the sensor is associated with an intrinsic binding affinity. However, instead of using a single coupling constant to describe the interactions between the pore and the calcium sensor, we use four different conformational state-dependent interaction terms (**Fig. 4A**). As detailed in the supplementary information, the classical models of allostery are a simplified version of this model with the different state-dependent interaction terms buried within the apparent equilibrium and coupling constants (Chowdhury and Chanda, 2010).

In the context of allosteric models, the net coupling energy between the sensor and pore domains can be calculated directly by measuring the difference between Hill transformed $Po$ values in the presence and absence of stimulus as described previously (Chowdhury and Chanda, 2010; Sigg, 2013). This approach is analogous to the Hill-plot analysis of ligand binding curves described by Wyman in his classical descriptions of allosteric linkage (Wyman, 1967). In **Fig. 3C**, the Hill-transformed $Po$ (i.e., $\ln [Po/(1\text{-}Po)]$) with calcium concentration were plotted at 21 °C and 39 °C.

In physical terms, the difference between the two asymptotes shown in **Fig. 3C**, $\Delta\chi$ (at a specific temperature), may be expressed as:

$$\Delta\chi = \ln \sum \frac{\theta_{BO}\theta_{UC}}{\theta_{BC}\theta_{UO}} \quad \text{Eq. 1}$$

where $-RTln\theta_{BO}$ and $-RTln\theta_{BC}$ are the interaction energies between a calcium-bound site with open-pore and close-pore respectively; while $-RTln\theta_{UO}$ and $-RTln\theta_{UC}$ are the interaction energies between an apo binding site with open-pore and close-pore respectively (see **Fig. 4A**). Thus, $\Delta\chi$ reflects the preference of the calcium-binding sites and the pore for "like" conformations (i.e., bound-open or unbound-closed) as opposed to "unlike" conformations (i.e., bound-closed or unbound-open).

Most interestingly, the Hill-plots at the two temperatures show that $\Delta\chi$ is different at the two temperatures. Going from 21 °C to 39 °C, $\Delta\chi$ changes from 4 to 2.4, which corresponds to a change in coupling energy from 2.3 to 1.4 kcal/mol. Thus, while the overall allosteric coupling is favorable at both temperatures (i.e., the calcium-binding sites and the pore prefer to exist in "like" conformations), the coupling interaction is much weaker at 39 °C with respect to 21 °C.

In the context of a general allosteric model, it worth considering the higher and lower asymptotes, $\chi_-$ and $\chi_+$, individually which are:

$$\chi_- = \ln L_0 \sum \frac{\theta_{UO}}{\theta_{UC}} \quad \text{Eq. 2a}$$

$$\chi_+ = \ln L_0 \sum \frac{\theta_{BO}}{\theta_{BC}} \quad \text{Eq. 2b}$$

where $L_0$ is the intrinsic equilibrium constant of pore opening. Our data on the MthK PO shows that $L_0$ is not significantly temperature-sensitive and, therefore, one or more of the interaction terms must contribute to temperature dependence. The Hill-plots reveal that the $\chi_-$ is much more sensitive to temperature than $\chi_+$ and, therefore, one or both of the interaction terms, $\theta_{UO}$ and $\theta_{UC}$, must contribute to this higher temperature dependence of $\chi_-$.

Simulations of the Hill-plots of our revised allosteric model (**Fig. 4B** and **Suppl. Fig. 4**) clearly show that temperature-dependent $\theta_{UO}$ or $\theta_{UC}$ is able to recapitulate the characteristic behavior of our experimental Hill-plots, namely a temperature-dependent $\Delta\chi$ and $\chi_-$ with a relatively modest temperature-sensitivity of $\chi_+$. We note that both $\theta_{UO}$ and $\theta_{UC}$ describes the interaction between the apo-sensor and pore domain. Based on open-dwell time and $Po$ measurements at low calcium concentrations, we have previously argued that temperature causes a profound increase in the forward rate of channel opening (see **Fig. 1**), which is also governed by $\theta_{UC}$. Therefore we must conclude that the primary effect of increasing temperature on MthK IR is to decrease the interaction energy between the closed pore and apo calcium-binding sites.

**Equivalence between a classical allosteric model with a single coupling parameter and an allosteric model state-dependent coupling parameters**

We consider the binary elements model depicted in **Fig. 4A**. In this model, the channel comprises two "binary elements" – the pore and the calcium sensor, each of which can exist in two conformations. The closed to the open transition of pore alone is associated with an intrinsic equilibrium constant, $L_0$, which is informed by the intrinsic stabilities of the open/closed conformations of the pore. The calcium sensor binds calcium with an intrinsic equilibrium (binding) constant, $K$, which is governed by the interaction between calcium ion and the sensor relative to the apo conformation of the sensor. The full channel thus is assumed to exist in four possible states. The closed pore interacts with apo (or unbound) calcium sensor, and the interaction is depicted by the coupling constant, $\theta_{UC}$. The closed pore also interacts with calcium sensor in its holo (bound) state, which is depicted by the parameter, $\theta_{BC}$. Similarly, the open pore also interacts with calcium sensors in the unbound and bound states, and the interactions are accounted for by the terms $\theta_{UO}$ and $\theta_{BO}$ respectively. The reference energy level for this system with four

conformational states is considered to be the closed pore-apo calcium sensor. For this system, the partition function can be written as:

$$Z = \theta_{UC} + L_0\theta_{UO} + Kx\theta_{BC} + L_0Kx\theta_{BO} \quad \text{Eq. 3}$$

Where $x$ is the calcium concentration. This is the most general partition function that can be written for the 4 state system. Now we can divide Eq. 3 with $\theta_{UC}$ to get:

$$\frac{Z}{\theta_{UC}} = 1 + \frac{L_0\theta_{UO}}{\theta_{UC}} + \frac{Kx\theta_{BC}}{\theta_{UC}} + \frac{L_0Kx\theta_{BO}}{\theta_{UC}} \quad \text{Eq. 4}$$

We define, $L_0' = \frac{L_0\theta_{UO}}{\theta_{UC}}$ and $K' = \frac{K\theta_{BC}}{\theta_{UC}}$ and use these parameters in Eq. 4 to get:

$$\frac{Z}{\theta_{UC}} = 1 + L_0' + K'x + L_0'K'x\frac{\theta_{UC}\theta_{BO}}{\theta_{UO}\theta_{BC}} \quad \text{Eq. 5}$$

Now if define $\theta = \frac{\theta_{UC}\theta_{BO}}{\theta_{UO}\theta_{BC}}$, which simply is the ratio of the 'like-state' interactions and the 'unlike-state' interactions and is a measure of the energetic preference of the two binary elements to exist in 'similar' functional states. Using $\theta$ and redefining the reference energy level to be the energy of the state closed pore-apo calcium sensor, including its interaction, Eq. 5 converts to:

$$Z' = 1 + L_0' + K'x + L_0'K'x\theta \quad \text{Eq. 6}$$

The above equation (Eq. 6) is mathematically analogous to the partition function of a binary elements model where the interaction between the binary elements is assumed to be restricted to the open-pore-bound calcium sensor as would be the case in classical allosteric models (**Suppl. Fig. 3**). Yet, by introducing parameter normalizations (to get to Eq. 5 from 4) and redefining the reference energy level, we are able to arrive at a similar mathematical expression even for a system where there are multiple conformational-state dependent interactions between the binary elements. However, it is essential to realize that in this normalized form, the contributions of the various state-dependent interactions are incorporated within the different 'normalized' parameters.

**Analytical derivation of the temperature dependence of χ-values for a model with a temperature sensor**

A more conventional model often used to describe temperature-dependent gating of ion channels invokes a specific temperature sensing domain, allosterically coupled to the channel pore (Diaz-Franulic et al., 2016). As shown in **Suppl. Fig. 5A**, this allosteric domain is associated with a temperature-dependent activation constant, $M_0$, and its interactions with the pore and the ligand-binding domains are associated with allosteric factors C and E, respectively. In this model, the coupling between the pore and ligand-binding domain is represented by the single allosteric parameter, D. For such a model, we are interested in understanding how the χ-values would change with temperature. The χ-values for ligand driven transformation of the channel can be represented as:

$$\chi_- = \ln\frac{L_0(1+M_0C)}{1+M_0} \quad \text{Eq. 7}$$

$$\chi_+ = \ln\frac{L_0D(1+M_0CE)}{1+M_0E} \quad \text{Eq. 8}$$

$$\Delta\chi = \ln\frac{D(1+M_0CE)(1+M_0)}{(1+M_0C)(1+M_0E)} \quad \text{Eq. 9}$$

We are interested in deriving the expressions for the temperature dependence of the χ-values which arises due to the logarithmic terms in Eqs. 7-9. Therefore we differentiate each of the above equations concerning temperature (T), noting that of the different parameters only $M_0$, the activation constant of the temperature sensor is the only model parameter which changes with temperature. The following equations are the temperature differentials of the χ-values:

$$\frac{\partial\chi_-}{\partial T} = \frac{\partial M_0}{\partial T}\frac{C-1}{(1+M_0)(1+M_0C)} \quad \text{Eq. 10}$$

$$\frac{\partial\chi_+}{\partial T} = \frac{\partial M_0}{\partial T}\frac{E(C-1)}{(1+M_0E)(1+M_0CE)} \quad \text{Eq. 11}$$

$$\frac{\partial\Delta\chi}{\partial T} = \frac{\partial M_0}{\partial T}\frac{(E-1)(C-1)(1-M_0^2CE)}{(1+M_0)(1+M_0C)(1+M_0E)(1+M_0CE)} \quad \text{Eq. 12}$$

From Eqs.10-12, we can see that when C = 1, all three differentials are zero indicating their lack of temperature dependence. When C ≠ 1 but E = 1, both $\chi_-$ and $\chi_+$ are temperature-dependent, but $\Delta\chi$ is temperature independent. Only when both E and C are different from unity are the differentials non-zero and unequal (**Suppl. Fig. 5B**).

Another interesting observation is that if $M_0$ is a monotonically increasing (or decreasing) function of temperature both $\chi_-$ and $\chi_+$ are monotonically temperature-dependent viz. for a specific 'C', the signs of the differentials are constant. For instance, in the case where C > 1 and $\frac{\partial M_0}{\partial T} > 0$, the sign of the differential is positive and thus as the temperature is increased, $\chi_-$ and $\chi_+$ both will keep increasing with temperature. However, $\Delta\chi$ may be a non-monotonic function of temperature. For a given value of E and C and a fixed sign of the differential $\frac{\partial M_0}{\partial T}$ (which governs whether the temperature sensing domain 'activates' or 'deactivates' with increasing temperature), the sign of the temperature differential of $\Delta\chi$ will change depending on whether $M_0$ is greater or less than $1/\sqrt{CE}$. Since $M_0$ is itself temperature dependent, it is possible that over a specific temperature range $M_0 < 1/\sqrt{CE}$ while at a different temperature regime $M_0 > 1/\sqrt{CE}$. It is important to realize, however, that this cross-over temperature might be inaccessible in electrophysiological experiments.

## Discussion

Temperature modulates the functional activity of virtually all known proteins to a varying extent by altering the fluctuations of atoms, which frequently manifests itself as a change in the kinetics of a reaction. However, in some instances, it also results in an altered equilibrium response as observed in temperature-sensitive ion channels. Mammalian thermoTRPs are founding members of temperature-sensitive ion channels that respond exquisitely to thermal stimuli (Caterina et al., 1997; McKemy et al., 2002; Peier et al., 2002). But in addition to thermoTRPs, many other structurally dissimilar ion channels such as the STIM1-Orai complex

are also activated by temperature (Xiao et al., 2011). This lack of structurally conserved temperature-sensing domain raises profound questions about the mechanisms of thermal sensing in biology.

Studies by various groups over the years have identified several structural motifs that could possibly act as temperature-sensing domains that drive the pore gating allosterically analogous to a ligand-binding domain regulating ligand-activated ion channel (Arrigoni et al., 2016; Brauchi et al., 2006; Cordero-Morales et al., 2011a; Fujiwara et al., 2012; Lishko et al., 2007; Takeshita et al., 2014; Voets et al., 2007). Here, we have examined the mechanism of temperature-sensitivity of archaebacterial MthK which have been exemplars for studying calcium activation mechanisms. Bilayer recordings of purified reconstituted MthK show that they are extremely sensitive to temperature change between 30 and 40 °C. Over this range, the open probability of inactivation deficient MthK (MthK IR) increases about two orders of magnitude in low calcium. The ablation of the RCK domain dramatically reduces the temperature-dependence of pore opening in these channels. By obtaining single-channel measurements under limiting conditions and combining it with model-independent linkage analysis, we find that temperature modulates the activity of MthK by altering the allosteric coupling between apo-RCK and the pore module rather than their intrinsic equilibrium constants. Interestingly, theoretical analyses of allosteric models had led Jara-Oseguera and Islas to previously proposed that temperature-sensitive allosteric coupling between stimulus sensing elements (such as voltage or ligand sensors) and a channel pore could underlie steep temperature-sensitivity of thermoTRPs (Jara-Oseguera and Islas, 2013). To the best of our knowledge, our study is the first known instance where the temperature is shown to affect an allosteric protein by altering coupling between its functional domains.

It is worth considering these coupling energies in the context of classic allosteric analysis by Horrigan and Aldrich on BK channels (Horrigan and Aldrich, 2002). The measured coupling between the RCK domains and the pore domain is about 5 kcal/mol which results in four orders

of increase in $Po$ values upon addition of calcium. In the case of MthK, we find that the measured coupling is 2.3 kcal/mol which increases $Po$ by about two orders of magnitude at room temperature. At elevated temperatures, this coupling energy reduces by 0.9 kcal/mol to 1.4 kcal/mol which corresponds to a 40% reduction in interaction energy. This is perhaps our most interesting finding which illustrates that when the coupling energies are modest, a change of 1 kcal/mol in interaction energy can profoundly regulate channel activity.

At a physical level, it is interesting to speculate how the coupling interactions between the pore and RCK domain is altered in a temperature-dependent manner. The structure of the full-length MthK shows that the pore and RCK domains are not in physical contact except through the connecting linker which was modeled as $\alpha$-helix (Kopec et al., 2019). Thus, one would posit that the linker helices may play a key role in coupling the apo-RCK domain to the conformation of the pore domain. Future studies probing the role of this linker helix may help provide a better understanding of the structural mechanisms that underlie temperature-dependent gating in these ion channels.

It is important to note that our analysis does not necessarily rule out the alternative model which invokes the existence of an allosteric temperature sensing domain. However, a noteworthy departure from the classical viewpoint, like Horrigan-Aldrich type model (Horrigan and Aldrich, 2002), is that this temperature sensing domain, if it exists, has to directly regulate not just the state of the pore domain but also the RCK domain. If either of these interactions is missing, the limiting asymptotes ($\chi_{\pm}$) will not exhibit characteristic temperature dependence observed here (**Suppl. Fig. 5**). Even within this nested allosteric framework, the effect of temperature can be distilled down to modulation of RCK and pore coupling. Whether this modulation is mediated directly by disrupting the interactions between RCK and pore or by a discrete temperature sensor that regulates RCK-pore coupling remains an open question. While further studies are required to clarify the structural and energetic mechanisms that underlie temperature-dependent gating in

MthK, our findings highlight a unique mechanism of temperature-dependent gating in this ancient ion channel.

## Figures

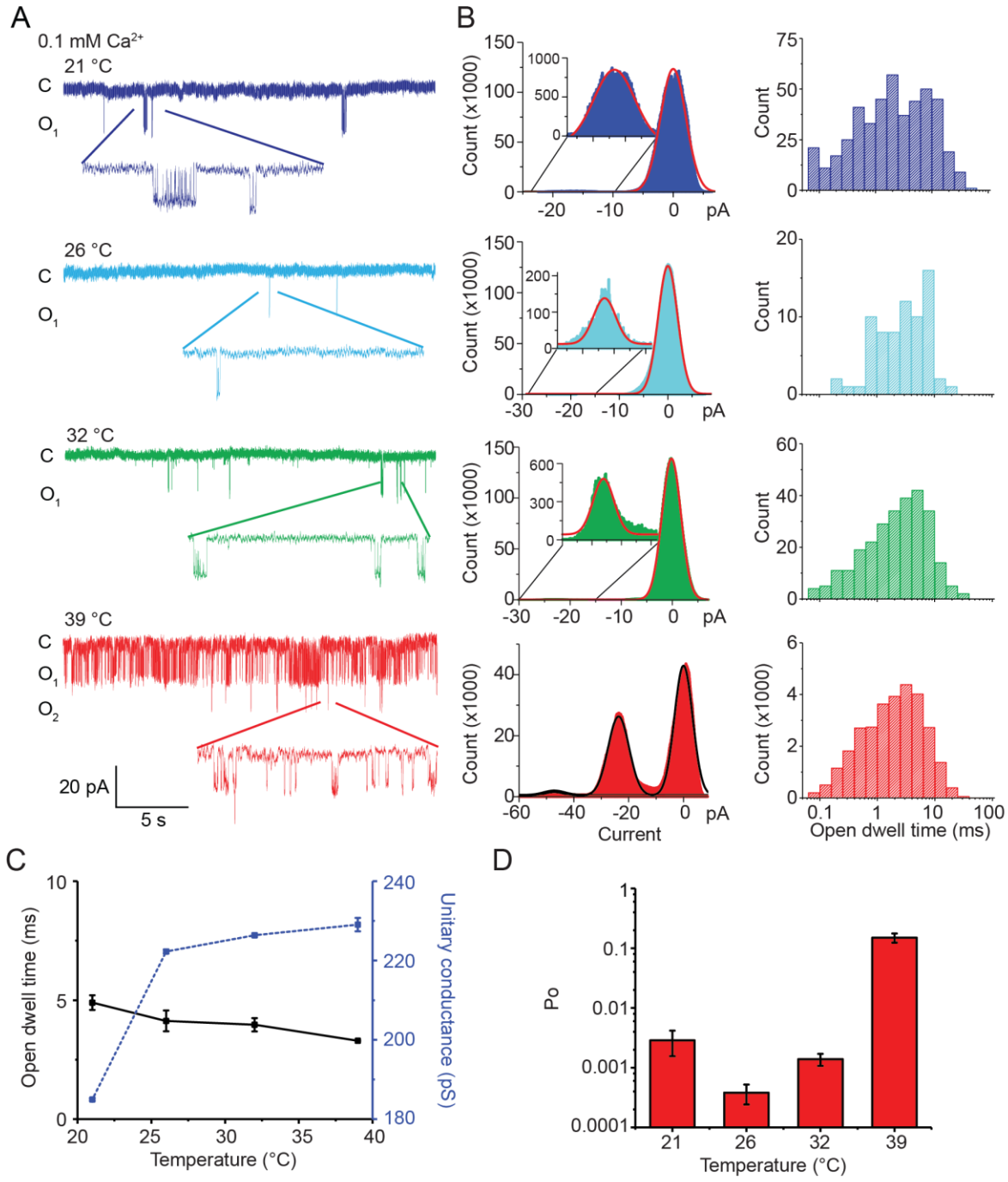


**Figure 1 | MthK IR channel is intrinsically heat-sensitive.**

**A.** Representative single channel recordings of purified MthK IR reconstituted in soybean polar lipids with 0.1 mM calcium at various temperatures. All traces were recorded at -100 mV from the

same patch. **B.** Current amplitude histograms (left) and open dwell time (right) of single channel recordings with same color scheme as in **A**. Inset. The current amplitude histograms corresponding to the open channels are enlarged for clarity. **C.** Open dwell time (solid black line) and unitary conductance (dotted blue line) of MthK IR plotted with respect to temperature. Mean open dwell time was calculated based on all the opening events identified in Clampfit after 5 minute of continuous recordings at each temperature. Error bars are standard error for open dwell time from all the recorded single channel events n = 457 for 21 °C, n = 73 for 26 °C, n = 274 for 32°C and n = 29,926 for 39 °C; error bars for unitary conductance are based on the Gaussian fitting (Origin) shown in (**B**). **D.** Bar graph of open probability at various temperatures. Error bars are SEM calculated by using bootstrapping from 10 sweeps of 30s length.

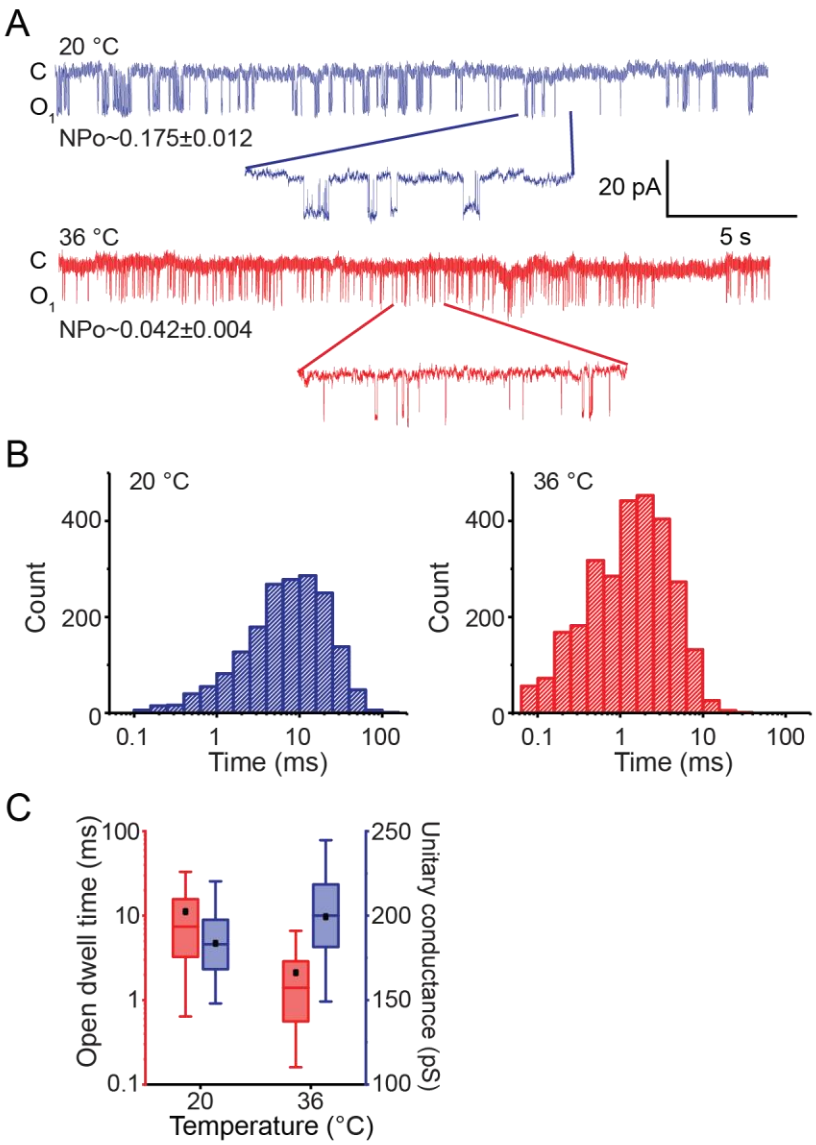


**Figure 2 | MthK pore itself is not responsible for the heat sensitivity of MthK.**

**A.** Representative single channel recordings of purified MthK PO reconstituted in soybean polar lipids with 1 mM calcium at 20 and 36 °C. Inset shows the enlarged traces. $nPo$ values are shown below each trace; the errors were calculated as SEM from bootstrapping the whole recordings. **B.** Open dwell time histograms at the two different temperatures. **C.** Box graphs showing the open dwell times (red) and unitary conductances (blue) of MthK PO plotted with respect to temperature. The boxes indicate 25 to 75 percentiles of the data; the whiskers show 5 to 95 percentiles of the data. Within each box, the line indicates the median value and black square is the mean.

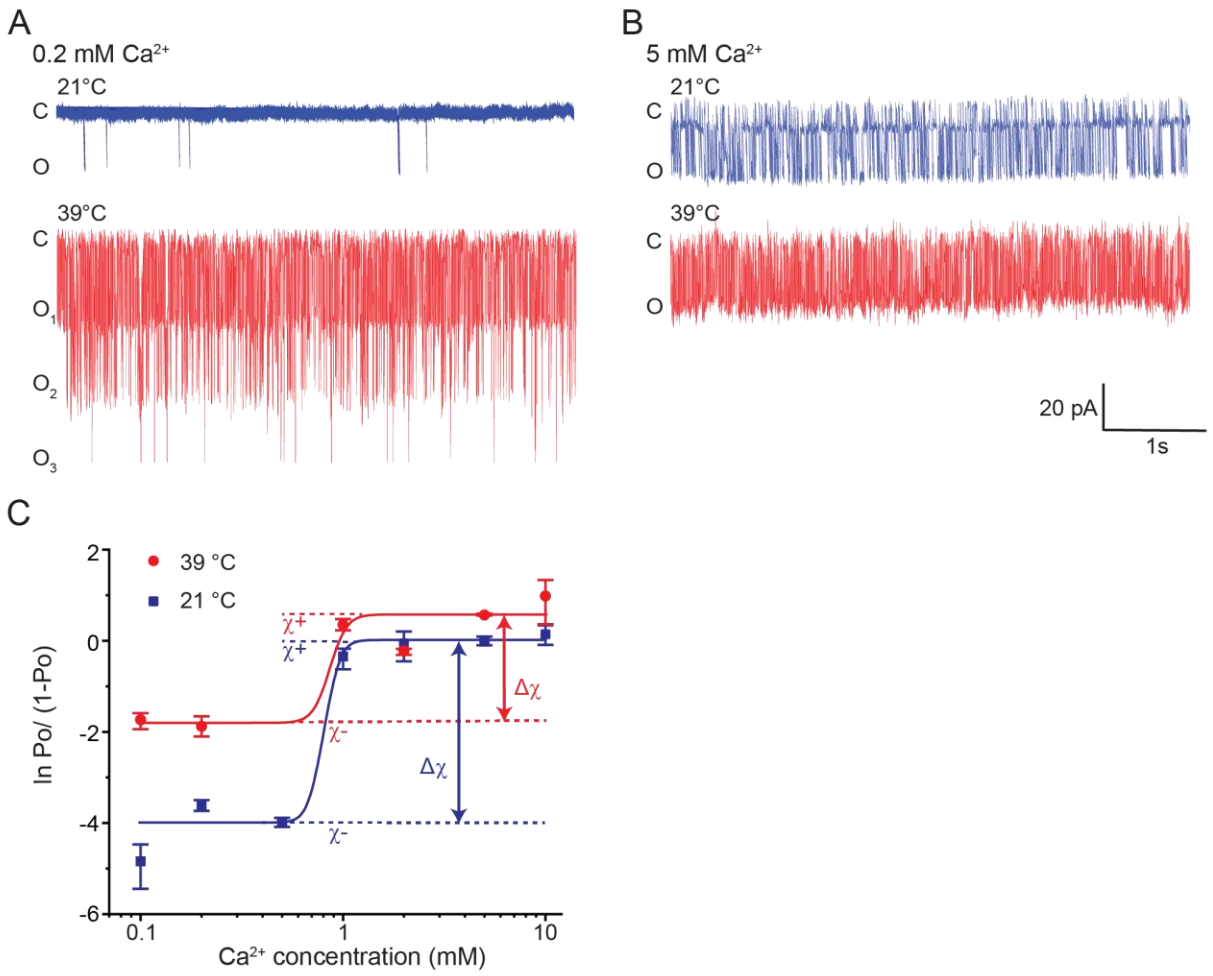


**Figure 3 | Temperature alters the coupling energy between the RCK domain and pore domain.**

Representative single channel recordings in the presence of 0.2 mM calcium (**A**) and 5 mM calcium (**B**) at two different temperatures. For a particular calcium concentration, the recordings were obtained from the same patch. **C.** Hill plot of $\ln [Po/(1\text{-}Po)]$ versus calcium concentration. Low temperature data are shown in blue while high temperature data are in red. The limiting asymptotes for each curve are depicted as dotted lines. $\Delta\chi$ values at each temperature correspond to the difference between asymptotes at the respective temperature (indicated by double headed arrows). Error bars are SEM calculated from bootstrapping of the whole single channel recordings.

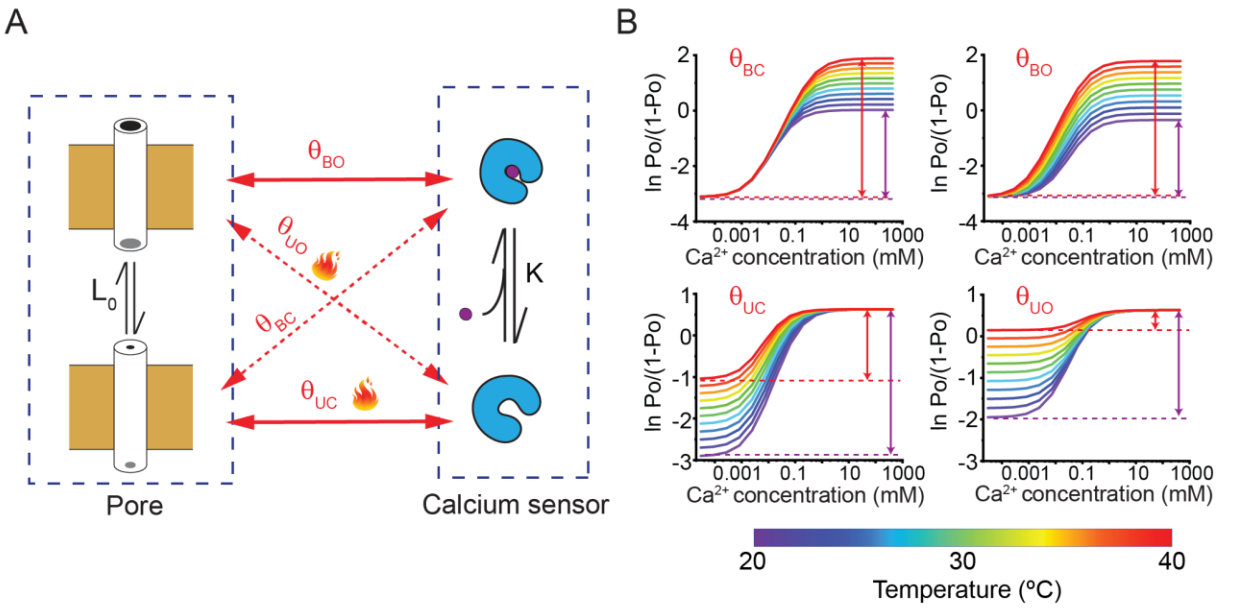


**Figure 4 | Two plausible models for the temperature activation mechanism of MthK.**

**A.** Four state binary elements model of MthK activation. The intrinsic equilibrium constant of pore opening is $L_0$ and the calcium binding affinity is $K$. The state-dependent interactions between the pore and calcium sensor are represented by $\theta_{XY}$, where $X$ indicates the conformation of the calcium sensor ($X=$ bound (B) or unbound (U)) and $Y$ indicates the conformation of the Pore ($Y=$ open (O) or closed (C)). Solid lines indicate the interactions between the "like" states and the dotted lines indicate the interaction between "unlike" states. **B.** Using the model of MthK channel gating, described in **A**, we simulated the Hill-plot of MthK (i.e. $\ln [Po/(1-Po)]$ vs $Ca^{2+}$) at different temperatures for various model parameters. In each graph, all parameters, except the state-dependent interaction marked in the graph, were kept constant across different temperatures. For all the simulations, the values of the parameters used were: $L_0 = 0.1$; $K = 20000$ $M^{-1}$; $\theta_{UO} = 8$; $\theta_{UC} = 18$; $\theta_{BO} = 150$; $\theta_{BC} = 8$. For temperature dependent simulations of $\theta_{BC}$, we use the following equation: $\theta_{BC}(T) = \exp(-(\Delta H_{BC} - T\Delta S_{BC})/RT)$, where $\Delta H_{BC}$ = -71 kJ and $\Delta S_{BC}$ = -220 J/K. Similarly, $\theta_{BO}$ ( $\Delta H_{BO} = 81$ kJ and $\Delta S_{BO} = 310$ J/K), $\theta_{UC}$ ($\Delta H_{UC}$ = -71 kJ and $\Delta S_{UC}$ = -220 J/K) and $\theta_{UO}$ ($\Delta H_{UO} = 80$ kJ and $\Delta S_{UO} = 300$ J/K) were calculated.

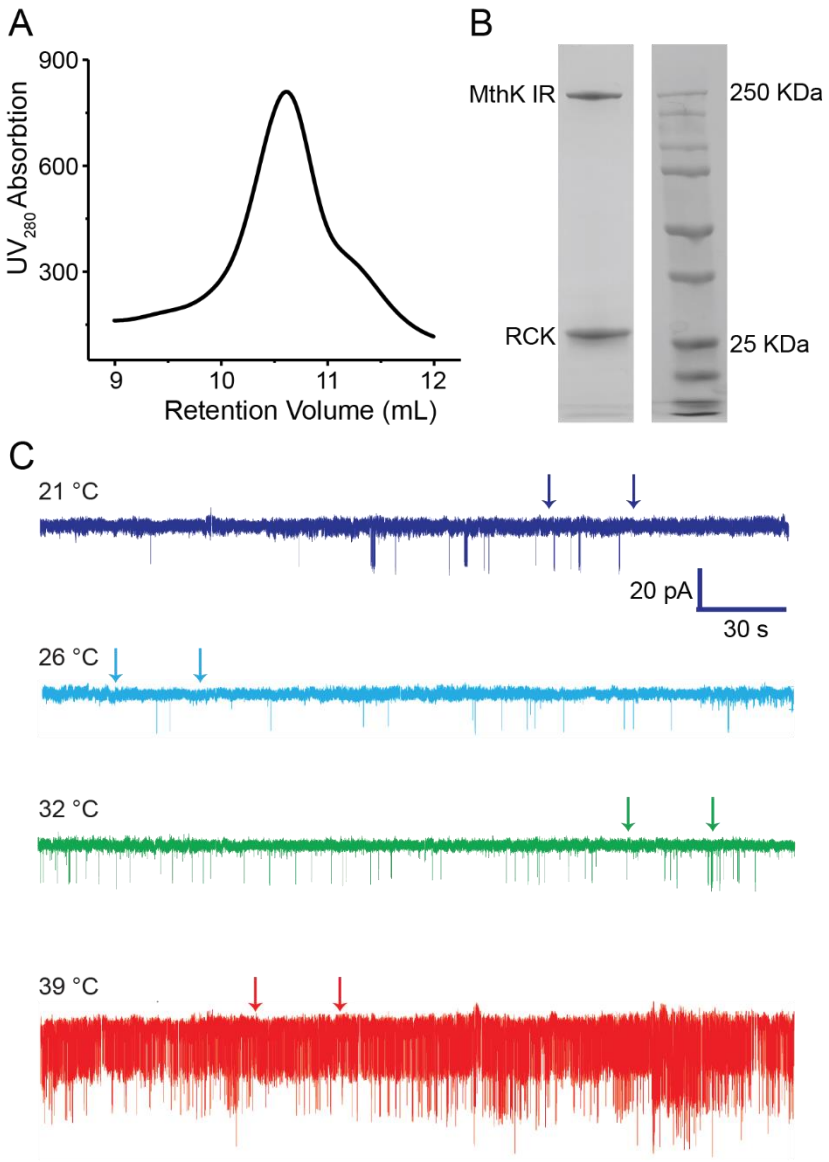


**Supplementary Figure 1 | Purification profile of MthK IR and single channel recordings.**

**A.** Size exclusion chromatography (SEC) of MthK IR in DM detergent in Superdex 200 column. **B.** The peak fraction from SEC in 10% SDS-PAGE, protein marker in the same gel is shown on the right. C. Long traces of single channel recordings of MthK IR at 0.1 mM $Ca^{2+}$. The traces between the two arrows are used as the representative data shown in **Fig. 1A**.

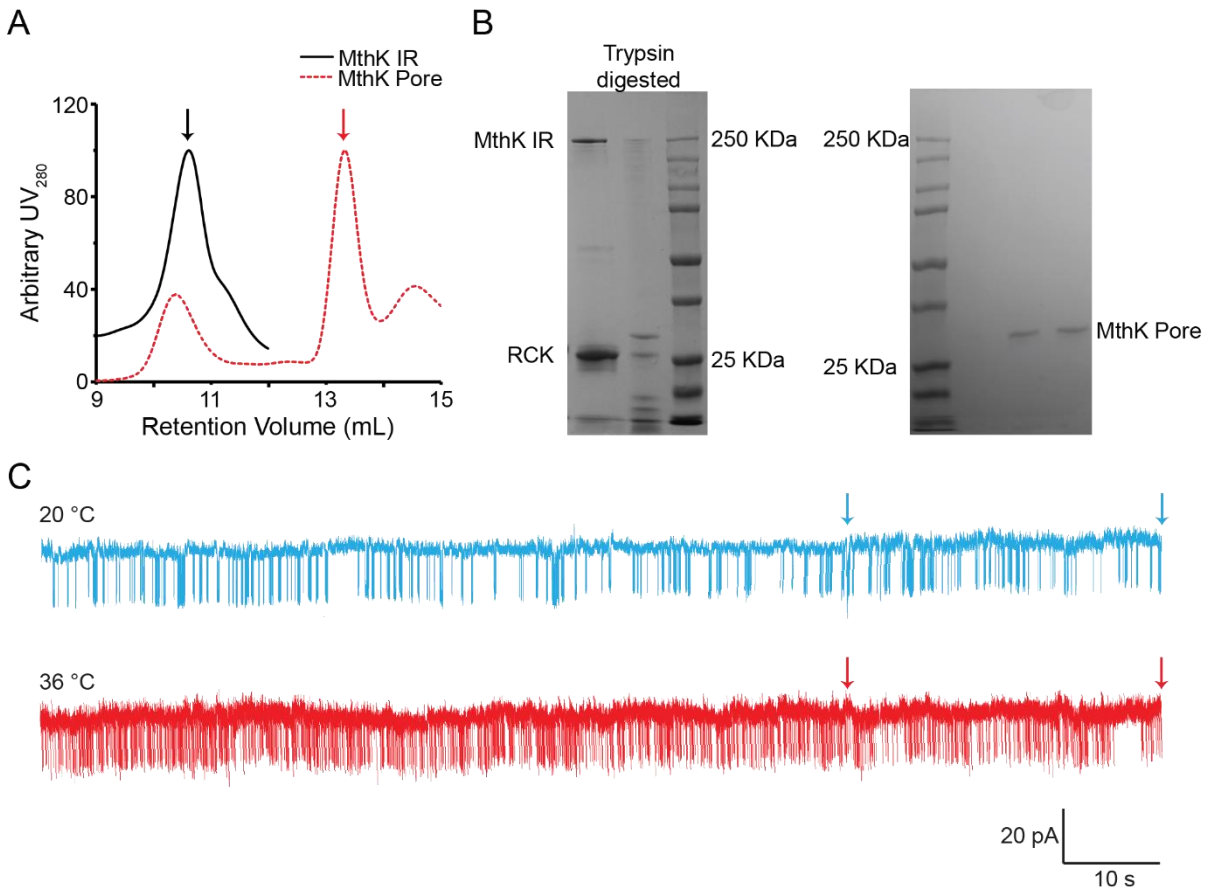


**Supplementary Figure 2 | Purification profile of MthK pore and single channel recordings.** **A.** SEC profile of MthK IR (black) and MthK PO (red) in Superdex 200 column. Black and red arrowheads mark the peaks for MthK IR and MthK PO respectively. **B.** SDS-PAGE analysis of MthK IR before and after trypsin digestion is shown on the left whereas the peak fraction from SEC of MthK PO is on the right. **C.** Extended single channel recordings of MthK PO at 1 mM calcium. The traces between the two arrows are used as the representative data shown in **Fig. 2A**.

.

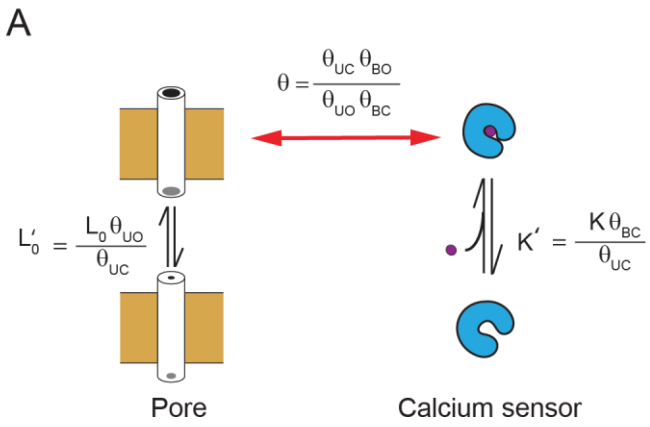


**Supplementary Figure 3 | Renormalization of state-dependent interaction parameters.**

**A.** The model shown in **Fig. 4A** can be described by a reduced set of parameters, as is common in classical representations of allosteric models. The apparent equilibrium constants of pore opening and ligand binding ($L_0'$ and $K_0'$) and the global coupling parameter, $\theta$, are now dependent on the state-dependent coupling parameters and the relationships between the model parameters with those of **Fig. 4A** as shown. This model and that in **Fig. 4A** thus represent the same process but the significance of the parameters is different. The intrinsic equilibrium constants $L_0$ and $K$can be obtained if the pore activation and calcium binding to the calcium sensor is measured in isolation and, thus, these will be different from $L_0'$ and $K_0'$ terms obtained by allosteric analysis of intact channels.

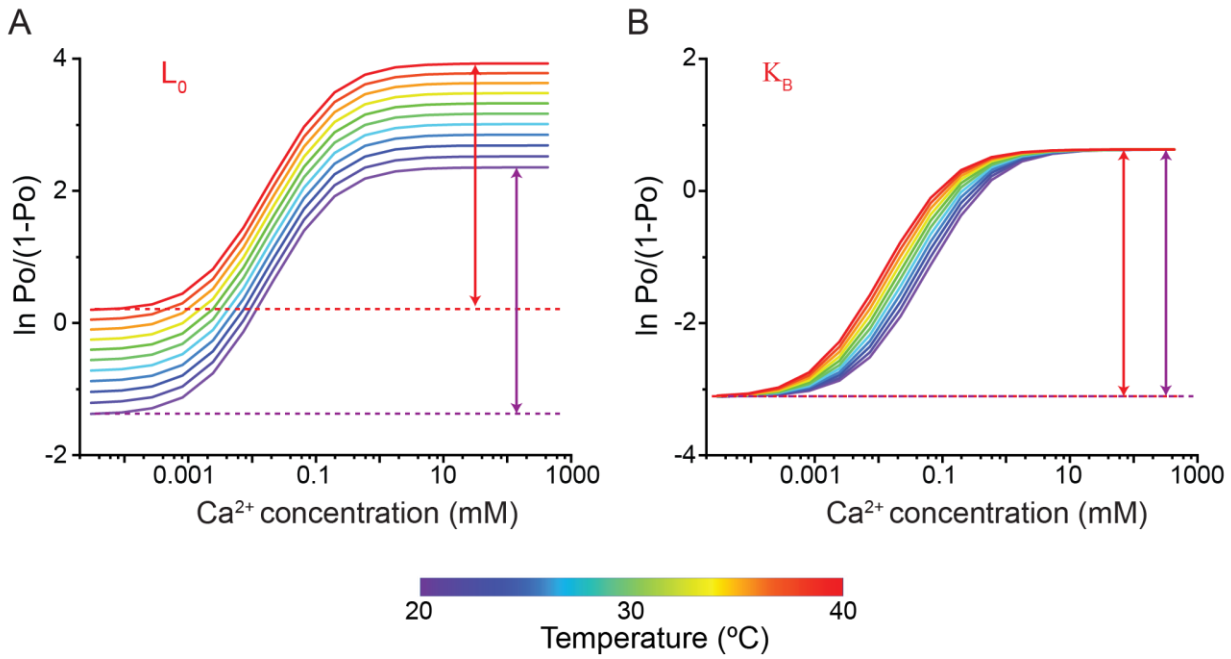


**Supplementary Figure 4: Effect of temperature-dependent parameters on simulated Hill-plots of calcium-dependent gating of MthK.**

Using the model of MthK channel gating, described in **Fig. 5A**, we simulated the Hill-plot of MthK channel (i.e. $\ln [Po/(1\text{-}Po)]$ vs $Ca^{2+}$) at different temperatures. **A.** All parameters, except $L_0$ were kept constant across the different temperatures. This represents the case where the pore opening is innately temperature sensitive. The simulations show that the Hill-plots symmetrically translate vertically with a change in temperature and there is no change in $\Delta\chi$ values. **B.** When the binding affinity, $K$, of calcium is temperature-dependent, the Hill curves are displaced horizontally along the calcium concentration, again with no change in $\Delta\chi$. For all the simulations, the values of the parameters used were: $L_0 = 0.1$; $K = 20000$ $M^{-1}$; $\theta_{UO} = 8$; $\theta_{UC} = 18$; $\theta_{BO} = 150$; $\theta_{BC} = 8$. For temperature dependent simulations of $L_0$ in panel **A**, $\Delta H_L = 60$ kJ and $\Delta S_L = 200$ J/K and the $L_0$ at each temperature was directly calculated as: $L_0(T) = \exp(-(\Delta H_L - T\Delta S_L)/RT)$. Similarly, for temperature dependent simulations of $K$ shown in panel **B**, $\Delta H_K = 60$ KJ and $\Delta S_K = 220$ J/K, respectively.

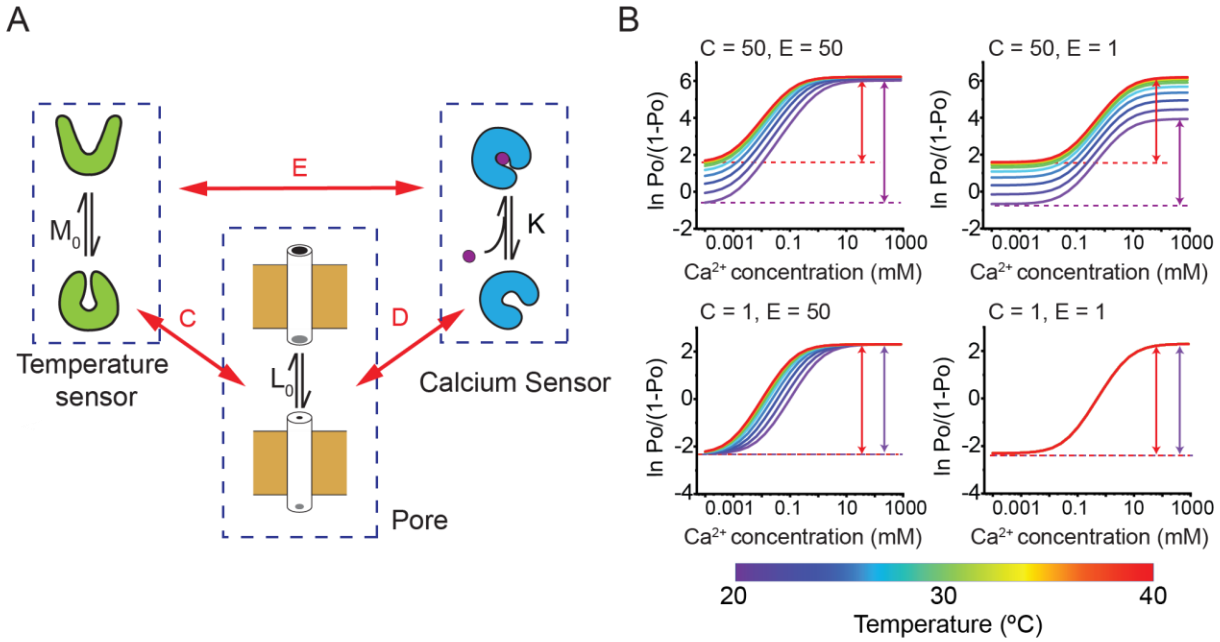


**Supplementary Figure 5. An alternate allosteric model of regulation of calcium activation of MthK by a discrete temperature sensing domain.**

**A.** Schematic model depicting pore domain, calcium-binding domain and temperature sensing domain each of which undergoes a change between active and passive forms. The intrinsic equilibrium constant for pore opening is $L_0$, the binding affinity of calcium to the RCK domain is $K$ and the intrinsic temperature-dependent activation constant of the thermosensor is $M_0$. Each of the three binary elements are allosterically coupled to each other. D, C and E indicate the coupling constants between voltage sensor and pore, temperature sensor and pore and voltage-sensor and temperature-sensor respectively. This model is an adaptation of the nested MWC model used by Horrigan and Aldrich (Horrigan and Aldrich, 2002). **B.** Hill plots of model simulations at different temperatures for various values of parameters C and E, as indicated in the inset. The remaining parameters were kept constant: $L_0 = 0.1$, $K = 200$, and D = 100. All the parameters, except $M_0$, were assumed to be temperature independent. For the temperature sensor, $\Delta H_M = 60$ kJ and $\Delta S_M = 200$ J/K respectively. As observed in the simulations, only when C is not equal to 1, the intercepts of the hyperpolarizing and depolarizing asymptotes change significantly with

temperature. However, only when both C and E are different from 1, $\Delta\chi$ changes with temperature.

# CHAPTER FIVE

## *Cryo-EM study of the MthK apo structure*

### Introduction

> Structure without function is a corpse; function without structure is a ghost.
>
> Vogel and Wainwright, 1969

Electrophysiology and structural biology are two major domains of modern science that allow us to probe ion channels from a structural and functional perspective. Temperature-sensitive ion channels, especially thermoTRPs, are involved in multiple physiological processes, including thermosensation and osmoregulation (Islas and Qin, 2014; Patapoutian et al., 2003). Besides, thermoTRPs are also regulated by multiple endogenous and exogenous ligands. For example, TRPV1 is sensitive to capsaicin, protons, tarantula toxins, peperine, and so on (Cao et al., 2013a; Caterina et al., 1997; Islas and Qin, 2014; Patapoutian et al., 2003; Yuan, 2019). A previous study also found that a lack of extracellular sodium can potentiate the activation of TRPV1 (Jara-Oseguera et al., 2016). It has long been an endeavor for researchers to understand the polymodal gating processes by solving the atomic resolution structure of thermoTRPs.

However, as conventional x-ray crystallography usually requires large quantities of well-behaved protein for crystallization screening (Drenth, 2007), one of the main obstacles for solving their structures is the high cost of expressing these eukaryotic channels. Moreover, as these channels are $Ca^{2+}$ permeable, overexpression of thermoTRPs could be toxic for eukaryotic expression systems (Cohen and Moiseenkova-Bell, 2014). The breakthrough came with the development of electron cryo-microscopy (cryo-EM). With the development of a direct electron detector for electron microscopy, researchers are able to resolve the atomic resolution structures by imaging hundreds of thousands of particles before radiation damage destroying their

conformations (Scheiner, 2015). This improvement was subsequently named as ‘resolution revolution’ and structures of large protein complexes solved with these types of equipment could have a resolution even reach 1 Å resolution (Merk et al., 2016).

In 2013, Cao et al. resolved the first structure of TRPV1 channels using cryo-EM (Cao et al., 2013b; Liao et al., 2013). Although the trials for crystallization failed, the process of screening for a higher expressing and better-behaved construct helps this study. To solve the structure, Cao et al. used a minimally functional construct of rat TRPV1, which is truncated at N-terminal, C-terminal, and a linker region. After this, more structures of TRPV1 were solved, including the capsaicin bound state and the tarantula toxin bound state (Cao et al., 2013b). These combined structures of the same protein in various states improve our understanding of the ligand gating mechanism, while little information is known about the temperature-activation mechanism (Yuan, 2019).

To understand the temperature gating mechanisms of bacterial voltage-gated sodium ($BacNa_V$) channel, Arrigoni et al. solved a bunch of structures of $BacNa_V$ homologs, which possess different temperature sensitivities. Their study reveals that temperature activates these $BacNa_V$ channels through the unfolding of the ‘neck domain’ in the cytoplasmic side underneath the pore (Arrigoni et al., 2016). This study revealed an isolated domain as a temperature sensor in natural ion channels. As this unfolding process correlates with the solvation of hydrophobic residues, this finding is in agreement with the hypothesis proposed by Clapham and Miller, that heat capacity change ($\Delta C_P$) between the open and closed states could contribute to the temperature sensitivity (Clapham and Miller, 2011).

Although Arrigoni et al. suggested that this unfolding or disruption of coiled-coil by temperature may also exist in thermoTRPs, there is no direct evidence that eukaryotic temperature-sensitive ion channels are gated with the same mechanism (Arrigoni and Minor, 2018; Arrigoni et al., 2016). But this study does enlighten us that the structural studies on prokaryotic channels may help us understand the temperature gating mechanism like in voltage-

gated ion channels (Cordero-Morales et al., 2011b; Cuello et al., 2010a; Jiang and MacKinnon, 2000; Kim and Nimigean, 2016; Lenaeus et al., 2005; Morais-Cabral et al., 2001; Shi et al., 2006; Zhou et al., 2001).

As MthK has been studied as a model system for potassium ion channels, multiple crystal structures of MthK are available. As of November 28th, 2019, there have been 25 structures of MthK available in RCSB protein data bank (PDB). Based on the constructs, these structures can be divided into three categories, namely, full-length, pore domain only, and RCK domain only. As for the ligand occupancy, these structures can also be categorized as apo state, calcium-bound state, barium-bound state, cadmium-bound state, and blocker-bound (TBsb) state.

These previous studies help us to better understand the molecular gating mechanism in MthK. As we found that the coupling energy between the RCK and the pore domain is involved in the temperature-dependent activation of MthK, it naturally raises questions about the structural basis of coupling. From the full-length structures, it seems that the linker region is the only interaction between the pore and the RCK domains. However, the electron density of the linker region is missing in these structures (Jiang et al., 2002; Pau et al., 2011). Moreover, to date, there is no structure of full-length MthK in the apo state. Therefore, we pursued a collaboration with Dr. Vera Moiseenkova-Bell at the University of Pennsylvania and her postdoc, Dr. Yaxian Zhao, to solve the apo structure of MthK with cryo-EM.

## Results

### Full-length structures of MthK are all in the bound states

For full-length MthK (MthK FL), there are three structures available. The first one was published in 2002 by Mackinnon and his colleagues with 3.3 Å resolution (PDB: 1LNQ) (Jiang et al., 2002). The protein crystal was achieved at 20 ºC by equal volume mixing of purified protein with buffer containing 23–26% polyethylene glycol 350 monomethyl ether (PEGMME), 100 mM MES, pH 6.5 and 200 mM $CaCl_2$ (Jiang et al., 2002). In this structure, the N-terminal (before

residue 19) and the linker (residue 97-115) are missing, which lack the information for the fast-inactivation as well as RCK regulation. With electron densities in the calcium-binding sites surrounded by Aspartate 184, Glutamate 210, and Glutamate 212, it is assumed that the channel is in an open state (Jiang et al., 2002). This structure, for the first time, showed the gating ring of RCK and identified flexible and stable interfaces in the RCK domain (**Fig. 1**).

From this structure, Jiang et al. proposed that, upon calcium binding, the flexible interfaces will undergo a major conformational change to drag the M2 transmembrane domain away from the center to open the pore (Jiang et al., 2002). However, this structure is solved with the M107I mutant construct, which removes the alternate start point. In lack of the soluble RCKs, two extracted channels bind to each other bottom-to-bottom to have a total of eight RCKs in a crystal unit. Besides, MthK is pH sensitive, and the acidic environment in the crystallization buffer may inhibit MthK (Kuo et al., 2007; Pau et al., 2010). Combined, this structure may not fully represent the open state. Moreover, due to the unresolved linker connecting the RCK domains and transmembrane domains, this structure leaves open questions about the coupling between pore gating and RCK activation.

Besides these questions, functional studies do not agree with one calcium-binding site observed in the RCK domain. First, single-channel recordings showed that the Hill coefficient for calcium is high, around 8 to 10, which suggests more calcium-binding sites should exist (Pau et al., 2011). Second, the neutralized mutations of the binding site (D184N, E210Q, E212Q) do not entirely abolish the calcium-dependent activation of the channel (Pau et al., 2011). Later on, to identify whether more regulatory calcium-binding sites were in the RCK domain, Pau et al. solved another MthK FL calcium bound structure. By soaking the purified protein in buffer containing 22% PEG3350, 100 mM 2-(N-morpholino)-ethanesulfonic acid (MES), pH 5.9, and 100 mM $CaCl_2$, Pao et al. solved a 3.4 Å resolution structure (PDB: 3RBZ) with the best x-ray diffracting crystal (Pau et al., 2011).

In this structure, they found two more calcium-binding sites in the interface of two RCKs, which gives a total of 24 calcium-regulatory sites per MthK channel (**Fig. 1B**). These binding sites were further tested with bilayer recording studies (Pau et al., 2011). Interestingly, by superimposing the two structures (RMSD: 0.686 Å), 1LNQ and 3RBZ, it is evident that the pore domain is twisted with respect to each other (**Fig. 1C**). As the structures were all solved at a similar pH and calcium concentration, this twisting may reflect the effect of detergents on MthK. Comparing to 1LNQ, the structure solved by Pau and his colleagues has an even shorter M2 transmembrane domain resolved, which misses the residues from 92 to 115 in the linker region. However, studies on BK, the eukaryotic counterpart of MthK, has shown that the linker region for BK is structured and functions as a 'repulsive spring' in regulating the function of BK (Niu et al., 2004). Furthermore, our studies on the coupling energy between the RCK domain and pore suggest that the linker should be structured.

The latest full-length structure of MthK (PDB: 6OLY) was available online on November 26$^{th}$, 2019 with 3.1 Å resolution, which is a collaborative work between Brad Rothberg and Bert de Groot (Kopec et al., 2019). From the structure, we could see that the linker is structured, which is consistent with our apo structure, while different from the proposed hypothesis from MacKinnon's structure (Jiang et al., 2002). The linker region, residues 110 to 114, was built based on the previous studies on BK channels and assumed it is an α-helix (Kopec et al., 2019). Interestingly, this structure is solved in a similar condition to the previous structure (3RBZ) with a crystallization buffer containing 22% PEG3350, 100 mM MES, pH 5.9, and 100 mM $CaCl_2$. The purpose of this structure was to study the reason behind the variable conductance of MthK and found that the dewetting from M2 to the linker could modify the selective filter stability and regulate the conductance of the channel (Kopec et al., 2019).

In summary, all of these structures were solved with M107I mutants in an acidic environment (Jiang et al., 2002; Kopec et al., 2019; Smith et al., 2013), which could cause a shift in the structures from a real open state of the channel. As all the structures are in the calcium

bound state, we need the MthK structure in apo state to understand how binding of calcium to RCK causes a structural change in the linker.

**Impact of purification temperature, detergent, and His-tag on biochemistry behavior of MthK**

We discovered that MthK requires room temperature purification and is unstable in cold (**Fig. 2A**). This apparently is not a general rule for membrane proteins, as a lot of sodium and potassium ion channels were purified in cold (4 °C) (Clairfeuille et al., 2017; Cuello et al., 2010a; Kim and Nimigean, 2016).

This preference for room temperature may be partly because of the temperature effect on detergents (Attwood, 1968; Balmbra et al., 1962). The detergent used for purification, n-Decyl-β-D-Maltopyranoside (DM), has a high critical micellar concentration (CMC) around 1.8 mM (Stetsenko and Guskov, 2017). During the purification, we used 5 mM DM, which is less than three fold of CMC. At low temperatures, the CMC of DM may increase, and there may not be enough micelles to solubilize MthK protein in our buffer. Changing to a similar detergent, n-Dodecyl-β-D-Maltopyranoside (DDM), which has two more carbons in the alkyl chain than DM but a much lower CMC (~0.17 mM) (Stetsenko and Guskov, 2017), does not solve the problem. On the contrary, more MthK aggregates with DDM at 4 °C, compared to DM (**Fig. 2B**). Even at room temperature, DDM decreases the stability of the intact MthK channel (**Fig. 2B)**, and most proteins were either aggregated or fell apart. But by adding both DM and DDM in the SEC buffer, this aggregation in cold is significantly reduced, as shown in **Fig. 2C**. This result could because in DDM and DM mixture, MthK prefers to interact with DM, which makes the channel remain intact. While in the presence of DDM, the micelle formation of DM breaks down to smaller sizes and the CMC decreases, which provides enough micelles at a low temperature.

Previously, purification tags have been shown to interfere with the biochemical behavior of the target protein (Kimple et al., 2013; Scopes, 2013). Following the protocol from Mackinnon's

lab, we added a Hexahistidine-tag at the C-terminus of MthK for purification, and a thrombin digestion site was inserted in between (Jiang et al., 2002; Parfenova et al., 2006). As the hexahistidine-tag is a small tag, presumably, it would not interfere with the behavior of MthK. However, without thrombin digestion, MthK is prone to aggregation with the His-tag (**Fig. 2D**). This is observed with two phenomena. First, after elution from the Ni-NTA column, precipitate would form if thrombin protease was not added immediately. Besides, after precipitates removal for the concentrated MthK with His-tag, the injected sample still has a broad SEC profile. This unexpected behavior is hard to explain, as, from the MthK FL structures, the c-terminus appears to be separated (Jiang et al., 2002; Pau et al., 2011). Besides, if the presence of His-tag would prevent the assembly of the channel, why would this construct express well in *E. coli*? Combined with the observation that most pore-only constructs of MthK could not form a functional channel, the RCK domain seems to play an essential role in channel assembly, which is not fully understood.

**Apo structure of MthK in digitonin**

Without a functional cryo-EM facility on campus, we collaborated with Professor Vera Moiseenkova-Bell at the University of Pennsylvania. With a collaborator off-campus, the first obstacle we faced is sample shipment. As the environment during shipment is uncontrolled, it is better to keep the sample on ice to sustain the stability of the sample. In the previous discussion, I have shown that MthK IR behaves well in the presence of both DM and DDM in cold (**Fig. 2C)**. However, to the best of my knowledge, none of the ion channel structures was solved in DM, due to a noisy background.

To solve this problem, I first tried MthK purification with digitonin, which is a mild detergent widely used in the membrane protein field (Stetsenko and Guskov, 2017). Most of the purified MthK ends up aggregated with digitonin in cold, shown in **Fig. 3A**, but compared with only DDM or DM, the SEC profile looks better. Even though digitonin does not produce a perfect SEC profile,

we obtained enough protein samples for cryo-EM from the corresponding peak fraction around 10. 5 ml in Superdex 200 increase column. Strikingly, later trials with glycol-diosgenin (GDN), a synthetic version of digitonin, solved this aggregation problem, shown in **Fig. 3B**. But the peak is still broader and slightly shifts to a higher molecular weight region compared with DDM and DM combined.

The purified MthK sample was shipped to Dr. Moiseenkova-Bell overnight and all the electron microscope images were collected and processed in their laboratory by Dr. Yaxian Zhao. With 2% uranyl acetate, the MthK IR sample in digitonin looks quite homogenous from the negative stain images (**Fig. 4A**). With this promising result, we further concentrated the sample to about 2 mg/ml for the data collection. To achieve an apo state of MthK, our SEC buffer included 5 mM EDTA and 5mM HEDTA. To further remove the calcium contamination from the blotting process, we used this buffer to wash the blotting paper as well (kindly suggested by Dr. Richard Hite).

With blotting and freezing conditions screened by Yaxian, we achieved grids that have a reasonable thickness of ice for cryo-EM (**Fig. 4B**). More than 7,000 movies from these cryo grids were collected, and 26,000 channel-like particles were picked through LoG-autopicking. Based on this pool, 2D classification was processed with Relion 3.1 and achieved 6 classes for MthK shown in **Fig. 4C**. Furthermore, based on the best 2D classification classes, 3D classification was processed and shown in **Fig. 4D**. After rounds of refinement, we finally achieved a density map for MthK with 4.8 Å resolution, shown in **Fig. 5A**. From this structure, we could clearly see the density for the linker region and RCK domains. Unfortunately, the transmembrane domain is covered by detergent micelle and could not be resolved in our density map.

Based on our structure, the linker region is slightly tilted to connect the RCK domain. Previous studies on the eukaryotic large-conductance $K^+$ channel, BK channel, have shown that differences in the linker length could impact the channel activity (Niu et al., 2004). Furthermore, structural studies have illustrated that the linker region of the BK channel is an α helix (Tao et al.,

2017). Although the resolution is not high enough for us to confirm whether it is an α helix or coiled-coil in our structure, we can confirm it is definitely not an unstructured loop. Similar to what we observed, in the latest MthK FL open structure (6OLY), the linker region is observed and constructed as an α-helix (Kopec et al., 2019). Their structure, as well as our structure, implies that the linker region of MthK is structured in both the open and closed states. This is in agreement with our finding that temperature mainly alters the coupling energy between the unbound (Apo) RCK to the pore. This mechanism proposes the existence of a structured linker, as intuitively, the linker region should contribute most to the coupling energy. Furthermore, compared with calcium bound structure, a dramatic conformation change was observed in the linker region.

Although the apo structure of the BK channel is solved (Tao and MacKinnon, 2019), however, the second RCK domain is connected by a linker to RCK1 in the BK, which is different from MthK. In MthK, the second gating ring is formed by the soluble RCK domain expressed from an internal alternate starting point M107 (Jiang et al., 2002). This is also observed in several RCK-gated ion channels originating from bacteria (Dong et al., 2005; Kuo et al., 2003; Schrecker et al., 2019). This soluble gating ring brings a question of dynamic assembly of RCK domains, which has been shown with various oligomerization states in the presence of different calcium concentrations and pH (Kuo et al., 2007).

Previously, the apo gating ring was solved with the isolated RCK domains (Kuo et al., 2007; Ye et al., 2006). The first one (PDB: 2FY8) was solved by Youxing Jiang and his colleagues with a mutation in the $Ca^{2+}$ binding site (D184N) (Ye et al., 2006). However, there is no calcium chelator during purification or crystallization, which may have some contaminated calcium in the purified sample. In this structure, they observed two conformations of the gating ring. One is closed, and the other is partially open. This partially open structure probably results from the contaminated calcium. Later, Kuo et al. used 1mM EDTA in the purified RCK and solved the apo structure (PDB:2OGU) (Kuo et al., 2007). Interestingly, these isolated RCK domains form a hexamer by itself in a triangular position, shown in **Fig. 5B**. This structure has minor variations

from the structure 2FY8, mainly at the interface between the neighboring RCK domains, as illustrated in **Fig. 5C**. Based on the analyses of the purification condition, we think 2OGU is the real apo state of the RCK gating ring. From these structures, the conformational interactions between the pore and apo RCK are missing, which require an apo structure of full-length MthK.

From our MthK structure, we did not see any density of calcium in all twenty four calcium binding sites. Furthermore, the apo RCK structure (2OGU) fits well with our density map, as shown in **Fig. 5D** and **5E**, which is different from the bound structure. Based on these observations, we are confident that we successfully achieved an apo structure of MthK. From the structure, we could see a few helices are misaligned, which suggests the pore domain in the apo state is constricted. This observation correlates well with our finding that at the apo state, there is coupling energy between the pore and gating ring. However, this density map is still low in resolution to give us details of the apo gating ring. In the future, as the SEC profile in GDN is promising, we will try to solve the structure in the presence of GDN.

**Nanodisc reconstitution of MthK**

To solve the structure in a lipid environment, we tried to reconstitute the purified MthK channel in nanodiscs. Nanodiscs are discoidal lipid bilayers with a constrained diameter (Bayburt and Sligar, 2010; Denisov and Sligar, 2016). They are stabilized and soluble in aqueous solutions via a self-encircling amphipathic helical protein called membrane scaffold protein (MSP), which originated from high-density lipoprotein Apo-AI (Bayburt et al., 2002; Bayburt and Sligar, 2010). The length of MSP determines the diameter of nanodisc, and in this study, MSP1E3D1 was used which generates discs with ~12 nm diameter (Bayburt and Sligar, 2010; Denisov et al., 2004). As MthK has only two transmembrane domains per monomer, the pore region is quite small (with diameter ~ 42 Å) (Jiang et al., 2002). This size of nanodisc should be enough for MthK IR reconstitution.

Nanodisc reconstitution has many protocols available (Bayburt et al., 2002; Bayburt and Sligar, 2010; Denisov and Sligar, 2016; Matthies et al., 2018). However, the details vary case by case. The reconstitution temperature, detergent type, concentration, and detergent removal speed could all vary the reconstitution results (Bayburt et al., 2002). Strikingly, even the MSP and target protein storage time may change the outcome (Matthies et al., 2018). To begin, we followed the protocol from Swartz's lab with minor modifications (see Method for detail) (Matthies et al., 2018). As the MthK channel is expressed in *E. coli*, we tested the reconstitution condition with *E. coli* lipids (Avanti). We first optimized the condition for nanodisc reconstitution without purified MthK to get a molar ratio range for MSP and *E. coli* lipids. Shown in **Fig. 6A**, empty nanodisc with *E. coli* lipids behaved well with a mono peak, and the best ratio range for MSP: lipids are between 1:50 to 1:100.

With these results, we further tested MthK reconstitution into nanodisc. As the insertion of MthK will replace some lipids, so the best MSP: lipids ratio should decrease. Moreover, in theory, each nanodisc should have one MthK protein with two MSP. However, it has been tested that the existence of extra empty nanodisc is helpful for the reconstitution (Matthies et al., 2018). With these in mind, we first tried with 1:10:500 and 1:10:1000 ratios for MthK: MSP: lipids. However, these two ratios produce too many empty nanodiscs. So in the second round, we tried the reconstitution with reduced MSP and tested another two ratios 1:8:640 and 1:8:800, shown in **Fig. 6B**. From the SEC profile, the ratio 1:8:640 looks better. Thus, we used this ratio for a medium scale reconstitution, and by SDS-PAGE, we found MthK was successfully reconstituted into nanodisc (**Fig. 6B**).

We observed turbidity in our MSP stock after two-days of storage at room temperature as well as at 4 °C. MSP is an amphipathic protein and purified as a soluble protein, however, it is not stable without the presence of strong detergent like sodium cholate in the buffer. This finding suggests we should prepare the cholate-free MSP right before the reconstitution and keep track of the storage time for each aliquot to improve the reproducibility of the protocol.

**Discussion**

This project is unfinished and I will continue the structural study as a postdoc in Baron's lab after graduation. Based on the preliminary studies, it is quite promising for us to achieve a high-resolution apo structure of MthK IR.

From the digitonin structure on hand, we could see that the linker region of MthK is structured, which is further confirmed with the latest MthK structure (PDB: 6OLY) (Kopec et al., 2019). However, whether this linker is an α helix as it is in its homolog BK remains to be investigated. Besides, we observed that the presence of the pore affected the apo structure of the RCK domain (**Fig. 5D** and **5E)**. This observation is a strong argument for our hypothesis that the apo gating ring is coupled with the pore. Furthermore, compared to the latest MthK FL calcium-bound structure, we observed a dramatic conformation change in the linker from our apo structure, however, whether this conformation change is related to the temperature activation of MthK requests a further investigation.

**Figures**

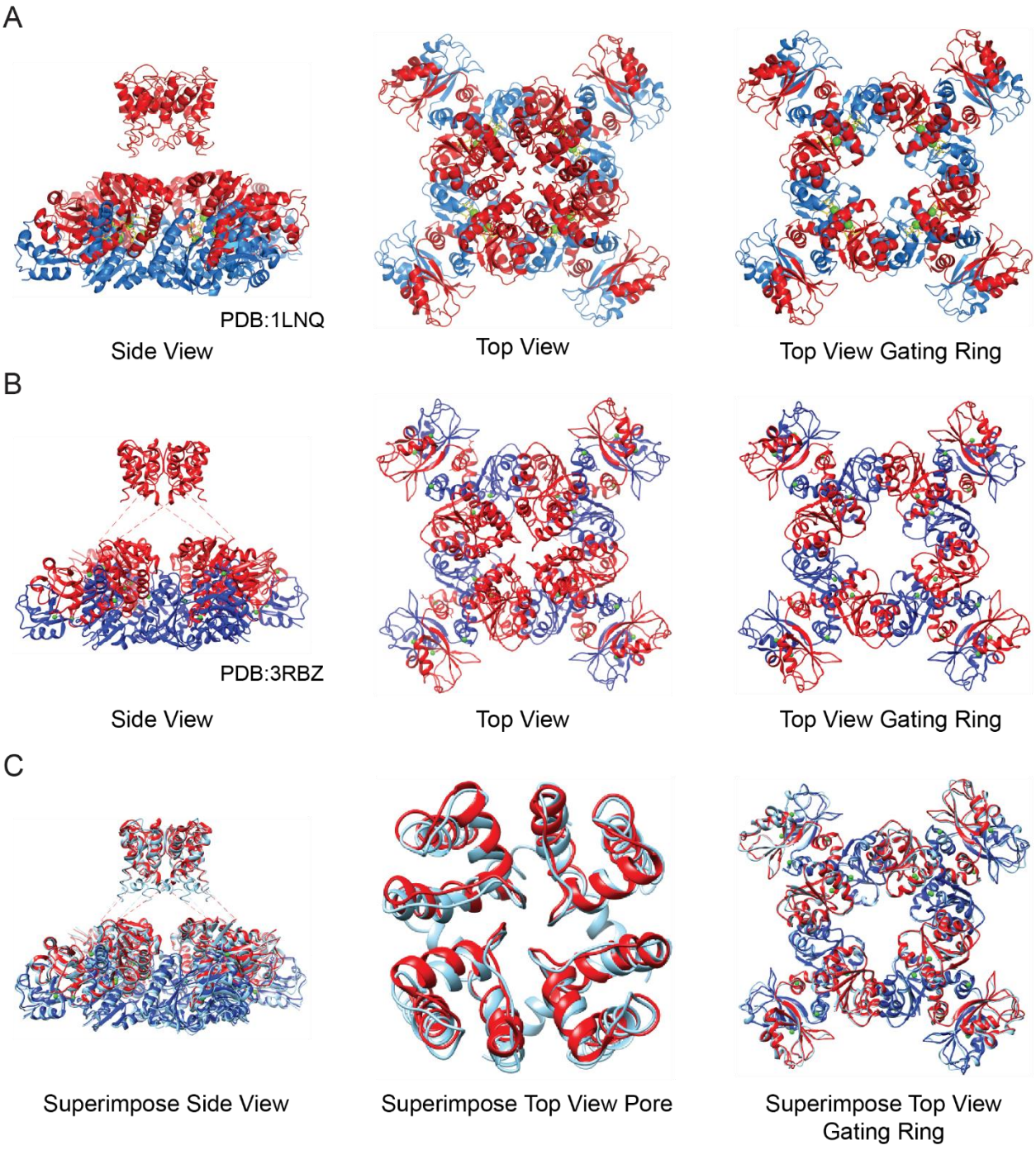


**Figure 1 | Structures of $Ca^{2+}$-bound full-length MthK (MthK FL).**

**A.** Side and top view of the MthK structure solved in Mackinnon's lab (PDB:1LNQ). The pore domain and the RCK linked to the pore are colored in red while the 'soluble' RCK is marked in blue. **B.** MthK structure solved in Rothberg's lab (PDB:3RBZ). Same color coding as in **A**. **C.**

Superimposing of the two structures (1LNQ and 3RBZ). 3RBZ is colored in red and blue, while 1LNQ is in cyan. As we can see, the RCK domain of the two structures fitted quite well, with minor differences in the loop while there is a slight twisting in the pore domain.

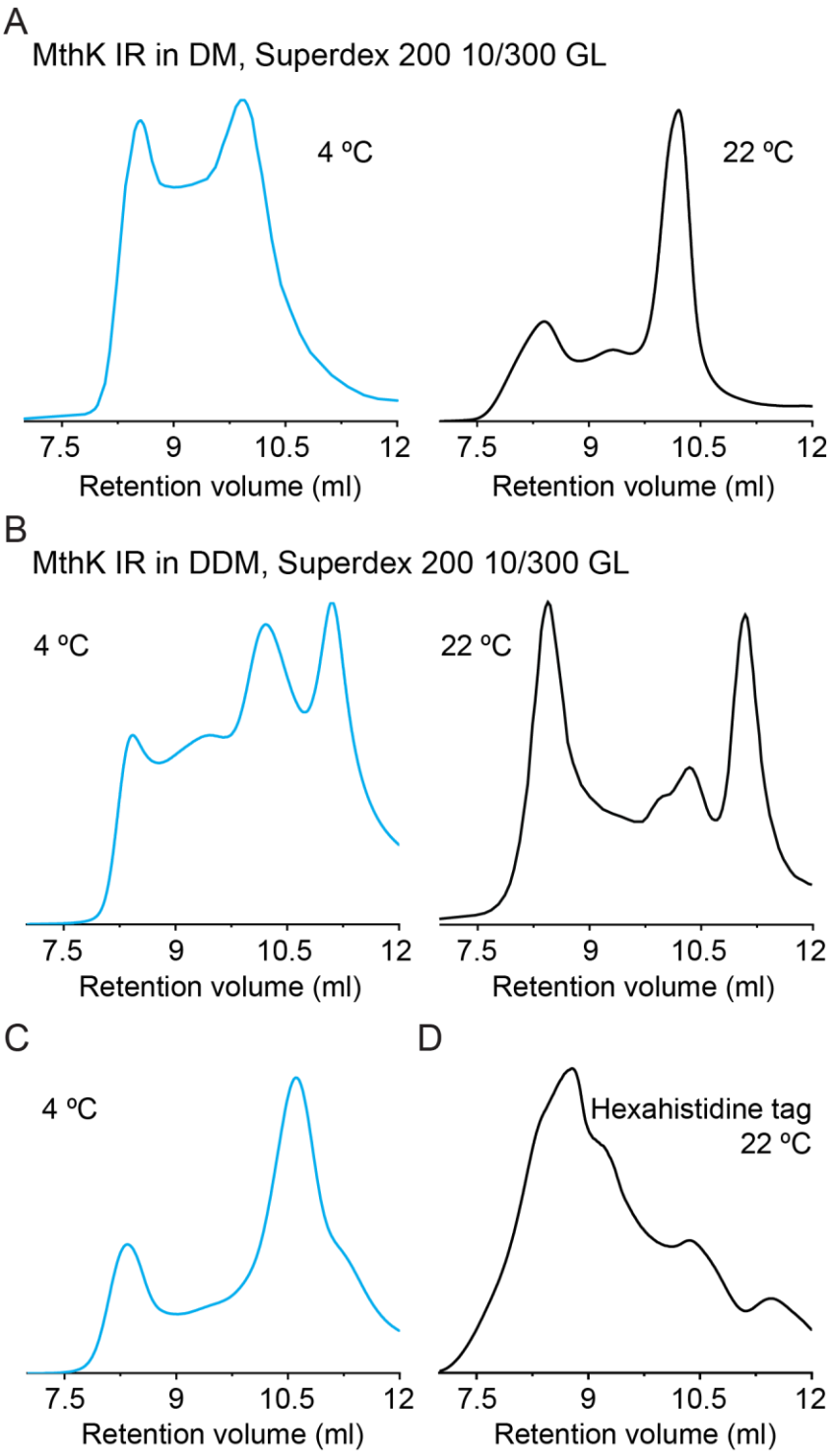


**Figure 2 | Temperature, detergent, and poly-Histidine tag impacts on biochemical behavior of MthK IR.**

**A.** Superdex 200 10/300 GL chromatography of affinity-purified MthK IR after thrombin digestion

(hexahistidine-tag removed). Both injections are in the same buffer containing 5 mM DM. On the left is injection at 4 °C (blue) and on the right is at 22 °C (black) (room temperature). The elution volume for MthK IR should be around 10.2 to 10.5 ml. **B.** Everything is the same as in **A**, except that the buffer contains 1 mM DDM instead of 5 mM DM. **C.** Size-exclusion chromatography (SEC) profile of purified tag-removed MthK IR in buffer containing 1 mM DDM and 5 mM DM at 4 °C. As we could see, the combination of these two detergents significantly decreases aggregation. **D.** SEC profile of purified hexahistidine-tag MthK IR in 5 mM DM buffer at room temperature. A significant amount of MthK was in aggregation.

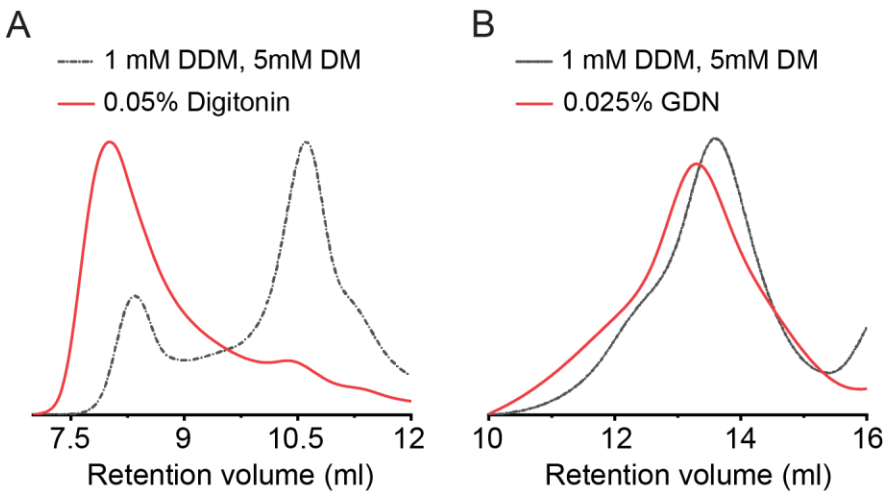


**Figure 3 | Size-exclusion chromatography profile of MthK IR in digitonin and GDN.**

**A.** Superdex 200 10/300 GL chromatography of affinity-purified MthK IR after thrombin digestion (hexahistidine-tag removed) at 4 °C. The dashed black line is with 1 mM DDM and 5 mM DM as a standard. The solid red line is in digitonin. As we could see, most purified protein is in aggregation with digitonin, while the small peak around 10.5 ml is collected for cryo-EM studies. **B.** SEC profile of MthK IR in Superose 6 10/300 chromatography after thrombin digestion (hexahistidine-tag removed) at 4 °C. The red line is in GDN, while the black line is for 1 mM DDM and 5 mM DM. As we could see, purified MthK IR in GDN has a broader peak compared with in DM and DDM dual detergents, and there is a slight peak shift to higher molecular weight.

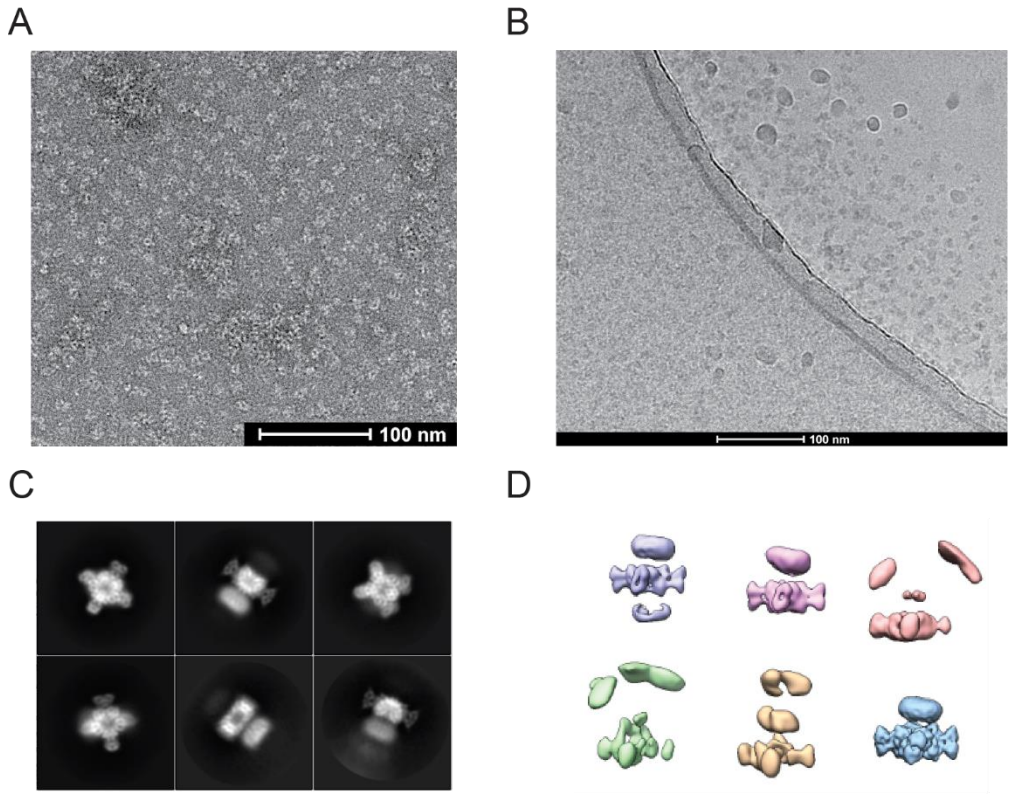


**Figure 4 | Data collection and image processing for MthK IR apo in digitonin.**

**A.** Negative stain of the MthK IR apo sample in digitonin. As we could see, the sample is quite homogenous with minor aggregation. Stained with uranyl acetate. Scale bar is 100 nm indicated in the downright corner. **B.** Frozen grids of the MthK IR apo sample. We could see the ice is quite thin for the grids. **C.** 2D-classifications of the particles from the gids sample. **D.** Result of first round of 3D classification. By picking the most promising ones, we further go through rounds of refinement to achieve a high-resolution density map.

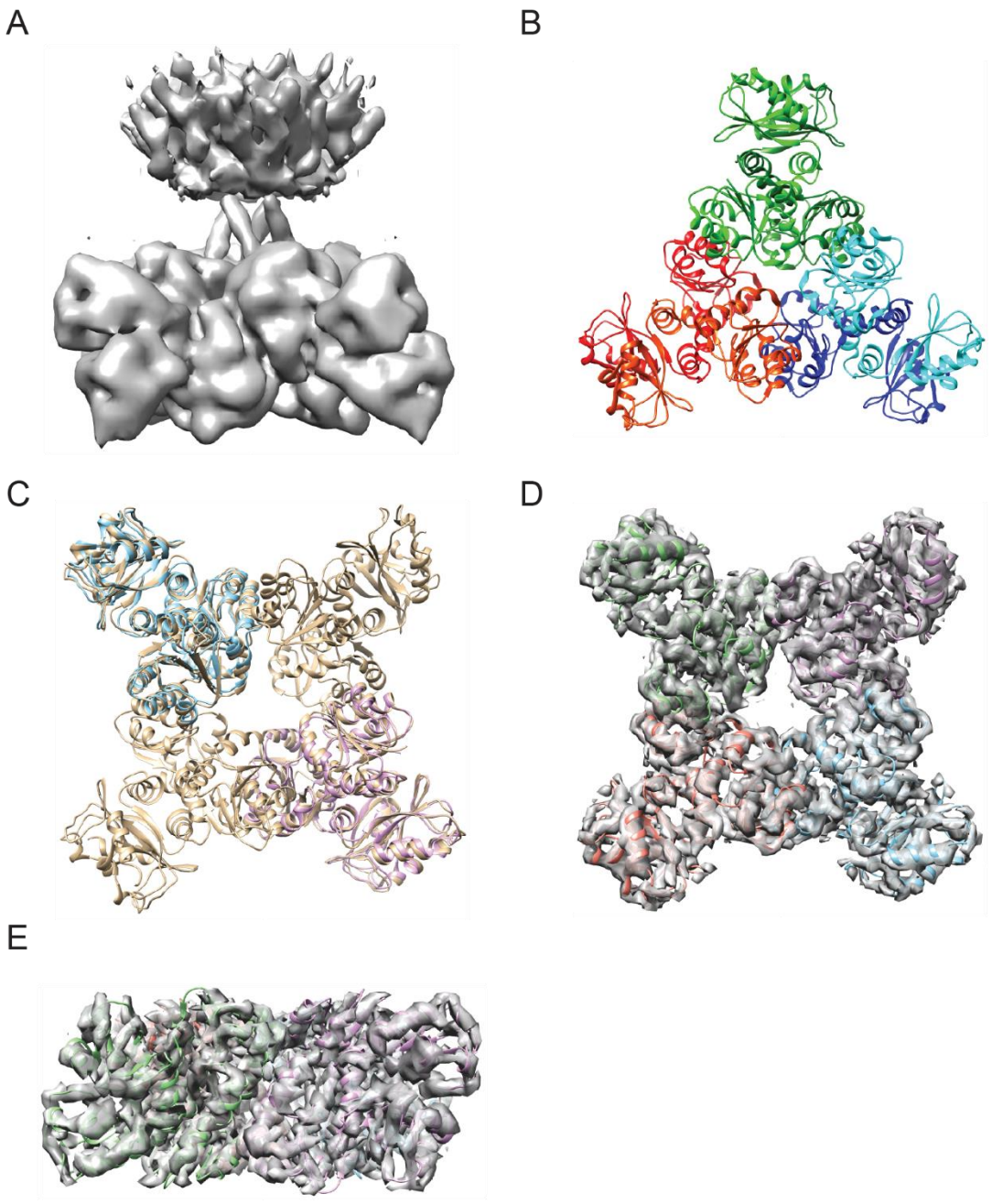


**Figure 5 | MthK IR apo structure in digitonin.**

**A.** Electron density map of the MthK IR apo state. From this structure, we can clearly see that the linker slightly tilted from the digitonin micelle to the RCK domain. The transmembrane domain is still buried in the hydrophobic micelle. **B.** Hexameric assembly of the gating ring of MthK (PDB:2OGU). **C.** Superimposing 2OGU onto the structural assembly of 2FY8 in chimera. 2FY8 is colored as beige, while 2OGU is colored as cyan and pale purple. Minor variations are observed

at the interface between neighboring RCKs and the flexible dimer interface. This superimposed image was completed in Chimera and achieved an RMSD of 1.055 Å. **D.** and **E.** Superimpose 2OGU (colored ribbon) into the MthK IR apo density map (transparent grey) solved in this study. **D** is a bottom view and **E** is sided view. As we could see, most parts fit well with the density map, while minor variations were observed.

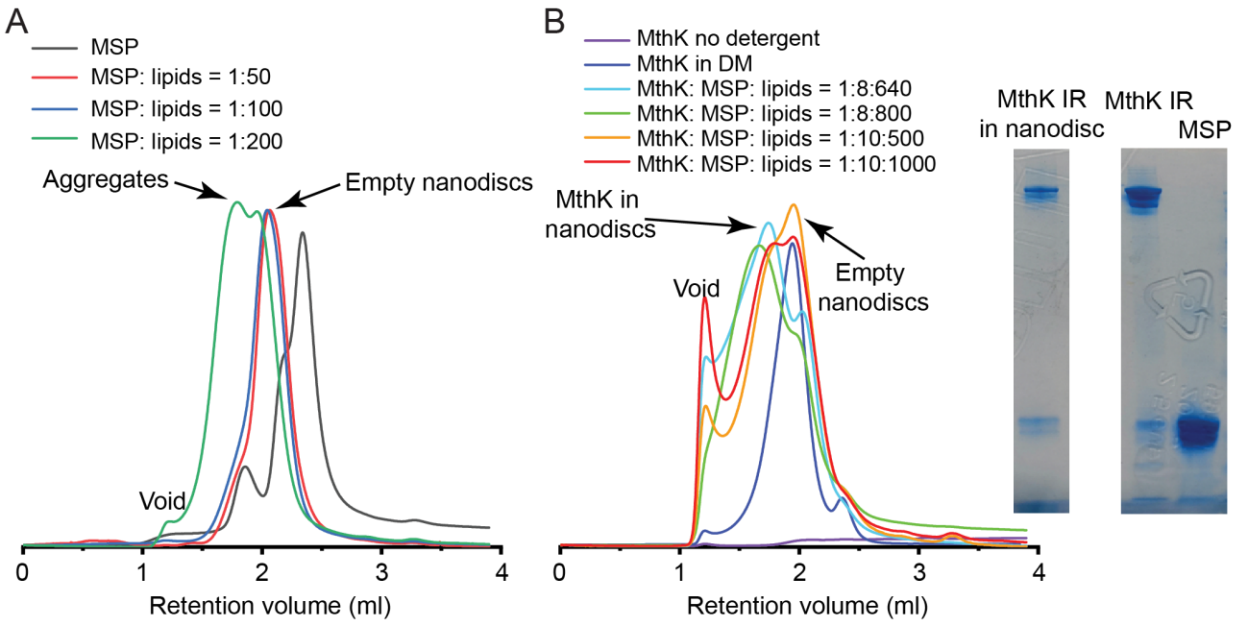


**Figure 6 | Nanodisc reconstitution of MthK IR.**

**A.** Size exclusion chromatography (SEC) of empty nanodisc reconstitution. Tryptophan fluorescence was used in this study with excitation at 295 nm and emission at 335 nm. For fast screening, Superose 6 5/150 GL column was used. The molar ratio of MSP1E3D1 versus lipids was indicated. **B.** MthK IR reconstitution into nanodisc. The SEC profile is collected the same as described in **A**. The peak correspondence was indicated in the chromatography. The SDS-PAGE was collected in a medium-scale preparation, and faction collected corresponds to the screen to indicate the fraction for MthK in nanodisc.

# CHAPTER SIX

## *Conclusions and Future directions*

### Temperature-dependent activation mechanism of MthK

#### *Conclusions*

My thesis work focused on understanding the mechanism of temperature-dependent activation of ion channels. To achieve this, I used MthK as a model system. I have characterized the temperature sensitivity of this channel, first utilizing a complementation assay in $K^+$ uptake deficient strain of bacteria and later through electrophysiology. Then we used a thermodynamic approach to analyze the open probability of MthK in various calcium concentrations at two different temperatures. Using this approach, we demonstrated that the coupling between the calcium sensor and pore plays an essential role in temperature sensation in MthK. To the best of our knowledge, this is the first experimental evidence demonstrating that coupling energy plays an essential role in temperature sensing. In the following section, I will elucidate the temperature-dependent activation mechanism of MthK in simple terms.

Although heat shock has been used in biological studies for decades, mechanistic studies on temperature-sensitive ion channels only have a history of around 20 years. Prior to this study, there were two prevailing ideologies to explain the mechanism of temperature-dependent activation. The most popular among them was that a specialized 'temperature sensor' will be activated upon a change in temperature and thereby lead to channel opening, as shown in **Fig. 1A**. However, after a plethora of mutagenesis and chimera studies, no single domain emerged as a consensus temperature sensor (Clapham and Miller, 2011; Islas and Qin, 2014). Instead, it appears that mutations in multiple regions of the channel could alter the temperature sensitivity (Boukalova et al., 2010; Chowdhury et al., 2014; Cui et al., 2012; Fujiwara et al., 2012; Jabba et al., 2014; Lishko et al., 2007; Saito et al., 2012). From these observations and inspired by protein

unfolding studies, Clapham and Miller proposed that the heat capacity change ($\Delta C_P$) associated with the solvation of buried hydrophobic residues upon channel opening could result in temperature sensitivity (Clapham and Miller, 2011). Based on this hypothesis, Chowdhury et al. repurposed a voltage sensor into a temperature sensor in Shaker potassium channel (**Fig. 1B)** (Chowdhury et al., 2014). Later, studies on bacterial channels, $BacNa_V$ and Hv1, show that a coiled-coil motif regulates the temperature-dependent activities in these channels (Arrigoni et al., 2016; Takeshita et al., 2014). These studies showed clearly that a specialized domain could function as a temperature sensor in some ion channels (Arrigoni and Minor, 2018). Additionally, these findings are consistent with Clapham and Miller's hypothesis. It should be noted, however, that the temperature dependence of these channels is much lower than that of the prototypical temperature-sensitive TRP channels (Islas and Qin, 2014).

Besides these two hypotheses, through model-based simulation, Jara-Oseguera and Islas brought up the possibility that changing the strength and temperature dependence of coupling energy between the pore and the temperature sensor could revert the temperature sensitivity (Jara-Oseguera and Islas, 2013). Unlike the HA model in BK (Horrigan and Aldrich, 2002), this hypothesis proposed that instead of shifting the equilibrium constant of the temperature sensor, temperature alters the coupling energy between the temperature sensor and the pore. However, in their model, a temperature sensor is still required.

With $\chi$-value analysis, my thesis work illustrated that the coupling energy between the calcium sensor and pore is altered by temperature in the temperature-sensitive ion channel, MthK (**Fig. 1C**). In our model, the presence of a temperature sensor is not required for a two order of magnitude change in open probability. Furthermore, through simulation and model building (with the help of Sandipan) we showed that the coupling energy between unbound (apo) calcium sensor and closed pore ($\Delta G_{UC}$) is mainly changed by temperature.

Although we could not eliminate the possibility of a temperature sensor based on our data, we demonstrated that even if the temperature sensor exists, there must be interactions between

the temperature sensor and the pore as well as the temperature sensor and the calcium sensor. In a way, it behaves like changing the coupling energy between the calcium sensor and the pore.

With all these functional studies, we want to strengthen our work with structural analysis. By solving an apo MthK structure in digitonin, we could see the linker region is slightly tilted beneath the digitonin micelle and firmly linked to the RCK domain. This well-ordered linker is further confirmed with the latest MthK bound structure (Kopec et al., 2019). Moreover, by docking the apo gating ring structure (PDB:2OGU) into our electron density map, we observed conformational changes between them, which shed light on the gating mechanism of the pore with an apo gating ring.

***Future directions***

Prokaryotic expression systems have the capability to screen much larger cloning libraries compared to mammalian cell expression systems (Grimm, 2004; Shuman and Silhavy, 2003). This advantage makes the bacterial protein more suitable for large scale forward mutagenesis. With a biochemically tractable temperature-sensitive ion channel, MthK, and functional assays established, we have the possibility to perform a full range of mutagenesis to understand the mechanism of temperature activation better.

As discussed in **Chapter Three**, we implied that the survival rate of LB2003, a $K^+$ uptake deficient *E. coli* strain, is positively correlated with the open probability of expressed MthK. These complementation results were in agreement with the open probability achieved from single channel recordings in **Chapter Four**. Taken together, these results suggest that this complementation assay can serve as a crude screening tool for temperature-sensitive mutants screening for MthK.

By using a cocktail of error-prone DNA polymerases, we created an unbiased library containing over a million independent clones with Dima's help. Most of these clones contain multiple mutations in the open reading frame (ORF) of MthK sequences. To improve the feasibility

of the complementation screen, we did the assay at room temperature (20 °C) and picked clones with a gain of function. In other words, we were screening for cold-sensitive mutants of MthK.

To better illustrating how temperature-sensitive each mutant is, with help from Dr. Vinay Idikuda in our group, we repeated the complementation assay with the wild-type MthK (MthK WT) as control at both 20 °C and at 37 °C. A few representative cold-sensitive mutants' phenotypes were shown in **Fig. 2**. Compared to MthK WT, these mutants have either increased complementation at 20 °C or decreased complementation at 37 °C. Among these mutants, mutant #73, #74 shows extreme cold sensitivity, while mutant #75 remains slightly heat sensitive. To better quantify the effects among different mutants, we used the difference between the highest dilution number of colonies grew at 20 °C, minus the number at 37 °C, shown in Eq. 1:

$$Weight = D_{20\,^{\circ}\mathrm{C}} - D_{37\,^{\circ}\mathrm{C}} \qquad \text{Eq. 1}$$

So if the weight of a mutant is zero, it means the LB2003 cells transformed with this mutant grows equal better at 20 °C versus at 37 °C in our complementation assay. If weight is one, then the transformed LB2003 grows 10-fold better at 20 °C.

With help from Vinay in our lab, we sequenced 49 temperature-sensitive mutants from our pool. With the weight number, we quantified the effect of a mutation in each residue and summarized in **Fig. 3**. The red line is marked at 2.81, which is the average of mutation effects of all 336 residues plus one magnitude of standard deviation. Every mutation at a specific residue has a higher value than this line is indicated as hot spots, summarized in **Table 1**. From the sequences, we could see that the 'hot spots' are all over the construct, but F38 is outstanding with the maximum value. In addition, between residues 79 and 96, there are 8 'hot spots' in these 17 residues, which is the most crowded area for cold-sensitive mutations.

To better illustrate the location of hot spots, we marked all the hot spots in the MthK structure (PDB:1LNQ) based on **Table 1**. As shown in **Fig. 4**, the residues which have values over mean plus standard deviation (SD) were marked as yellow and residues over mean plus 2-fold SD were labeled as orange.

From the structure, we can see that a few areas have clusters of mutations. The linker region is one of these areas, but unfortunately missing from the structure (PDB: 1LNQ). Based on our hypothesis that the coupling energy is altered by heat, which in turn activates the MthK channels, we believe that the residues in the linker region will be critical in reverting temperature sensitivity to the MthK. Hot spot residues E96, A113, V119, and C121 were all in the linker, and residues right above and below the linker are hot spots as well. Surprisingly, besides the linker region, the RCK domain interfaces are areas of interest as well (**Fig. 4C)**. These interfaces are essential in regulating the gating ring to activate the channel upon calcium binding. This finding intrigues us to solve structures for some of these mutants and get a molecular understanding of how these mutants revert the temperature sensitivity in MthK.

Going forward, we will sequence more cold-sensitive mutants to reveal temperature-sensitive hot spots. With the knowledge of all these hot spots, we will systematically identify the areas involved in temperature sensation in MthK. By designing rational mutations in these areas, we will further characterize the most promising ones with electrophysiology and structural studies. Hopefully, with this set of experiments, we could get a deeper understanding of how temperature regulates conformational changes in MthK.

## Figures

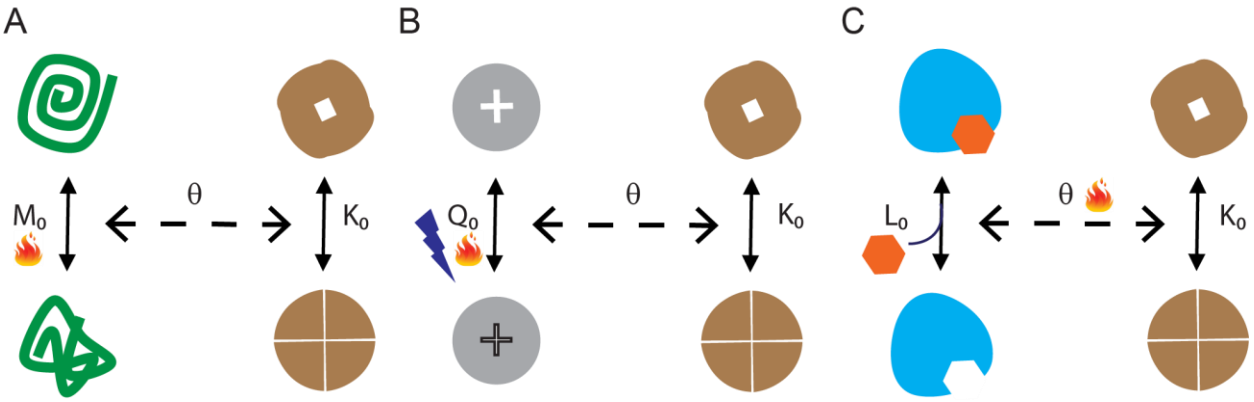


**Figure 1 | Three allosteric mechanisms of temperature regulation.**

**A.** Specialized sensor model. A classical allosteric model where the pore domain (brown tetramer) is allosterically coupled to a specialized domain (green) whose conformation is temperature-dependent. Examples of specialized temperature sensors include bacterial sodium channels and Hv1 channels (Arrigoni et al., 2016; Takeshita et al., 2014). **B.** Polymodal sensor model. A variant of the classical allosteric model wherein the ligand-binding domain or voltage-sensing domain (shaded grey) itself is sensitive to temperature. In the engineered temperature-sensitive Shaker mutants, the mutations likely alter the temperature-dependence of voltage-sensor movement (Chowdhury et al., 2014). **C.** Allosteric modifier model. The primary effect of temperature is to alter the allosteric coupling interaction between the ligand-sensing domain (cyan) and the pore domain.

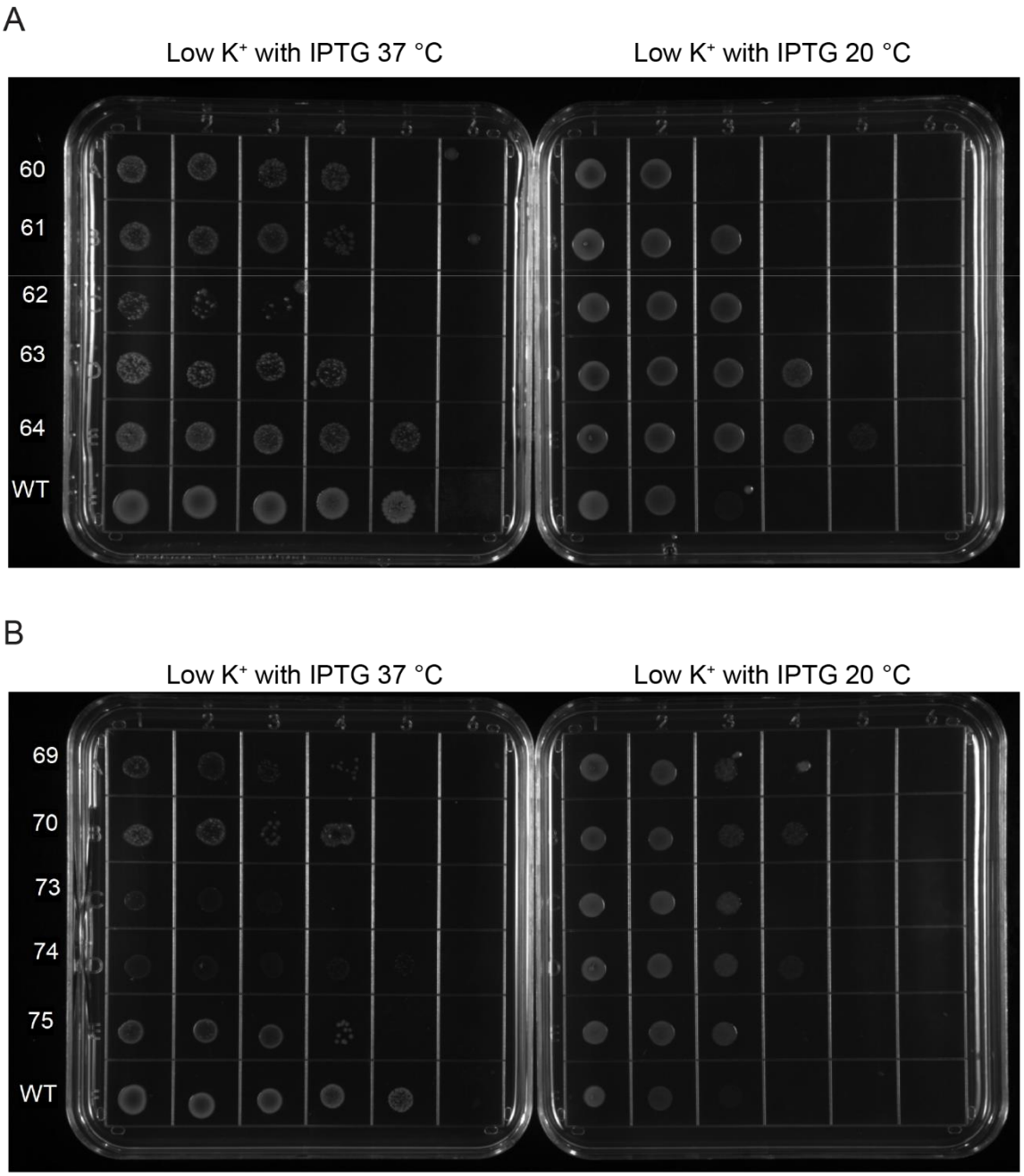


**Figure 2 | Representative temperature sensitive mutants in complementation assay.**

**A.** and **B.** The number codes in the figure are the cold-sensitive mutants selected from more than a million unbiased mutants created with error-prone PCR. The complementation ability of each mutant was evaluated by comparison of the transformed LB2003 cell recovery incubated at 20 °C and 37 °C. The low $K^+$ plates used are Luria broth plates containing IPTG and antibiotics. To quantitatively analyze the complementation ability, we did serial dilution of each mutant with wild

type MthK construct as a control. As shown, the ‘cold-sensitive’ mutants we selected are not all cold-sensitive, some of them behave less heat-sensitive compared with wild type.

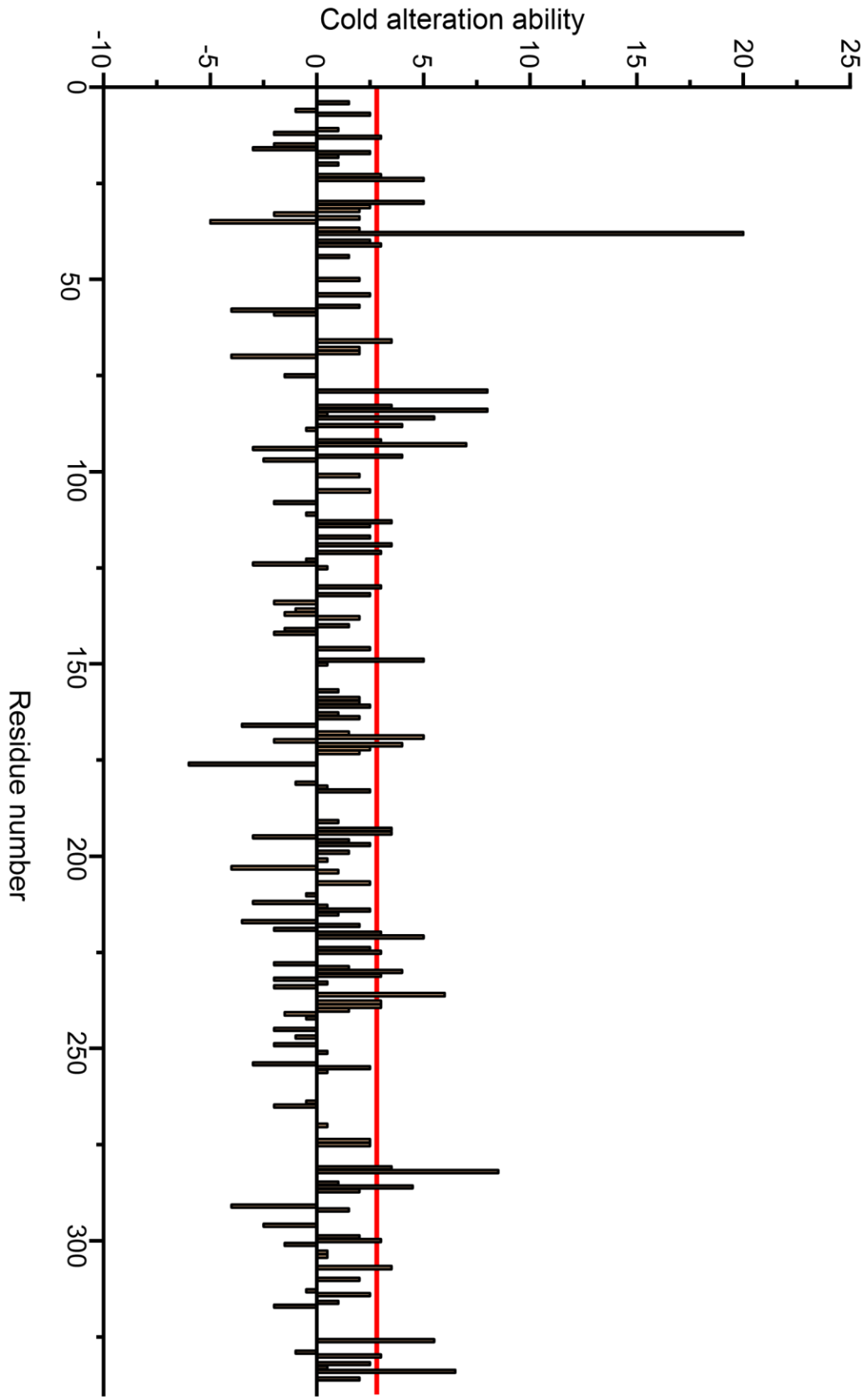
Cold alteration ability
-10
-5
0
5
10
15
20
25
0
50
100
150
200
250
300
Residue number

**Figure 3 | Bar graph of cold alteration ability of each residue in MthK.**

With 49 cold-sensitive mutants sequenced, we weighted the mutation based on the complementation assay. The weight is 0 if the recovery at 20 °C equals with the result at 37 °C, 1 for one order of magnitude better complementation at 20 °C, and -1 for one order better complementation at 37 °C. Every mutation in this mutant has the same weight, and we summarized the number of all 49 mutants based on each residue and shown here as a bar graph. The red line is the threshold, which equals the average plus one standard deviation (average = 0.606, SD = 2.206, threshold = 2.81).

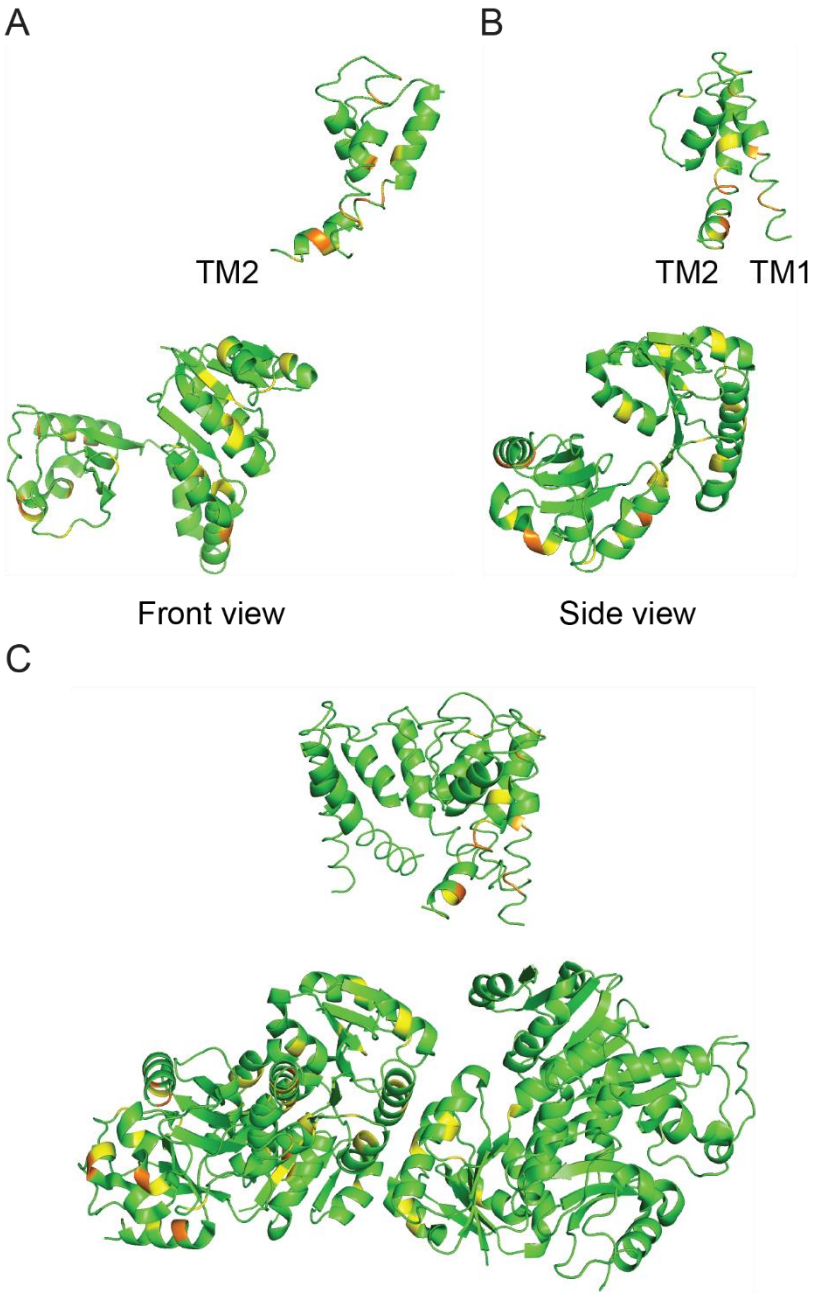


**Figure 4 | Structural illustration of the temperature-sensitive 'hot spots' mutations.**

**A.** and **B.** are front and side views of an MthK monomer (without the soluble RCK domain), 'hot spot' residues are colored based on their value (Value > mean + SD are colored yellow; Value> mean + 2*SD are colored orange). This figure is made in Pymol with $Ca^{2+}$-bound MthK structure (PDB: 1LNQ). As can be seen, the mutations are all over the structure. The linker region is missed in the structure. **C.** Mutations are indicated in a full-length channel (Part of the pore and RCK

domains are deleted for better illustration). Color code is the same as in **A** and **B**. From the structure, we could see that ‘hot spot’ residues clusters in the interfaces of RCK domains.

**Table 1. 'Hot spot' residues summarized from the sequencing results.**

| Mean + SD | Mean + 2*SD |
|---|---|
| P13, I23, L24, V30, F38, I41, S66, L79, G83, I84, T86, A88, E92, R93, E96, A113, V119, C121, C130, R149, D169, E171, H193, C194, L220, R221, A225, S230, P231, G236, L238, M239, L281, D282, H286, D300, P307, E326, L330, I334 | F38, L79, I84, T86, R93, G236, D282, E326, I334 |

Residues that have values higher than the threshold (mean + SD on the left, mean + 2*SD on the right) are summarized in the corresponding category. These residues are 'hot spots' for temperature sensitivity in MthK.

# REFERENCES

Alessandri-Haber, N., Yeh, J.J., Boyd, A.E., Parada, C.A., Chen, X., Reichling, D.B., and Levine, J.D. (2003). Hypotonicity induces TRPV4-mediated nociception in rat. Neuron *39*, 497-511.

Arrigoni, C., and Minor, D.L. (2018). Global versus local mechanisms of temperature sensing in ion channels. Pflugers Arch *470*, 733-744.

Arrigoni, C., Rohaim, A., Shaya, D., Findeisen, F., Stein, R.A., Nurva, S.R., Mishra, S., Mchaourab, H.S., and Minor, D.L. (2016). Unfolding of a Temperature-Sensitive Domain Controls Voltage-Gated Channel Activation. Cell *164*, 922-936.

Attwood, D. (1968). Light-scattering study of the effect of temperature on the micellar size and shape of a nonionic detergent in aqueous solution. The Journal of Physical Chemistry *72*, 339-345.

Balmbra, R.R., Clunie, J.S., Corkill, J.M., and Goodman, J.F. (1962). Effect of temperature on the micelle size of a homogeneous non-ionic detergent. Transactions of the Faraday Society *58*, 1661-1667.

Bayburt, T.H., Grinkova, Y.V., and Sligar, S.G. (2002). Self-Assembly of Discoidal Phospholipid Bilayer Nanoparticles with Membrane Scaffold Proteins. Nano Letters *2*, 853-856.

Bayburt, T.H., and Sligar, S.G. (2010). Membrane protein assembly into Nanodiscs. FEBS Lett *584*, 1721-1727.

Bernèche, S., and Roux, B. (2001). Energetics of ion conduction through the K+ channel. Nature *414*, 73-77.

Block, S.M., Segall, J.E., and Berg, H.C. (1982). Impulse responses in bacterial chemotaxis. Cell *31*, 215-226.

Boukalova, S., Marsakova, L., Teisinger, J., and Vlachova, V. (2010). Conserved residues within the putative S4-S5 region serve distinct functions among thermosensitive vanilloid transient receptor potential (TRPV) channels. J Biol Chem *285*, 41455-41462.

Brauchi, S., Orio, P., and Latorre, R. (2004). Clues to understanding cold sensation: thermodynamics and electrophysiological analysis of the cold receptor TRPM8. Proc Natl Acad Sci U S A *101*, 15494-15499.

Brauchi, S., Orta, G., Salazar, M., Rosenmann, E., and Latorre, R. (2006). A hot-sensing cold receptor: C-terminal domain determines thermosensation in transient receptor potential channels. J Neurosci *26*, 4835-4840.

Bullock, T.H., and Diecke, F.P. (1956). Properties of an infra-red receptor. The Journal of physiology *134*, 47-87.

Cao, E., Cordero-Morales, J.F., Liu, B., Qin, F., and Julius, D. (2013a). TRPV1 channels are intrinsically heat sensitive and negatively regulated by phosphoinositide lipids. Neuron *77*, 667-679.

Cao, E., Liao, M., Cheng, Y., and Julius, D. (2013b). TRPV1 structures in distinct conformations reveal activation mechanisms. Nature *504*, 113-118.

Carpenter, D.O., and Alving, B.O. (1968). A contribution of an electrogenic Na+ pump to membrane potential in Aplysia neurons. J Gen Physiol *52*, 1-21.

Caterina, M.J., Leffler, A., Malmberg, A.B., Martin, W.J., Trafton, J., Petersen-Zeitz, K.R., Koltzenburg, M., Basbaum, A.I., and Julius, D. (2000). Impaired nociception and pain sensation in mice lacking the capsaicin receptor. Science *288*, 306-313.

Caterina, M.J., Rosen, T.A., Tominaga, M., Brake, A.J., and Julius, D. (1999). A capsaicin-receptor homologue with a high threshold for noxious heat. Nature *398*, 436-441.

Caterina, M.J., Schumacher, M.A., Tominaga, M., Rosen, T.A., Levine, J.D., and Julius, D. (1997). The capsaicin receptor: a heat-activated ion channel in the pain pathway. Nature *389*, 816-824.

Chakrapani, S., Cordero-Morales, J.F., and Perozo, E. (2007). A quantitative description of KcsA gating II: single-channel currents. J Gen Physiol *130*, 479-496.

Cheng, W., Sun, C., and Zheng, J. (2010). Heteromerization of TRP channel subunits: extending functional diversity. Protein Cell *1*, 802-810.

Cheng, W., Yang, F., Takanishi, C.L., and Zheng, J. (2007). Thermosensitive TRPV channel subunits coassemble into heteromeric channels with intermediate conductance and gating properties. J Gen Physiol *129*, 191-207.

Cho, H., Yang, Y.D., Lee, J., Lee, B., Kim, T., Jang, Y., Back, S.K., Na, H.S., Harfe, B.D., Wang, F.*, et al.* (2012). The calcium-activated chloride channel anoctamin 1 acts as a heat sensor in nociceptive neurons. Nat Neurosci *15*, 1015-1021.

Chowdhury, S., and Chanda, B. (2010). Deconstructing thermodynamic parameters of a coupled system from site-specific observables. Proc Natl Acad Sci U S A *107*, 18856-18861.

Chowdhury, S., and Chanda, B. (2012). Perspectives on: conformational coupling in ion channels: thermodynamics of electromechanical coupling in voltage-gated ion channels. J Gen Physiol *140*, 613-623.

Chowdhury, S., Jarecki, B.W., and Chanda, B. (2014). A molecular framework for temperature-

dependent gating of ion channels. Cell *158*, 1148-1158.

Clairfeuille, T., Xu, H., Koth, C.M., and Payandeh, J. (2017). Voltage-gated sodium channels viewed through a structural biology lens. Curr Opin Struct Biol *45*, 74-84.

Clapham, D.E., and Miller, C. (2011). A thermodynamic framework for understanding temperature sensing by transient receptor potential (TRP) channels. Proc Natl Acad Sci U S A *108*, 19492-19497.

Clausen, M.V., Hilbers, F., and Poulsen, H. (2017). The Structure and Function of the Na,K-ATPase Isoforms in Health and Disease. Front Physiol *8*, 371.

Cohen, M.R., and Moiseenkova-Bell, V.Y. (2014). Chapter Seven - Structure of Thermally Activated TRP Channels. In Current Topics in Membranes, L.D. Islas, and F. Qin, eds. (Academic Press), pp. 181-211.

Cordero-Morales, J.F., Gracheva, E.O., and Julius, D. (2011a). Cytoplasmic ankyrin repeats of transient receptor potential A1 (TRPA1) dictate sensitivity to thermal and chemical stimuli. Proc Natl Acad Sci U S A *108*, E1184-1191.

Cordero-Morales, J.F., Jogini, V., Chakrapani, S., and Perozo, E. (2011b). A multipoint hydrogen-bond network underlying KcsA C-type inactivation. Biophys J *100*, 2387-2393.

Coronado, R. (1985). Effect of divalent cations on the assembly of neutral and charged phospholipid bilayers in patch-recording pipettes. Biophys J *47*, 851-857.

Cosens, D.J., and Manning, A. (1969). Abnormal electroretinogram from a Drosophila mutant. Nature *224*, 285-287.

Craven, K.B., and Zagotta, W.N. (2006). CNG and HCN channels: two peas, one pod. Annu Rev Physiol *68*, 375-401.

Cuello, L.G., Jogini, V., Cortes, D.M., and Perozo, E. (2010a). Structural mechanism of C-type inactivation in K(+) channels. Nature *466*, 203-208.

Cuello, L.G., Jogini, V., Cortes, D.M., Sompornpisut, A., Purdy, M.D., Wiener, M.C., and Perozo, E. (2010b). Design and characterization of a constitutively open KcsA. FEBS Lett *584*, 1133-1138.

Cui, Y., Yang, F., Cao, X., Yarov-Yarovoy, V., Wang, K., and Zheng, J. (2012). Selective disruption of high sensitivity heat activation but not capsaicin activation of TRPV1 channels by pore turret mutations. J Gen Physiol *139*, 273-283.

Darian-Smith, I., Johnson, K.O., LaMotte, C., Shigenaga, Y., Kenins, P., and Champness, P. (1979). Warm fibers innervating palmar and digital skin of the monkey: responses to thermal stimuli. J Neurophysiol *42*, 1297-1315.

Deming, J.W. (2002). Psychrophiles and polar regions. Curr Opin Microbiol *5*, 301-309.

Denisov, I.G., Grinkova, Y.V., Lazarides, A.A., and Sligar, S.G. (2004). Directed self-assembly of monodisperse phospholipid bilayer Nanodiscs with controlled size. J Am Chem Soc *126*, 3477-3487.

Denisov, I.G., and Sligar, S.G. (2016). Nanodiscs for structural and functional studies of membrane proteins. Nat Struct Mol Biol *23*, 481-486.

Diaz-Franulic, I., Poblete, H., Miño-Galaz, G., González, C., and Latorre, R. (2016). Allosterism and Structure in Thermally Activated Transient Receptor Potential Channels. Annu Rev Biophys *45*, 371-398.

Dib-Hajj, S.D., Yang, Y., and Waxman, S.G. (2008). Genetics and molecular pathophysiology of Na(v)1.7-related pain syndromes. Adv Genet *63*, 85-110.

Dong, J., Shi, N., Berke, I., Chen, L., and Jiang, Y. (2005). Structures of the MthK RCK domain and the effect of Ca2+ on gating ring stability. J Biol Chem *280*, 41716-41724.

Doyle, D.A., Morais Cabral, J., Pfuetzner, R.A., Kuo, A., Gulbis, J.M., Cohen, S.L., Chait, B.T., and MacKinnon, R. (1998). The structure of the potassium channel: molecular basis of K+ conduction and selectivity. Science *280*, 69-77.

Drenth, J. (2007). Principles of Protein X-Ray Crystallography (Springer New York).

Dumon-Seignovert, L., Cariot, G., and Vuillard, L. (2004). The toxicity of recombinant proteins in Escherichia coli: a comparison of overexpression in BL21(DE3), C41(DE3), and C43(DE3). Protein Expr Purif *37*, 203-206.

Falke, J.J., and Hazelbauer, G.L. (2001). Transmembrane signaling in bacterial chemoreceptors. Trends Biochem Sci *26*, 257-265.

Feng, Q. (2014). Temperature sensing by thermal TRP channels: thermodynamic basis and molecular insights. Curr Top Membr *74*, 19-50.

Fujiwara, Y., Kurokawa, T., Takeshita, K., Kobayashi, M., Okochi, Y., Nakagawa, A., and Okamura, Y. (2012). The cytoplasmic coiled-coil mediates cooperative gating temperature sensitivity in the voltage-gated H(+) channel Hv1. Nat Commun *3*, 816.

Garrity, P.A., Goodman, M.B., Samuel, A.D., and Sengupta, P. (2010). Running hot and cold: behavioral strategies, neural circuits, and the molecular machinery for thermotaxis in C. elegans and Drosophila. Genes Dev *24*, 2365-2382.

Glauser, D.A. (2013). How and why Caenorhabditis elegans uses distinct escape and avoidance regimes to minimize exposure to noxious heat. Worm *2*, e27285.

Glauser, D.A., Chen, W.C., Agin, R., Macinnis, B.L., Hellman, A.B., Garrity, P.A., Tan, M.W., and Goodman, M.B. (2011). Heat avoidance is regulated by transient receptor potential (TRP) channels and a neuropeptide signaling pathway in Caenorhabditis elegans. Genetics *188*, 91-103.

Goldschen-Ohm, M.P., and Chanda, B. (2017). SnapShot: Channel Gating Mechanisms. Cell *170*, 594-594.e591.

Gong, J., Liu, J., Ronan, E.A., He, F., Cai, W., Fatima, M., Zhang, W., Lee, H., Li, Z., Kim, G.H.*, et al.* (2019). A Cold-Sensing Receptor Encoded by a Glutamate Receptor Gene. Cell *178*, 1375-1386.e1311.

Graber, Z.T., Shi, Z., and Baumgart, T. (2017). Cations induce shape remodeling of negatively charged phospholipid membranes. Phys Chem Chem Phys *19*, 15285-15295.

Gracheva, E.O., Ingolia, N.T., Kelly, Y.M., Cordero-Morales, J.F., Hollopeter, G., Chesler, A.T., Sánchez, E.E., Perez, J.C., Weissman, J.S., and Julius, D. (2010). Molecular basis of infrared detection by snakes. Nature *464*, 1006-1011.

Grandl, J., Hu, H., Bandell, M., Bursulaya, B., Schmidt, M., Petrus, M., and Patapoutian, A. (2008). Pore region of TRPV3 ion channel is specifically required for heat activation. Nat Neurosci *11*, 1007-1013.

Grimm, S. (2004). The art and design of genetic screens: mammalian culture cells. Nat Rev Genet *5*, 179-189.

Guo, R., Zeng, W., Cui, H., Chen, L., and Ye, S. (2014). Ionic interactions of Ba2+ blockades in the MthK K+ channel. J Gen Physiol *144*, 193-200.

Güler, A.D., Lee, H., Iida, T., Shimizu, I., Tominaga, M., and Caterina, M. (2002). Heat-evoked activation of the ion channel, TRPV4. J Neurosci *22*, 6408-6414.

Harteneck, C., Plant, T.D., and Schultz, G. (2000). From worm to man: three subfamilies of TRP channels. Trends in Neurosciences *23*, 159-166.

Haug, T., Olcese, R., Toro, L., and Stefani, E. (2004a). Regulation of K+ flow by a ring of negative charges in the outer pore of BK Ca channels. Part II: Neutralization of aspartate 292 reduces long channel openings and gating current slow component. J Gen Physiol *124*, 185-197.

Haug, T., Sigg, D., Ciani, S., Toro, L., Stefani, E., and Olcese, R. (2004b). Regulation of K+ flow by a ring of negative charges in the outer pore of BK Ca channels. Part I: Aspartate 292 modulates K+ conduction by external surface charge effect. J Gen Physiol *124*, 173-184.

Heginbotham, L., Lu, Z., Abramson, T., and MacKinnon, R. (1994). Mutations in the K+ channel signature sequence. Biophys J *66*, 1061-1067.

Hille, B. (1992). Ionic Channels of Excitable Membranes (Oxford University Press, Incorporated).

Hodgkin, A.L., and Keynes, R.D. (1955). The potassium permeability of a giant nerve fibre. The Journal of Physiology *128*, 61-88.

Hoffmann, A.A., Sørensen, J.G., and Loeschcke, V. (2003). Adaptation of Drosophila to temperature extremes: bringing together quantitative and molecular approaches. Journal of Thermal Biology *28*, 175-216.

Horrigan, F.T., and Aldrich, R.W. (2002). Coupling between voltage sensor activation, Ca2+ binding and channel opening in large conductance (BK) potassium channels. J Gen Physiol *120*, 267-305.

Hoshi, T., Zagotta, W.N., and Aldrich, R.W. (1994). Shaker potassium channel gating. I: Transitions near the open state. J Gen Physiol *103*, 249-278.

Hänelt, I., Löchte, S., Sundermann, L., Elbers, K., Vor der Brüggen, M., and Bakker, E.P. (2010). Gain of function mutations in membrane region M2C2 of KtrB open a gate controlling K+ transport by the KtrAB system from Vibrio alginolyticus. J Biol Chem *285*, 10318-10327.

Islas, L., and Qin, F. (2014). Thermal Sensors (Elsevier Science).

Jabba, S., Goyal, R., Sosa-Pagán, J.O., Moldenhauer, H., Wu, J., Kalmeta, B., Bandell, M., Latorre, R., Patapoutian, A., and Grandl, J. (2014). Directionality of temperature activation in mouse TRPA1 ion channel can be inverted by single-point mutations in ankyrin repeat six. Neuron *82*, 1017-1031.

Jara-Oseguera, A., Bae, C., and Swartz, K.J. (2016). An external sodium ion binding site controls allosteric gating in TRPV1 channels. Elife *5*.

Jara-Oseguera, A., and Islas, L.D. (2013). The role of allosteric coupling on thermal activation of thermo-TRP channels. Biophys J *104*, 2160-2169.

Jiang, Y., Lee, A., Chen, J., Cadene, M., Chait, B.T., and MacKinnon, R. (2002). Crystal structure and mechanism of a calcium-gated potassium channel. Nature *417*, 515-522.

Jiang, Y., and MacKinnon, R. (2000). The barium site in a potassium channel by x-ray crystallography. J Gen Physiol *115*, 269-272.

Kang, K., Panzano, V.C., Chang, E.C., Ni, L., Dainis, A.M., Jenkins, A.M., Regna, K., Muskavitch, M.A., and Garrity, P.A. (2011). Modulation of TRPA1 thermal sensitivity enables sensory discrimination in Drosophila. Nature *481*, 76-80.

Kikuchi, K., Sugiura, M., Nishizawa-Harada, C., and Kimura, T. (2015). The application of the Escherichia coli giant spheroplast for drug screening with automated planar patch clamp system.

Biotechnol Rep (Amst) *7*, 17-23.

Kim, D.M., and Nimigean, C.M. (2016). Voltage-Gated Potassium Channels: A Structural Examination of Selectivity and Gating. Cold Spring Harbor Perspectives in Biology *8*, 19.

Kimple, M.E., Brill, A.L., and Pasker, R.L. (2013). Overview of affinity tags for protein purification. Curr Protoc Protein Sci *73*, 9.9.1-9.9.23.

Kopec, W., Rothberg, B.S., and de Groot, B.L. (2019). Molecular mechanism of a potassium channel gating through activation gate-selectivity filter coupling. Nature Communications *10*, 5366.

Kuo, M.M., Baker, K.A., Wong, L., and Choe, S. (2007). Dynamic oligomeric conversions of the cytoplasmic RCK domains mediate MthK potassium channel activity. Proc Natl Acad Sci U S A *104*, 2151-2156.

Kuo, M.M., Maslennikov, I., Molden, B., and Choe, S. (2008). The desensitization gating of the MthK K+ channel is governed by its cytoplasmic amino terminus. PLoS Biol *6*, e223.

Kuo, M.M.C., Saimi, Y., and Kung, C. (2003). Gain-of-function mutations indicate that Escherichia coli Kch forms a functional K+ conduit in vivo. The EMBO journal *22*, 4049-4058.

Kuriyan, J., Konforti, B., and Wemmer, D. (2012). The Molecules of Life: Physical and Chemical Principles (CRC Press).

Lee, C.-H., and MacKinnon, R. (2017). Structures of the Human HCN1 Hyperpolarization-Activated Channel. Cell *168*, 111-120.e111.

Lee, U.S., and Cui, J. (2010). BK channel activation: structural and functional insights. Trends Neurosci *33*, 415-423.

Leffler, A., Linte, R.M., Nau, C., Reeh, P., and Babes, A. (2007). A high-threshold heat-activated channel in cultured rat dorsal root ganglion neurons resembles TRPV2 and is blocked by gadolinium. European Journal of Neuroscience *26*, 12-22.

Lenaeus, M.J., Vamvouka, M., Focia, P.J., and Gross, A. (2005). Structural basis of TEA blockade in a model potassium channel. Nat Struct Mol Biol *12*, 454-459.

Li, Y., Berke, I., Chen, L., and Jiang, Y. (2007). Gating and inward rectifying properties of the MthK K+ channel with and without the gating ring. J Gen Physiol *129*, 109-120.

Liao, M., Cao, E., Julius, D., and Cheng, Y. (2013). Structure of the TRPV1 ion channel determined by electron cryo-microscopy. Nature *504*, 107-112.

Liedtke, W., Choe, Y., Martí-Renom, M.A., Bell, A.M., Denis, C.S., Sali, A., Hudspeth, A.J.,

Friedman, J.M., and Heller, S. (2000). Vanilloid receptor-related osmotically activated channel (VR-OAC), a candidate vertebrate osmoreceptor. Cell *103*, 525-535.

Lishko, P.V., Procko, E., Jin, X., Phelps, C.B., and Gaudet, R. (2007). The ankyrin repeats of TRPV1 bind multiple ligands and modulate channel sensitivity. Neuron *54*, 905-918.

Liu, B., Hui, K., and Qin, F. (2003a). Thermodynamics of heat activation of single capsaicin ion channels VR1. Biophys J *85*, 2988-3006.

Liu, B., Yao, J., Zhu, M.X., and Qin, F. (2011). Hysteresis of gating underlines sensitization of TRPV3 channels. J Gen Physiol *138*, 509-520.

Liu, L., Yermolaieva, O., Johnson, W.A., Abboud, F.M., and Welsh, M.J. (2003b). Identification and function of thermosensory neurons in Drosophila larvae. Nat Neurosci *6*, 267-273.

Ludwig, A., Zong, X., Jeglitsch, M., Hofmann, F., and Biel, M. (1998). A family of hyperpolarization-activated mammalian cation channels. Nature *393*, 587-591.

Maeda, K., Imae, Y., Shioi, J.I., and Oosawa, F. (1976). Effect of temperature on motility and chemotaxis of Escherichia coli. J Bacteriol *127*, 1039-1046.

Maingret, F., Lauritzen, I., Patel, A.J., Heurteaux, C., Reyes, R., Lesage, F., Lazdunski, M., and Honoré, E. (2000). TREK-1 is a heat-activated background K(+) channel. EMBO J *19*, 2483-2491.

Martinac, B., Rohde, P.R., Cranfield, C.G., and Nomura, T. (2013). Patch clamp electrophysiology for the study of bacterial ion channels in giant spheroplasts of E. coli. Methods Mol Biol *966*, 367-380.

Matthies, D., Bae, C., Toombes, G.E., Fox, T., Bartesaghi, A., Subramaniam, S., and Swartz, K.J. (2018). Single-particle cryo-EM structure of a voltage-activated potassium channel in lipid nanodiscs. Elife *7*.

McKemy, D.D., Neuhausser, W.M., and Julius, D. (2002). Identification of a cold receptor reveals a general role for TRP channels in thermosensation. Nature *416*, 52-58.

Merk, A., Bartesaghi, A., Banerjee, S., Falconieri, V., Rao, P., Davis, M.I., Pragani, R., Boxer, M.B., Earl, L.A., Milne, J.L.S.*, et al.* (2016). Breaking Cryo-EM Resolution Barriers to Facilitate Drug Discovery. Cell *165*, 1698-1707.

Michaelis, L. Menten. ML (1913) Die kinetik der invertinwerkung. Biochem Z *49*, 333-3691.

Michaelis, L., Menten, M.L., Johnson, K.A., and Goody, R.S. (2011). The original Michaelis constant: translation of the 1913 Michaelis-Menten paper. Biochemistry *50*, 8264-8269.

Mittman, S., Flaming, D.G., Copenhagen, D.R., and Belgum, J.H. (1987). Bubble pressure

measurement of micropipet tip outer diameter. J Neurosci Methods *22*, 161-166.

Monod, J., Wyman, J., and Changeux, J.P. (1965). On the nature of allosteric transitions: a plausible model. J Mol Biol *12*, 88-118.

Moparthi, L., Kichko, T.I., Eberhardt, M., Högestätt, E.D., Kjellbom, P., Johanson, U., Reeh, P.W., Leffler, A., Filipovic, M.R., and Zygmunt, P.M. (2016). Human TRPA1 is a heat sensor displaying intrinsic U-shaped thermosensitivity. Sci Rep *6*, 28763.

Moqrich, A., Hwang, S.W., Earley, T.J., Petrus, M.J., Murray, A.N., Spencer, K.S., Andahazy, M., Story, G.M., and Patapoutian, A. (2005). Impaired thermosensation in mice lacking TRPV3, a heat and camphor sensor in the skin. Science *307*, 1468-1472.

Morais-Cabral, J.H., Zhou, Y., and MacKinnon, R. (2001). Energetic optimization of ion conduction rate by the K+ selectivity filter. Nature *414*, 37-42.

Muraki, K., Iwata, Y., Katanosaka, Y., Ito, T., Ohya, S., Shigekawa, M., and Imaizumi, Y. (2003). TRPV2 is a component of osmotically sensitive cation channels in murine aortic myocytes. Circ Res *93*, 829-838.

Neely, G.G., Keene, A.C., Duchek, P., Chang, E.C., Wang, Q.P., Aksoy, Y.A., Rosenzweig, M., Costigan, M., Woolf, C.J., Garrity, P.A.*, et al.* (2011). TrpA1 regulates thermal nociception in Drosophila. PLoS One *6*, e24343.

Nernst, W. (1889). Die elektromotorische Wirksamkeit der Jonen. In Zeitschrift für Physikalische Chemie, pp. 129.

Nimigean, C.M., Chappie, J.S., and Miller, C. (2003). Electrostatic tuning of ion conductance in potassium channels. Biochemistry *42*, 9263-9268.

Niu, X., Qian, X., and Magleby, K.L. (2004). Linker-gating ring complex as passive spring and Ca(2+)-dependent machine for a voltage- and Ca(2+)-activated potassium channel. Neuron *42*, 745-756.

Nugent, P.W., Shaw, J.A., and Vollmer, M. (2015). Colors of thermal pools at Yellowstone National Park. Appl Opt *54*, B128-139.

Parfenova, L.V., Crane, B.M., and Rothberg, B.S. (2006). Modulation of MthK potassium channel activity at the intracellular entrance to the pore. J Biol Chem *281*, 21131-21138.

Paster, E., and Ryu, W.S. (2008). The thermal impulse response of Escherichia coli. Proc Natl Acad Sci U S A *105*, 5373-5377.

Patapoutian, A., Peier, A.M., Story, G.M., and Viswanath, V. (2003). ThermoTRP channels and beyond: mechanisms of temperature sensation. Nat Rev Neurosci *4*, 529-539.

Pau, V.P., Abarca-Heidemann, K., and Rothberg, B.S. (2010). Allosteric mechanism of Ca2+ activation and H+-inhibited gating of the MthK K+ channel. J Gen Physiol *135*, 509-526.

Pau, V.P., Smith, F.J., Taylor, A.B., Parfenova, L.V., Samakai, E., Callaghan, M.M., Abarca-Heidemann, K., Hart, P.J., and Rothberg, B.S. (2011). Structure and function of multiple Ca2+-binding sites in a K+ channel regulator of K+ conductance (RCK) domain. Proc Natl Acad Sci U S A *108*, 17684-17689.

Peier, A.M., Reeve, A.J., Andersson, D.A., Moqrich, A., Earley, T.J., Hergarden, A.C., Story, G.M., Colley, S., Hogenesch, J.B., McIntyre, P.*, et al.* (2002). A heat-sensitive TRP channel expressed in keratinocytes. Science *296*, 2046-2049.

Posson, D.J., McCoy, J.G., and Nimigean, C.M. (2013). The voltage-dependent gate in MthK potassium channels is located at the selectivity filter. Nat Struct Mol Biol *20*, 159-166.

Pumroy, R.A., Samanta, A., Liu, Y., Hughes, T.E., Zhao, S., Yudin, Y., Rohacs, T., Han, S., and Moiseenkova-Bell, V.Y. (2019). Molecular mechanism of TRPV2 channel modulation by cannabidiol. Elife *8*.

Quallo, T., Vastani, N., Horridge, E., Gentry, C., Parra, A., Moss, S., Viana, F., Belmonte, C., Andersson, D.A., and Bevan, S. (2015). TRPM8 is a neuronal osmosensor that regulates eye blinking in mice. Nat Commun *6*, 7150.

Saito, S., Nakatsuka, K., Takahashi, K., Fukuta, N., Imagawa, T., Ohta, T., and Tominaga, M. (2012). Analysis of transient receptor potential ankyrin 1 (TRPA1) in frogs and lizards illuminates both nociceptive heat and chemical sensitivities and coexpression with TRP vanilloid 1 (TRPV1) in ancestral vertebrates. J Biol Chem *287*, 30743-30754.

Salkoff, L., and Wyman, R. (1981). Genetic modification of potassium channels in Drosophila Shaker mutants. Nature *293*, 228-230.

Scheiner, G. (2015). The Resolution Revolution. Diabetes Self Manag *32*, 28-29, 33.

Schrecker, M., Wunnicke, D., and Hänelt, I. (2019). How RCK domains regulate gating of K+ channels. Biol Chem *400*, 1303-1322.

Scopes, R.K. (2013). Protein Purification: Principles and Practice (Springer New York).

Shi, N., Ye, S., Alam, A., Chen, L., and Jiang, Y. (2006). Atomic structure of a Na+- and K+-conducting channel. Nature *440*, 570-574.

Shuman, H.A., and Silhavy, T.J. (2003). The art and design of genetic screens: Escherichia coli. Nat Rev Genet *4*, 419-431.

Sigg, D. (2013). A linkage analysis toolkit for studying allosteric networks in ion channels. J Gen

Physiol *141*, 29-60.

Smith, F.J., Pau, V.P., Cingolani, G., and Rothberg, B.S. (2012). Crystal structure of a Ba(2+)-bound gating ring reveals elementary steps in RCK domain activation. Structure *20*, 2038-2047.

Smith, F.J., Pau, V.P., Cingolani, G., and Rothberg, B.S. (2013). Structural basis of allosteric interactions among Ca2+-binding sites in a K+ channel RCK domain. Nat Commun *4*, 2621.

Sourjik, V., and Wingreen, N.S. (2012). Responding to chemical gradients: bacterial chemotaxis. Curr Opin Cell Biol *24*, 262-268.

Stetsenko, A., and Guskov, A. (2017). An Overview of the Top Ten Detergents Used for Membrane Protein Crystallization. Crystals *7*, 197.

Stetter, K.O. (2006). Hyperthermophiles in the history of life. Philos Trans R Soc Lond B Biol Sci *361*, 1837-1842; discussion 1842-1833.

Sun, Y., Sun, T.L., and Huang, H.W. (2014). Physical properties of Escherichia coli spheroplast membranes. Biophys J *107*, 2082-2090.

Sánchez-Moreno, A., Guevara-Hernández, E., Contreras-Cervera, R., Rangel-Yescas, G., Ladrón-de-Guevara, E., Rosenbaum, T., and Islas, L.D. (2018). Irreversible temperature gating in trpv1 sheds light on channel activation. Elife *7*.

Takeshita, K., Sakata, S., Yamashita, E., Fujiwara, Y., Kawanabe, A., Kurokawa, T., Okochi, Y., Matsuda, M., Narita, H., Okamura, Y.*, et al.* (2014). X-ray crystal structure of voltage-gated proton channel. Nat Struct Mol Biol *21*, 352-357.

Tao, X., Hite, R.K., and MacKinnon, R. (2017). Cryo-EM structure of the open high-conductance $Ca^{2+}$-activated $K^{+}$ channel. Nature *541*, 46-51.

Tao, X., and MacKinnon, R. (2019). Molecular structures of the human Slo1 K+ channel in complex with β4. eLife *8*, e51409.

Tilegenova, C., Vemulapally, S., Cortes, D.M., and Cuello, L.G. (2016). An improved method for the cost-effective expression and purification of large quantities of KcsA. Protein Expr Purif *127*, 53-60.

Träuble, H., and Eibl, H. (1974). Electrostatic effects on lipid phase transitions: membrane structure and ionic environment. Proc Natl Acad Sci U S A *71*, 214-219.

Vlachová, V., Teisinger, J., Susánková, K., Lyfenko, A., Ettrich, R., and Vyklický, L. (2003). Functional role of C-terminal cytoplasmic tail of rat vanilloid receptor 1. J Neurosci *23*, 1340-1350.

Voets, T., Owsianik, G., Janssens, A., Talavera, K., and Nilius, B. (2007). TRPM8 voltage sensor

mutants reveal a mechanism for integrating thermal and chemical stimuli. Nat Chem Biol *3*, 174-182.

Voets, T., Talavera, K., Owsianik, G., and Nilius, B. (2005). Sensing with TRP channels. Nat Chem Biol *1*, 85-92.

Vogel, S., and Wainwright, S.A. (1969). A Functional Bestiary: Laboratory Studies about Living Systems (Addison-Wesley Publishing Company).

Watanabe, H., Vriens, J., Suh, S.H., Benham, C.D., Droogmans, G., and Nilius, B. (2002). Heat-evoked activation of TRPV4 channels in a HEK293 cell expression system and in native mouse aorta endothelial cells. J Biol Chem *277*, 47044-47051.

Welch, J.M., Simon, S.A., and Reinhart, P.H. (2000). The activation mechanism of rat vanilloid receptor 1 by capsaicin involves the pore domain and differs from the activation by either acid or heat. Proc Natl Acad Sci U S A *97*, 13889-13894.

Wyman, J. (1967). Allosteric linkage. J Am Chem Soc *89*, 2202-&.

Xiao, B., Coste, B., Mathur, J., and Patapoutian, A. (2011). Temperature-dependent STIM1 activation induces $Ca^{2+}$ influx and modulates gene expression. Nat Chem Biol *7*, 351-358.

Xu, H., Ramsey, I.S., Kotecha, S.A., Moran, M.M., Chong, J.A., Lawson, D., Ge, P., Lilly, J., Silos-Santiago, I., Xie, Y*., et al.* (2002). TRPV3 is a calcium-permeable temperature-sensitive cation channel. Nature *418*, 181-186.

Yang, F., Cui, Y., Wang, K., and Zheng, J. (2010). Thermosensitive TRP channel pore turret is part of the temperature activation pathway. Proc Natl Acad Sci U S A *107*, 7083-7088.

Yao, J., Liu, B., and Qin, F. (2009). Rapid temperature jump by infrared diode laser irradiation for patch-clamp studies. Biophys J *96*, 3611-3619.

Yao, J., Liu, B., and Qin, F. (2010). Kinetic and energetic analysis of thermally activated TRPV1 channels. Biophys J *99*, 1743-1753.

Ye, S., Li, Y., Chen, L., and Jiang, Y. (2006). Crystal structures of a ligand-free MthK gating ring: insights into the ligand gating mechanism of K+ channels. Cell *126*, 1161-1173.

Yuan, P. (2019). Structural biology of thermoTRPV channels. Cell Calcium *84*, 102106.

Zadek, B., and Nimigean, C.M. (2006). Calcium-dependent gating of MthK, a prokaryotic potassium channel. J Gen Physiol *127*, 673-685.

Zakharian, E., Cao, C., and Rohacs, T. (2010). Gating of transient receptor potential melastatin 8 (TRPM8) channels activated by cold and chemical agonists in planar lipid bilayers. J Neurosci *30*,

12526-12534.

Zeikus, J.G., and Wolfe, R.S. (1973). Fine structure of Methanobacterium thermoautotrophicum: effect of growth temperature on morphology and ultrastructure. J Bacteriol *113*, 461-467.

Zhang, F., Jara-Oseguera, A., Chang, T.H., Bae, C., Hanson, S.M., and Swartz, K.J. (2018). Heat activation is intrinsic to the pore domain of TRPV1. Proc Natl Acad Sci U S A *115*, E317-E324.

Zheng, J., and Sigworth, F.J. (1997). Selectivity changes during activation of mutant Shaker potassium channels. J Gen Physiol *110*, 101-117.

Zheng, J., and Trudeau, M.C. (2015). Handbook of Ion Channels (CRC Press).

Zhong, L., Bellemer, A., Yan, H., Ken, H., Jessica, R., Hwang, R.Y., Pitt, G.S., and Tracey, W.D. (2012). Thermosensory and nonthermosensory isoforms of Drosophila melanogaster TRPA1 reveal heat-sensor domains of a thermoTRP Channel. Cell Rep *1*, 43-55.

Zhou, Y., Morais-Cabral, J.H., Kaufman, A., and MacKinnon, R. (2001). Chemistry of ion coordination and hydration revealed by a K+ channel-Fab complex at 2.0 A resolution. Nature *414*, 43-48.

Zimmermann, K., Lennerz, J.K., Hein, A., Link, A.S., Kaczmarek, J.S., Delling, M., Uysal, S., Pfeifer, J.D., Riccio, A., and Clapham, D.E. (2011). Transient receptor potential cation channel, subfamily C, member 5 (TRPC5) is a cold-transducer in the peripheral nervous system. Proc Natl Acad Sci U S A *108*, 18114-18119.